Alma Mater Studiorum · University of Bologna

Department of Physics and Astronomy
Department of Biological, Geological and Environmental Sciences

Master Degree in Science of Climate

Marine Productivity in Eastern Boundary Upwelling Systems under Climate Change

Supervisor:
Prof. Antonio Navarra

Co-supervisors:
Prof. Laurent Bopp
Dr. Lester Kwiatkowski

Submitted by:
Erica Cioffi

Academic Year 2023/2024

Abstract

The impact of climate change on the highly sensitive Eastern Boundary Upwelling Systems (EBUS) is currently a significant concern. These regions-California, Canary, Humboldt, and Benguela-contribute disproportionately to global marine productivity, supporting essential ecosystem services. Consequently, it is crucial to reduce the substantial uncertainties that still persist regarding the impact of climate change on these regions and on the ecosystems they support. This study utilizes scenario simulations (SSP5-8.5, SSP2-4.5, and SSP5-3.4-OS) from several Earth System Models of the CMIP6, in particular the latest model by IPSL (IPSL-CM6A-LR), to evaluate early theories and state-of-the-art hypotheses explaining the mechanisms driving changes in Net Primary Productivity (NPP). The findings reveal that the current understanding of these processes is partial, primarily accounting for large-scale atmospheric changes associated with Hadley cell expansion, which causes the poleward shift of upwelling regions and of NPP hotspots. While upwelling-favorable winds changes are recognized as significant drivers of NPP patterns, they alone cannot fully explain the projected changes in NPP across all regions. Through a correlative approach and a quantitative analysis of growth rates, this thesis emphasizes the central role in shaping productivity of temperature limitation and of changes in the concentrations of subsurface nutrients. The analysis of the overshoot scenario further highlights the importance of deep nutrient reservoirs in sustaining NPP within the euphotic layer. The study demonstrates the complexity of the subject, due to the intricate interplay of changes in upwelling intensity, source-water nutrient content, and other dynamical and biogeochemical processes, and highlights the potential ecological and economical impacts of changes in net primary productivity on marine ecosystems.

Contents

1 Introduction **4**
- 1.1 Understanding Phytoplankton Dynamics . . . 5
  - 1.1.1 Global carbon cycle . . . 5
  - 1.1.2 Marine food web . . . 7
  - 1.1.3 Key Drivers of Phytoplankton Variability . . . 7
- 1.2 Eastern Boundary Upwelling Systems . . . 9
  - 1.2.1 EBUS features . . . 9
  - 1.2.2 Ecological and socioeconomic importance . . . 13
- 1.3 Past and state-of-the-art research . . . 14
  - 1.3.1 Climate change in the EBUS . . . 14
  - 1.3.2 Mechanisms of change of marine productivity . . . 16
  - 1.3.3 Mitigation scenarios . . . 17
- 1.4 Thesis objectives . . . 19

2 Methods **21**
- 2.1 CMIP6 and ScenarioMIP . . . 21
- 2.2 The IPSL model . . . 24
- 2.3 Sources of uncertainty . . . 27
- 2.4 Variables . . . 28
- 2.5 Analysis methods . . . 29

3 Results and discussion **32**
- 3.1 Global overview . . . 32
- 3.2 EBUS Net Primary Productivity . . . 37
- 3.3 Correlative analysis . . . 43
  - 3.3.1 Nitrates . . . 44
  - 3.3.2 Upwelling-favorable winds . . . 50
  - 3.3.3 Community composition changes . . . 52
- 3.4 Growth rates decomposition . . . 56
- 3.5 Overshoot scenario . . . 58

4 Future work and open questions **66**
- 4.1 Biogeochemical aspects . . . 66
- 4.2 Observations . . . 67
- 4.3 Spatial resolution . . . 68

4.4 Projection uncertainty 68
4.5 Natural variability 69

5 Conclusions **71**

Chapter 1

Introduction

Climate change is significantly altering global ecosystems and represents a major cause for concern in contemporary science. Variations in greenhouse gas concentrations due to increasing human emissions strongly affect oceans that, uptaking one third of anthropogenic atmospheric carbon, play a central role in controlling climate by regulating the partial pressure of CO_2 in the atmosphere [1], [2]). The consequences may be far-reaching, with rising sea temperatures, acidification, deoxygenation, and variations of nutrient availability in the oceans [3].
These changes influence the growth and distribution of phytoplankton, thus representing a potential threat to marine ecosystems worldwide, because these microorganisms form the base of the marine food web, providing a fundamental ecological function for higher trophic levels, and mediate the carbon cycle, acting as a crucial component of the biological pump.
Understanding how phytoplankton will respond to climate change is especially important in the highly sensitive Eastern Boundary Upwelling Systems (EBUS), that play a disproportionate role for global ocean productivity and provide crucial ecosystem services [4].
However, projections of primary productivity trends in these regions are uncertain, due to the several factors that may influence them, potentially with opposing effects and varying time scales. The issue further complicates when considering mitigation scenarios and the reversibility of changes.

In this chapter, the main features of phytoplankton are introduced and the EBUS regions are described, highlighting their central support for human society. Moreover, an overview of past and state-of-the-art research on this topic is provided, summarizing the existing knowledge on climate change impacts under both standard and mitigation scenarios.

1.1 Understanding Phytoplankton Dynamics

Phytoplankton, derived from the Greek words *phyton*, meaning 'plant', and *planktos*, meaning 'wanderer' or 'drifter', are unicellular autotrophs[1] (with some species even exhibiting a mixotrophic behavior) and phototrophic organisms with the ability of synthesizing organic material using light. With more than 5000 species, phytoplankton cover a vast range of size, morphology and biogeochemical roles, and different groups have distinct functionalities and growth rates.

Phytoplankton play a central role in the marine biogeochemical cycles of elements like carbon, nitrogen, phosphorus, and oxygen. These cycles involve all the transformations and exchanges between various oceanic reservoirs and help regulate the climate system [5].
Thanks to their contribution to the marine biological pump in the global carbon cycle and their role as primary producers of organic matter, which supports the higher levels of the trophic web, phytoplankton are essential in the equilibria of regional and global ecosystems, and understanding the characteristics and functioning of the main factors affecting their variability, mainly temperature, light and nutrient availability, is of great importance.

1.1.1 Global carbon cycle

Phytoplankton play a central role in marine ecosystems: in Figure 1.1 a schematic of the processes in which they are involved is presented, illustration from [6].
Despite constituting only about 1% of the global photosynthetic biomass, these organisms account for approximately half of the conversion of inorganic compounds into organic matter [7]. In the euphotic zone (the sunlit surface layers) **photosynthesis** occurs: carbon dioxide and water are converted into glucose and oxygen using light energy. The chemical reaction of this is:

$$6\,CO_2 + 6\,H_2O \xrightarrow{light} C_6H_{12}\,O_6 + 6\,O_2$$

Most of the material synthesized by phytoplankton undergoes remineralization [8]. This process involves the breakdown of organic matter back into inorganic forms using an oxidant such as oxygen, and it is primarily carried out by bacteria and zooplankton, that convert the organic matter back into carbon dioxide and dissolved nutrients. Most of the remineralization activity occurs in the uppermost ocean layers. However, some material is exported to the twilight zone (the layer below the euphotic zone, spanning 150 to 1000 meters), where remineralization continues at a slower rate. This process replenishes the nutrient reservoir and contributes to oxygen depletion in these deeper waters.

[1] *Autotroph* organisms can create organic matter directly from nutrients (mainly nitrogen and phosphorus) using photosynthesis; they differ from *heterotrophs*, that take nutrition from preexisting sources of organic carbon.

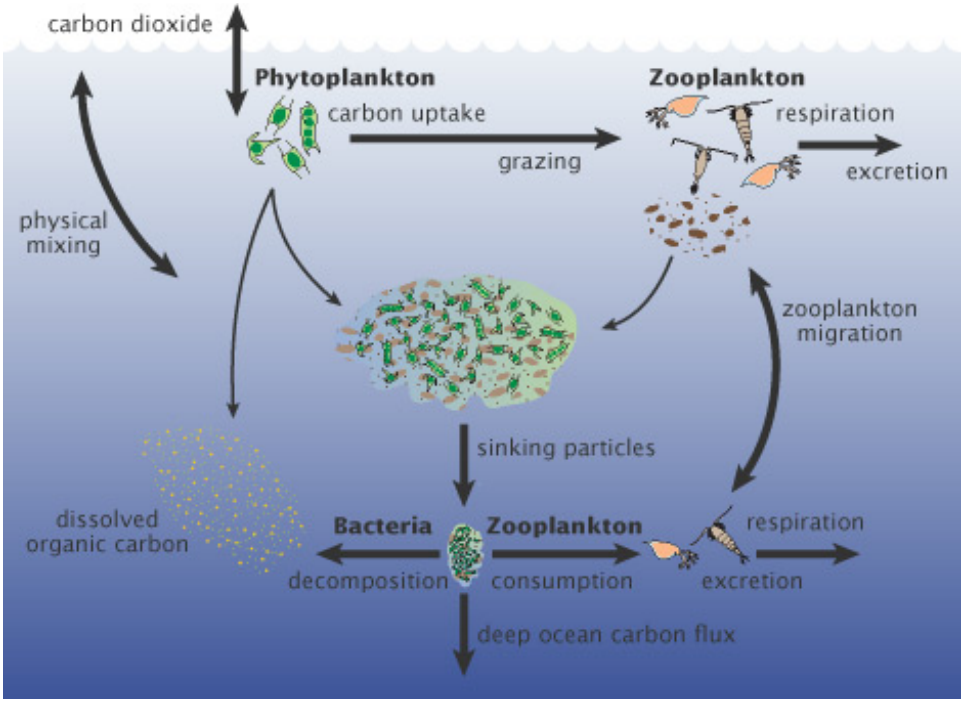

Figure 1.1: **The role of phytoplankton.** Phytoplankton are part of the ocean carbon cycle, fixing CO_2 in the euphotic layer by photosynthesis. Then, the carbon compounds generated can be directly remineralised in the upper ocean, they can sink to deeper ocean layers as dead organic matter (soft-tissue pump), or they can be sequestered in the shells of species with inorganic carbonate structures (hard-tissue pump).

The remaining part of the produced organic matter is involved in the *biological pump* and can either sink to deeper ocean layers as dead organic matter (*soft-tissue pump*, responsible for 70% of the vertical DIC[2] gradient) or be sequestered in the shells of species with inorganic carbonate structures (*hard-tissue pump*, responsible for 20% of the surface-to-deep DIC gradient[3]) [9], [2]. This process of carbon sequestration is crucial for regulating atmospheric CO_2 levels by storing carbon in the ocean's depths for extended periods. Eventually, when these materials are remineralized and dissolved, carbon is released back into the water, primarily as DIC.
Multiple processes can be responsible for the transport of carbon into the deep ocean as part of the biological carbon pump. A major role is played by sinking particles, but also diel vertical migration and the physical pump (subduction and vertical mixing of particles) can have an impact on carbon export and sequestration, as highlighted by Stukel et al. 2023 [10], who provided a description of these processes in a coastal upwelling biome (the California Current Ecosystem).
Important in the biological pump and upper layers nutrient supply is the general ocean circulation, which acts through vertical and horizontal processes, determining distinct

[2]Dissolved Inorganic Carbon.

[3]The remaining 10% of the surface-to-deep DIC gradient is achieved through the solubility pump, which encompasses all physical and chemical processes involved in gas exchange at the air-sea interface, as well as the carbon sequestration and burial driven by the enhanced solubility of deep, cold bottom waters.

biogeochemical provinces, which are large-scale ecosystems characterized by coherent physical forcing and environmental conditions, for instance, in the case of this study, the Eastern Boundary Upwelling Systems.

1.1.2 Marine food web

In addition to the role played in the global carbon cycle, phytoplankton are essential to the oceanic food web because they constitute the first trophic level, serving as the primary source of nutrition for the marine food web by autotrophically producing biomass through photosynthesis.
The primary consumers of the food chain are zooplankton, the heterotrophic constituents of the plankton community, which are mostly filter feeders and graze on the organic matter suspended in the water.

These herbivorous zooplankton are then consumed by larger zooplankton or forage fish (like sardine and anchovy), which in turn are eaten by predatory fish, marine mammals, and seabirds.

It is worth noting that some ecosystems, rather than on photosynthesis, rely on chemosynthesis, which uses the oxidation of inorganic compounds (like hydrogen gas, hydrogen sulfide, or ferrous ions) as source of energy, converting carbon-containing molecules and nutrients into organic matter. This process occurs in environments where sunlight does not penetrate, such as deep-sea hydrothermal vents or cold seeps [11]. However, despite the existence of chemosynthesis-based ecosystems, photosynthesis-based ones are the most widespread in supporting marine life.

Evaluating the impact of climate change on the marine trophic chain involves understanding the relative role of *bottom-up control*, that occurs through nutrient concentrations, food abundance, vertical stability, light availability, day length, and temperature, and *top-down control*, that acts through grazing, predation and fishery [12].

1.1.3 Key Drivers of Phytoplankton Variability

To understand phytoplankton dynamics, the drivers of their growth rate variability must be identified [13].
One first factor is **temperature**, that influences the growth rates of organisms [14], [15]. Modifying the metabolic rates, warmer temperatures lead to faster growth rates until the optimal temperature, at which metabolic processes become most efficient [16]. After this threshold, the thermal tolerance of the species is exceeded and higher temperatures become harmful.
Light availability is also important, since phytoplankton rely on photosynthesis and can only proliferate in the euphotic zone, where photons can penetrate and be captured by the pigments (mostly chlorophyll) [17].
Finally, as shown by Behrenfeld et al. 2006 [18], vital for phytoplankton are the **nutri-**

ents, in particular nitrogen, phosphorus, iron, and silicon, which constitute the building blocks needed to carry out photosynthesis, build cellular structures, and produce energy. Their availability can be often influenced by seasonal changes, determining the depth of the mixed-layer, and by regional factors and oceanic processes, such as subsurface currents or upwelling phenomena, that bring nutrient-rich waters from the depths to the surface.
Moreover, nutrient availability can be affected by river runoff, which carries materials from land into coastal waters, and anthropogenic activities, such as pollution, atmospheric deposition and agricultural or industrial discharge.

Because of the many factors having influence over phytoplankton, these organisms are characterized by a wide range of variability across different time scales, ranging from day-to-day variations (mainly associated with weather conditions or river runoff, which can alter the salinity and temperature of the ocean's upper layers [19], [20]), to seasonal variability (triggered by changes in vertical mixing), interannual variability (for example, associated with phenomena like El Niño [18], [21]), and, ultimately, to long-term trends like decadal oscillations or climate change.

Focusing on seasonality, phytoplankton dynamics are characterized by **blooms**, which are rapid and strong increases in the abundance of these organisms in specific areas. The timings of the blooms varies depending on the region and species involved, and these phenomena can differ in magnitude, duration, and spatial extent. Various hypotheses have been proposed to describe blooms, identifying both bottom-up and top-down control factors. At high latitudes, like in the North Atlantic, where nutrients are typically available year-round due to the deep mixed layer, blooms mainly occur in spring. One theory explaining this phenomenon, the Sverdrup's critical depth hypothesis (Sverdrup, 1953 [22]), suggests that during this season, the mixed layer shoals and temperatures rise, so the net growth rate of phytoplankton increases and surpasses the mortality rate, leading to a bloom.
At lower latitudes, in tropical and subtropical regions that are nutrients-limited, blooms are associated with the entrainment of nutrients from the deep ocean, driven by the deepening of the mixed layer, which starts in fall, when winds become stronger [23].
Very peculiar are blooms in the Indian Ocean, strongly connected to monsoonal circulation, which play a role in the transport of nutrients. This region experiences two blooms: a stronger one during the summer monsoon and a weaker one during the winter monsoon [24].
In coastal upwelling systems, instead, phytoplankton blooms are associated with the supply of nutrients to the surface by upwelling. This process is enhanced in summer due to stronger upwelling-favorable winds, leading to the most intense blooms typically occurring during the warmest season.

1.2 Eastern Boundary Upwelling Systems

The Eastern Boundary Upwelling Systems of California, Canary, Humboldt, and Benguela are ecosystems situated along the eastern portions of ocean basins and are associated with wind-driven coastal upwelling, which brings nutrient-rich deep waters to the surface. In this section the EBUS are described: the geographic features and the dominant physical mechanisms characterizing them are detailed. The ecological and socioeconomic importance of these regions is also highlighted.

1.2.1 EBUS features

In this study, to identify the EBUS, the predefined masks obtained from the ISIMIP[4] Repository [25] are used. These masks are presented in Figure 1.2.

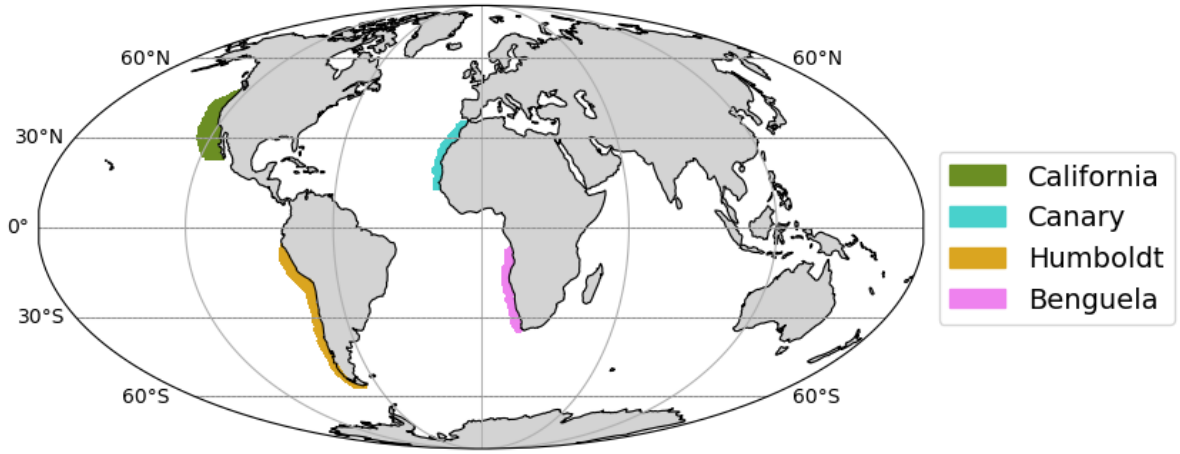

Figure 1.2: **The Eastern Boundary Upwelling Systems.** Global map depicting the masks (as defined in the ISIMIP Repository) used to identify the four Easter Boundary Upwelling Systems: California, Canary, Humboldt, and Benguela.

In this study, when defining the latitudinal and longitudinal domains of the EBUS, the circulation features of the regions are taken into account. The systems are characterized by the presence of surface eastern boundary currents, flowing towards the equator. Here's a brief overview of the considered regions:

- The **California System** stretches from 22°N to 47°N of latitude, with a longitudinal extent of about 9°. The associated California Current flows from southern British Columbia, Canada, up to Baja California, Mexico, and connects the North Pacific Current with the North Equatorial and Kuroshio Currents, forming the North Pacific Gyre.
- The **Canary System** extends from 10°N to 36°N of latitude, spanning about 4° of longitude; its associated oceanic current is part of the North Atlantic Subtropical Gyre and goes from northern Morocco southwestward to the North Atlantic

[4]ISIMIP (Inter-Sectoral Impact Model Intercomparison Project) is an international network of research collaboration on climate-change impacts across different sectors.

Equatorial Current. The related Canary Current, connected to the North Atlantic Gyre, extends southward from the North Atlantic Current and flows southwest until reaching Senegal, where it turns west, merging with the Atlantic North Equatorial Current.

- The **Humboldt System** is the largest of the four EBUS, stretching from 5°S to 55°S of latitude, with a longitudinal width of about 5°. The associated equatorward Humboldt Current is part of the South Pacific Gyre, running along Chile up to the North of Peru, connecting the northern part of the Antarctic Circumpolar Current with the Pacific South Equatorial Current.

- The **Benguela System** extends from 1°S to 36°S of latitude and for about 4° of longitude. The Benguela Current is a northward current, flowing along the southwest coast of Africa. It originates from the cold and eastward South Atlantic Current, and forms the eastern part of the South Atlantic Ocean gyre.

Moreover, undercurrents flowing poleward along the continental slope or outer shelf characterize each system.

Ocean dynamics of the globe and in coastal upwelling regions come from the combination of small and large scale atmospheric and oceanic forcing with a high temporal and spatial variability, and are strongly influenced by the specific geographic features (especially at the shorter time scales), as highlighted by Mackas et al. 2006 [26].
In the EBUS, dynamical processes can occur at different time scales. At the *diurnal timescale* the associated variability is dominated by tides and by the cycle of solar radiation, with effects on the upper ocean stratification, on primary production, and on the vertical migration of marine life. Processes occurring at the *intraseasonal timescale* are mainly characterised by coastal trapped waves (CTWs) and local instabilities in alongshore currents, leading to meanders, filaments, and eddies, while at the *annual timescale*, the dominant source of variability are the intensity and variability of alongshore wind stress and the associated wind-driven upwelling alterations, with broad-scale consequences on the seasonality of phytoplankton productivity and biomass. At the *interannual* and *decadal timescales* mechanisms occur over vast spatial extents, spanning thousands of kilometers up to the size of entire ocean basins, and include teleconnections and decadal oscillations. Finally at *centennial* and *millennial timescales* processes involve the global climate system, including surface wind-driven circulations, such as subtropical and subpolar gyres, the global overturning circulation, and the impacts of climate change.

In particular, the interannual teleconnections such as the El Niño-Southern Oscillation (ENSO), the Pacific Decadal Oscillation (PDO), the North Pacific Gyre Oscillation (NPGO), the North Atlantic Oscillation (NAO), and the Atlantic Multidecadal Oscillation (AMO), are known to have significant impacts on marine ecosystems, and may also overcome the human influence at global or regional scales [27], [28].
Jacox et al. 2015 [29] found links between variations in the upwelling intensity in the

Pacific EBUS and large-scale ocean-atmosphere processes: ENSO is the leading mode of variability of the Humboldt and California Systems, while the PDO and the NPGO are strongly linked to California Current System variability. Chenillat et al. 2012 [30] reported that fluctuations in the NPGO modulate the timing of the seasonal upwelling onset in the central California Current System. On the other hand, in the Atlantic, some studies highlighted the influence of the NAO and the AMO on upwelling magnitudes and interannual to decadal variability in the Canary Current System [31], while the Benguela EBUS appears to be more influenced by regional and smaller-scale processes.

Overall, the physical features in these coastal areas depend both on local and on remote locations, with a key role played by mechanisms, such as upwelling, mixing, and advection, able to transport water both horizontally and vertically.
Among these processes, in the EBUS the most biologically important is **upwelling**.
The upwelling intensity (the total volume of upwelled water) can be influenced by different mechanisms, including *Ekman transport*, driven by the wind, and *cross-shore geostrophic transport*. Although the latter process has not received significant attention, it has been identified as a potentially important contributor to the upwelling intensity and variations [32].
Regarding wind-driven upwelling, two main contributions can be distinguished: *offshore Ekman transport*, due to prevailing alongshore wind stress, and *Ekman pumping*, that is due to cyclonic wind stress curl, is associated with decreases in wind stress and may extend farther offshore.
Bravo et al. 2016 [33] highlighted that the relative contribution of each wind-driven mechanism to vertical transport along the coast depends on orography and coastline topography. They found a meridional alternation between these processes, where one mechanism is intense when the other is weak. Their study concluded that the largest portion of vertical transport was induced by coastal divergence rather than Ekman suction. Moreover, most literature on the topic typically examines the alongshore wind stress when investigating the upwelling strength [34], [35].

Therefore, this study mainly focuses on the upwelling associated with alongshore winds, whose physical mechanism is illustrated in Figure 1.3, adapted from Talley 2011 [36]. Each boundary system is characterized by prevailing equatorward winds blowing parallel to the shore. These winds result from the cross-shore atmospheric pressure gradient between the dominant high-pressure systems over subtropical ocean basins and the low-pressure systems over the adjacent land masses. This gradient intensifies during summer due to land warming, causing equatorward wind stress to fluctuate seasonally and to exhibit cross-shore variations in magnitude. Thus, alongshore winds induce coastal divergence and subsequent offshore Ekman transport, which triggers coastal upwelling of deeper waters.

Dealing with the biogeochemical aspects of the EBUS, similar oxygen and nutrient concentrations are shared across the four regions. These areas naturally experience hypoxia,

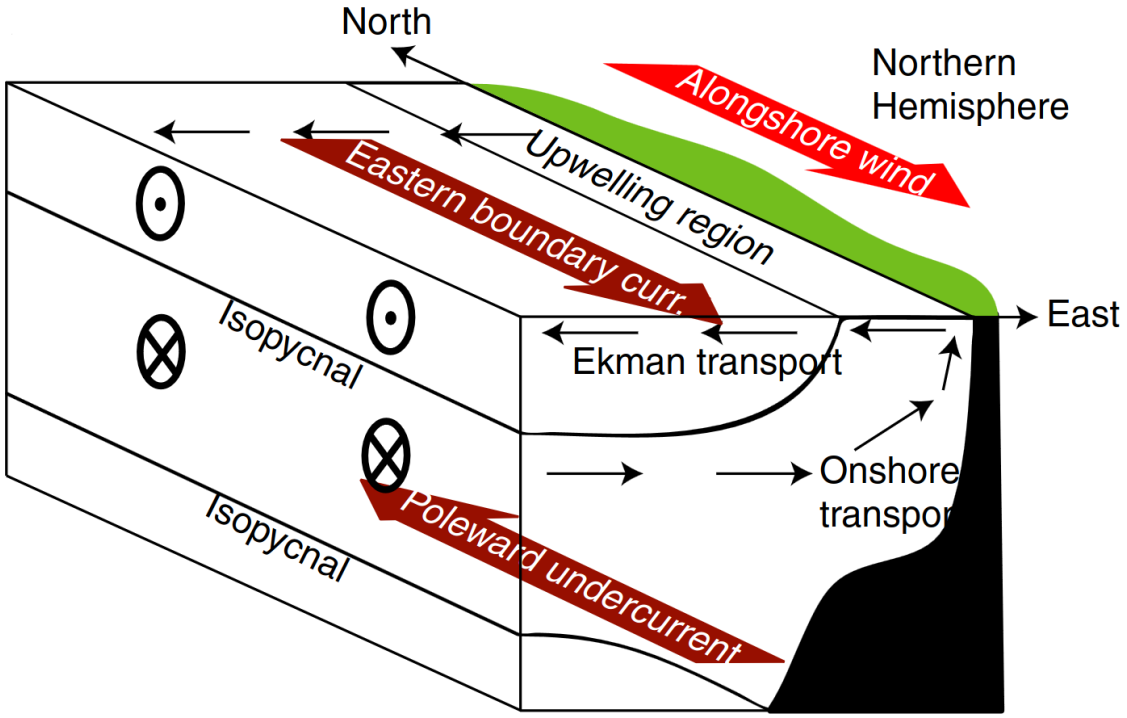

Figure 1.3: **Coastal upwelling system** associated with an alongshore wind with offshore Ekman transport (Northern Hemisphere). Figure adapted from Talley 2011 [36].

being characterized by persistent oxygen minimum zones (OMZs) with extremely low oxygen concentrations (less than 20-45 μmol kg^{-1}). This condition results from the high biological activity within these ecosystems, where respiration by living organisms depletes the oxygen supplied by physical transport, air-sea fluxes, and photosynthesis [37].

Regarding nutrient profiles, particularly nitrates, high concentrations are generally found in layers below the thermocline, where light availability is limited [38]. Conversely, in the upper euphotic region, nutrient levels are significantly lower. This peculiar vertical structure of nutrients reveals the importance of upwelling in sustaining the availability of nutrients at surface for phytoplankton life.
Dugdale and Goering 1967 [39] explained that the nitrate supply in the surface layer has two contributions: the new production, supported by nutrients from outside the euphotic zone (that is the main production source in upwelling systems), and the regenerated production, sustained by recycled nutrients within the euphotic zone (which is the primary source in oligotrophic regions). An estimation of the new production supported by external nutrients was carried out by Messié et al. 2009 [40], who assumed that during an upwelling event, which occurs over a daily/weekly time scale, the water brought to the surface comes from a depth of 60 meters, and calculated nitrate supply as the product of nitrate concentration and vertical transport. They found that the Canary, Humboldt, and Benguela systems have similar levels of nitrate supply and potential new production, whereas the California system has about 60% of the others.

Different mechanisms can affect the biogeochemical features of the EBUS over different timescales. Remote processes, like variations in water-mass formation and ventilation at high latitudes, can affect the properties of EBUS by altering the characteristics (oxygen, nutrients, or inorganic carbon concentrations) of the upwelled water masses. Moreover, remineralization processes exhibit a wide range of timescales, depending on factors such as sediment matrix, redox conditions, temperature, biotic activity, and the location of the remineralization process, with decreasing remineralization rates for increasing distance from the continent [41].

These physical and biological attributes are shared across the four EBUS, even if each region has unique characteristics due to geographical shape, coastal topography, and latitudinal position and extent. These features can generate spatial variations even within the same system, giving rise to localized areas of intensified coastal upwelling and productivity.
Moreover, there are significant differences between systems in the Pacific and in the Atlantic oceans. At subtropical latitudes, the Pacific basin is broader, with generally narrower continental shelves (with the exception of the Southern California Bight) [26]. Its water masses, circulating within the thermohaline circulation, are older, with higher nutrient levels and lower oxygen concentrations. In contrast, the Atlantic Ocean is narrower, with broader continental shelves, and its deep water masses are younger. Furthermore, while the Pacific region experiences a strong impact from the El Niño–Southern Oscillation [42], the Atlantic is subject to more limited influence from oceanic and atmospheric teleconnections.

Considering all these factors, when evaluating the impacts of climate change on Eastern Boundary Upwelling Systems, certain commonalities exist among all regions. This suggests that systems may exhibit comparable responses, including warming of surface waters, increased stratification, and a decline in subsurface oxygen levels. However, regional peculiarities should not be overlooked, as these may play significant roles in determining the primary productivity of each region.

1.2.2 Ecological and socioeconomic importance

The Eastern Boundary Upwelling Systems are recognized as "hotspots" of both productivity and biodiversity since, despite comprising less than 2% of the ocean's area, they contribute significantly to global marine primary production, nearly 7%. Given the high marine productivity, the EBUS support a diversity of mid-trophic-level species, giving rise to habitats for a wide range of species, sustaining a large biodiversity of fishes, seabirds, and marine mammals.

Moreover, these regions contribute to over 20% of the world's marine capture fisheries, [43]. The fish catches in these coastal areas are mostly sardines, anchovies, and mackerel, with variations across the different systems [44]. Over the last century catches fluctuated considerably, due to natural interannual or decadal variability and to direct

human impact through overexploitation of the resources. In the California EBUS, fish catches remained relatively stable at approximately 0.6 million tonnes per year (making it the lowest catch among the EBUS), in the Canary region they have stabilized around 2 million tonnes per year since the 1970s, in the Humboldt system they currently exceed 5 million tonnes per year (driven mostly by the anchoveta fishery), while in the Benguela region, they peaked in the late 1970s at 2.8 million tonnes per year, but have since then declined to around 1 million tonnes per year (data from [45]).

The combined effects of climate change and extensive overexploitation of the fisheries sector could severely impact the EBUS. Hence, these ecosystems and their associated resources should be protected and well managed, to assure their health and resilience, preventing extinctions, preserving biodiversity, and maintaining the services on which many communities depend.

1.3 Past and state-of-the-art research

Extensive studies were made to evaluate possible responses to climate change of the Eastern Boundary Upwelling Systems. The four regions were found to be highly sensitive to climate change [35], [44], and this section offers an overview on the current knowledge on its impacts there, with a particular focus on primary production and on mitigation scenarios.

1.3.1 Climate change in the EBUS

Since the pre-industrial period, **anthropogenic climate change** has been superimposed on natural variability of ecosystems, significantly affecting global oceans (as shown by Kwiatkowski et al. 2020 [3]) and the EBUS (as highlighted by Bograd et al. 2023 [4]). The rising CO_2 concentrations and atmospheric temperatures are driving *ocean warming*. Investigations of temperature trends in coastal areas found that the warming rate of nearshore areas in the EBUS is about half that of coastal regions outside the systems, with this difference being stronger in the Pacific [46]. In 92% of upwelling regions, the temperature increase is more intense offshore than nearshore, indicating that coastal upwelling might mitigate the effects of large-scale global warming [47].

At a global level, the scientific community identified as a major consequence of ocean warming the increased *stratification*. Upper ocean stratification, defined as the density difference between surface and 200 meters depth, indicates the degree of interaction and nutrient exchange between surface and deeper waters, with the mixed layer depth controlling light availability and nutrient supply at shallow levels, since the density gradient at its base influences processes like entrainment and particle sinking/export from the euphotic zone.
The alteration of water-column stability has significant impacts on ocean dynamics globally [48]. Changes in the mixed-layer depth, that is projected to shoal worldwide and

also in the EBUS (though with a large model spread), and variations in the depth from which upwelling waters are drawn, can alter the nutrient supply. Because of this process, most state-of-the-art Earth System Models have suggested decreases in net primary productivity at global levels, however projections show large regional variations, often differing considerably from the latitudinal tendencies. In particular, in coastal upwelling regions, other factors may drive contrasting trends with respect to the global increased stratification, as will be investigated in the next section.

Another evident human-induced change in the oceans is the *deoxygenation* of waters. Many studies have shown that oxygen concentrations are globally decreasing, due to reduced solubility of oxygen in water, increased rates of oxygen consumption via respiration, and smaller rate of oxygen resupply from the atmosphere to the ocean interior (due to enhanced stratification and reduced ventilation) [49], [37].
These decreased O_2 levels may have extensive consequences, given the vital role of oxygen in marine ecosystems and in many biogeochemical cycles. In coastal regions, other biophysical interactions may regulate oxygen concentrations, and the reduction is aggravated by increased nutrient loading (from anthropogenic activities) and organic matter, which leads to a higher frequency of hypoxic events and to increased coastal ocean dead zones.

Another significant consequence of the increased emissions is the *acidification* of oceans. Waters uptake atmospheric carbon, so the seawater levels of CO_2, H^+ and HCO_3^- increase, while CO_3^{2-} concentrations decrease. Since the industrial revolution, the decline of global surface waters pH was about 0.1 pH units [50], and the decline is projected to worsen for high-emission scenarios [51]. These acidified conditions largely influence seawater chemistry and the timing of response is very long [52]. Indeed, in the carbon cycle, atmospheric carbon is absorbed by the ocean's surface layers within approximately 100 years, while full equilibration with the deep ocean takes around 1,000 years. For example, the study by Cao et al. 2014 [53] proved that, while surface ocean chemistry variations closely follow atmospheric CO_2 changes, the deep ocean shows a significant lag due to the long timescales required for excess carbon dioxide to penetrate these depths. This means that the carbon dioxide emitted today will continue to be absorbed by the ocean for a very long time, even if emissions start to decrease, continually lowering the pH and having large implications on marine ecosystems, especially on calcifying organisms like corals, molluscs or foraminifera [54].
Particularly in the EBUS, the pH trends may differ from the global one, due to dynamical or biological interactions and upwelling intensity changes. For instance, in the Pacific EBUS, modeling studies project decreases in pH [55], [56], while in the Canary EBUS it was found an increasing trend [57].

All these changes are affecting the whole ecosystem functioning, with alterations of the community structure: the rising temperatures are leading to a migration of many species poleward or at deeper levels [58], while spots of intensified upwelling, mitigating locally

the warming, may represent a climate refugia for some species [59]; moreover, acidification and decreased levels of O_2 may degrade the ecosystem, restricting the viable zone and potentially creating a lethal environment. This may result in a reorganization of trophic interactions, possibly leading to fluctuations in fish catch.

In addition to the climate-related variations, marine ecosystems are also directly exposed to human stress through fishing [60], that, combined with climate change, can have cascading effects throughout the whole ecosystems.

1.3.2 Mechanisms of change of marine productivity

Dealing with the climate change impacts on marine productivity, several hypotheses have been made to describe its future evolution, but there is still limited consensus on which are the major drivers in each location of the EBUS and a quantitative assessment of the contribution of each forcing is still to be made.
One first branch of study underlines the role of stratification: as introduced in the previous section, the enhanced stratification due to global warming would reduce the vertical mixing and the nutrient supply from deeper waters, limiting productivity at shallower levels [61], [62].
However, the most corroborated theories suggest a dominant role of winds in the EBUS. In particular, one prominent theory was proposed in 1990 by **Bakun** [63], who focused on the mechanism of wind-induced upwelling intensification associated with the rising temperatures. He suggested that global warming will cause a greater increase of surface temperature over continents relative to adjacent ocean areas, accentuating the land-sea temperature gradient. As a result, he projected an intensification of continental low-pressure systems, particularly during the summer season, which would also increase the land-sea sea level pressure gradient. This, in turn, would enhance alongshore wind stress on the ocean surface, consequently accelerating coastal upwelling. The consequence, would be an increase in marine productivity in the EBUS region, thanks to the greater availability of nutrients at surface.

In more recent literature, different latitudinal changes in NPP were identified along the EBUS regions, and large focus was put on the consequences of the Hadley cell response to global warming.
The Hadley cell is a direct large-scale atmospheric circulation, thermally driven by the temperature gradient between the tropics and the subtropics. It transports heat from the equator towards higher latitudes, with warm air rising near the equator (tropical low-pressure regions), flowing poleward close to the tropopause, cooling and descending in the subtropics at around 25° latitude (subtropical high-pressure regions), and then returning equatorward close to the surface.

A consistent weakening and poleward expansion of this circulation is projected, with a significant shift in global atmospheric patterns [64], [65]. Specifically, the major high-pressure regions will move towards higher latitudes, leading to an expansion of

the subtropical dry zones, pushing them further towards the poles. The movement of high-pressure regions will have profound impacts on weather patterns, precipitation distribution, and overall climate dynamics across the globe.

Studies, such as those by **Rykaczewski** et al. 2015 [34] and by **Bograd** et al. 2023 [4], highlighted that this expected expansion could result in strengthening of upwelling-favorable winds during summertime in the poleward portions of the EBUS, while weakening near the equatorward boundaries. This would result in increased marine productivity in the poleward portions of the regions, thanks to the greater availability of nutrients provided by the stronger upwelling.

A less explored area of research emphasizes the impact of source water concentrations and suggests that nutrient enrichment in the upwelled waters could drive increased productivity [66].

1.3.3 Mitigation scenarios

Recognizing the urgency of the climate crisis, in December 2015 in Paris, 196 Parties at the United Nations Climate Change Conference (COP21) adopted the Paris Agreement, an international treaty on climate change [67]. It set the target of limiting the increase of the global average temperature to well below 2°C above pre-industrial levels, while also pursuing efforts to limit the temperature increase to 1.5°C above pre-industrial levels.

To reach these targets, mitigation efforts have been implemented and countries are expected to undertake increasingly ambitious climate actions through plans like the Nationally Determined Contributions (NDCs), commitments to reduce greenhouse gas emissions by undergoing economic and social transformations, including strategies like carbon capture and storage [68], [69], energy efficiency measures, and advancements in decarbonization technologies [70], [71]. An overview of science and policy features of this goal and of the implications for mitigation pathways is provided by Schleussner et al. 2016 [72].
More than 140 countries, (including China, the United States, India and the European Union, which are the major polluters) committed to achieving net-zero emissions, accounting for about 88% of global emissions. However, the result of current political choices and climate actions by 2030 is expected to be the increase in global greenhouse gas emissions of almost 9% relative to 2010 levels [73].
Therefore, the current efforts to reach the fixed targets are insufficient: to limit global warming below 1.5°C, emissions must be reduced by 45% by 2030 and reach net zero by 2050 [74], [75]. This requires all governments to take immediate actions to cut emissions, thus the possibility of temperature overshoot should receive greater attention from the scientific community.

Because achieving the temperature goals necessitates dramatic reductions in greenhouse gas emissions, it is of central importance to gain a comprehensive understanding of the

implications on climate resulting from mitigation strategies.
In past research, many idealized mitigation pathways have been explored. As explained by Rogelj et al. 2018 [76], the features of mitigation pathways can be different, since they can be characterized by their associated radiative forcing (RF) [77], [78], by the atmospheric concentrations [79], [80] or by the associated temperature outcomes [81], [82].
These scenarios include instantaneous stabilization of radiative forcing or cessation of emissions [83], artificial restoration of carbon dioxide to preindustrial levels [84], or overshoot scenarios, where atmospheric CO_2 concentrations peak before being reduced to lower levels.

When evaluating the future developments of the different quantities under such scenarios, it is important to assess both the magnitude and the permanence of anthropogenic climate impacts. Boucher et al. 2012 [85] highlighted the importance of assessing if changes are reversible, so whether and to what extent they can be reversed if the factors causing their changes are mitigated or reversed. Moreover, an issue is also determining if this **reversibility** can be accomplished in a usefully short time frame for all climate system constituents.
The atmosphere adjusts rapidly to external forcings, while the entire Earth's climate system responds over much longer timescales, due to the inertia introduced by physical climate system components (ocean, cryosphere, land surface) and biogeochemical cycles (like the carbon cycle).
Focusing on the ocean, it is characterized by low frequency timescales due to its large heat capacity, slow circulation processes and mixing into deep ocean, and to the associated biogeochemical processes, particularly those involving deep-sea carbon dynamics. Therefore, the response to changes in atmospheric CO_2 concentrations can show a considerable lag after the onset of the forcing.
The IPCC in 2021 defined the *climate change commitment* as the 'unavoidable future climate change resulting from inertia in the geophysical and socio-economic systems' [86]. These inertial changes will regard temperature, but also the hydrological cycle, extreme weather events, and sea level. In particular, the *Zero CO_2 Emissions Commitment* is the amount of global mean temperature change that is still expected to occur after a complete cessation of anthropogenic carbon dioxide emissions [87], while the *warming commitment* is the process of continued warming of the global ocean, even under mitigation scenarios, due to its lagged response [88].

Therefore, even if greenhouse gas concentrations remain stable or even return to preindustrial levels, the climate may not return to its former state. This divergence from the original trajectory, despite CO_2 concentration adjustments, is known as *hysteresis*. The response of the system is not only influenced by its current environment, but also by its past conditions, and the backward path may deviate from the original trajectory, in the worst case leading to irreversibility, when the system cannot be restored to its initial state, or cannot do so within any meaningful time frame for human planning and

decision-making. One dramatic example of irreversible changes of the climate system are the *tipping points*, critical thresholds beyond which systems reorganize, often abruptly and/or irreversibly [89].
The EBUS regions are not directly involved in the recognized alarming tipping points, however, due to their high sensitivity to environmental variations and their ecological, economic and social value, there is large scientific and policy interest on how they may change under mitigation strategies, in particular in overshoot scenarios where the forcing pathways exceed a certain threshold, then peak and eventually decrease.

The current understanding of the impact of a temperature overshoot on various components of the climate system is limited, particularly when it comes to primary productivity, which is already challenging to model under unidirectional climate forcing.
Studies on reversibility mostly focus on acidification [53], weakening of the global ocean circulation [53], [90], sea-ice extension [90], [85], temperature or precipitation patterns [85], while only few studies were conducted on the primary productivity response. A study by John et al. 2015 [91] investigated global marine productivity after mitigation, using ramp-up and ramp-down scenarios. It highlighted that, after a global NPP increase due to global warming, the cooling of upper ocean layers (associated to the reduction of emissions) in a mitigation scenario should ideally bring back to past values of NPP (with a lag). However the study found a counterintuitive trend, with increased global mean NPP, overshooting to values above contemporary means, in an ocean slowly recovering from acidification.
In another study by Heinze et al. 2023 [90], the primary productivity response to the overshoot scenario was analyzed for the Arctic ocean, and no hysteresis was detected in NPP, which reversed its trend around 2065, approximately 25 years after emissions began to decline.

1.4 Thesis objectives

This work aims to analyse the anthropogenic impact on marine ecosystems in the Eastern Boundary Upwelling Systems. It provides a comprehensive evaluation of the physical and biogeochemical factors influencing primary production. The study examines the roles of temperature and nutrient limitations and analyses the drivers of changes in nutrient availability in the euphotic layer, particularly upwelling intensity and subsurface nutrient concentrations.

The thesis is structured as follows:

- In the *Methods* Chapter 2, the tools used in the investigation are presented, introducing the climate scenario approach and the CMIP6 framework, presenting the use of Shared Socioeconomic Pathways of Earth System Models (focusing especially on the IPSL-CM6A-LR model) for assessing the impacts of climate change. Moreover, the sources of uncertainties associated with this approach are described, and the main variables and types of analysis used during this study are presented.

- In the *Results and discussion* Chapter 3, the main findings of the research are presented, first at a global level, to provide a large-scale overview of climate change impacts, and then focusing of the Eastern Boundary Upwelling Systems. Net primary productivity ensemble projections are presented, and the subsequent analysis aims at explaining the reasons of the observed patterns. Particularly, IPSL-CM6A-LR is used to investigate the mechanisms that drive the variability of primary production. At first, a correlative analysis is carried out, evaluating the roles of source water nutrient concentrations and of upwelling-favorable winds in driving NPP variability. Then, a more quantitative analysis of growth rates evaluates the impact of the various limiting factors in the different EBUS. Finally, once an understanding of the response of marine productivity under the traditional scenarios SSP5-8.5 and SSP2-4.5 is obtained, the knowledge is used to evaluate, in specific portions of the EBUS, the overshoot pathway SSP5-3.4-OS, in order to assess the reversibility of changes.

- In the *Open questions and future work* Chapter 4 the main drawbacks of the study are explained, presenting potential solutions and future improvements of the study.

Chapter 2

Methods

This chapter introduces the methods used for the analysis. To gain insight into the dynamic and biogeochemical processes essential for projecting future ocean productivity, it was employed a scenario projection approach using outputs from the Coupled Model Intercomparison Project Phase 6 (CMIP6), with a focus on the IPSL model.
The methodology mirrors that of Kwiatkowski et al. 2020 [3], who investigated the impacts of anthropogenic climate change using Shared Socioeconomic Pathways from Earth System Models in CMIP6. That study projected significant changes in key climatic variables affecting marine ecosystems over the twenty-first century, including ocean warming, acidification, deoxygenation, reductions in near-surface nutrients, and alterations in primary production, highlighting that the extent of future emissions largely determines the projected exposure of marine ecosystems to these drivers of ocean change.

In this thesis, a similar approach was adopted, focusing specifically on the Eastern Boundary Upwelling Systems, to assess the regional impacts of climate change on phytoplankton dynamics and the associated factors that may influence or be influenced by it.
The following chapter will provide a detailed account of the methods used, outlining the CMIP6 framework, describing the key features of the IPSL model, and introducing the main variables and computational approaches of the study.

2.1 CMIP6 and ScenarioMIP

To evaluate future changes in marine productivity in the regions of interest, outputs from climate models within the framework of the **Coupled Model Intercomparison Project Phase 6** (CMIP6) were utilised.
CMIP6 is the sixth phase of the Coupled Model Intercomparison Project, which began in 1995 under the guidance of the World Climate Research Programme (WCRP). It serves as a collaborative platform aimed at facilitating integrated research across the climate science, leading to a better understanding of climate change dynamics by comparing independent model activities and coordinating them with a common infrastructure for gathering, organizing, and distributing output from standardized experiments. Additionally, CMIP takes into account model dependence and includes the assessment of model

performances and quantification of the causes of projection uncertainties.

Inside the integrated design of the CMIP6, the focus in this thesis centers on the **ScenarioMIP** component, which offers a suite of multi-model climate projections based on diverse scenarios of future emissions and land use changes, as presented by O'Neill et al. 2016 in [92]. These projections directly inform societal concerns regarding climate change vulnerability and impacts, and they provide a valuable foundation for addressing targeted scientific issues, thereby guiding mitigation and adaptation strategies.

To provide insights into the potential impacts of future climate change on human societies and ecosystems, climate researchers initially utilized *Representative Concentration Pathways* (RCPs). RCPs provide a set of greenhouse gas concentration trajectories and associated emissions scenarios, serving as inputs for climate models, and are classified based on their radiative forcing level in the year 2100 relative to pre-industrial levels, see Meinshausen et al. 2011 [93].
However, present research rather utilises *Shared Socioeconomic Pathways* (SSPs), which are alternative societal development pathways that provide additional context for climate model projections, encompassing factors such as population and urbanisation growth, technological advancements, economic policies, and environmental strategies.
State-of-the-art climate models prefer the SSPs because of this richer and more detailed overview of both climatic and socioeconomic dimensions; however, the RCPs and the SSPs have analogies which make past studies and more recent ones still comparable.
The SSPs introduced in 2021 for the IPCC Sixth Assessment Report outline five distinct narratives for future global development:

- **Sustainability**: This pathway prioritizes environmental conservation and sustainable development, aiming for reduced resource and energy intensity alongside decreased inequality. It emphasizes advancements in education, healthcare, and overall human well-being.
- **Middle of the Road**: Global trends largely follow historical trajectories, resulting in uneven progress in development, persistent environmental degradation, albeit with a decline in resource and energy use. Moderate population growth and ongoing inequality characterize this pathway.
- **Regional Rivalry**: This scenario is marked by increasing nationalism and a shift in policy focus towards regional concerns, diverging from broader developmental goals. Environmental degradation worsens, regional disparities increase, and population growth varies significantly by region.
- **Inequality**: Highly unequal investments exacerbate economic disparities, leading to widening inequalities in economic opportunity. Economic growth takes precedence over environmental considerations, which are addressed only at a local level.
- **Fossil-fueled Development**: This pathway features high economic growth, rapid technological advancements, and heavy reliance on competitive markets and inno-

vation, as well as continued exploitation of fossil fuel resources. While population growth is expected to peak and decline in the 21st century, significant environmental degradation persists, with environmental issues managed primarily at local levels.

As described by Riahi et al. 2017 [94], using the Shared Socioeconomic Pathways as a foundation, researchers constructed Integrated Assessment Models (IAMs) scenarios. These scenarios provide numerical representations of future pathways, integrating insights from diverse fields to explore the intricate interplay between human actions, societal factors, and the environment. IAM scenarios convert the descriptive narratives of SSPs into quantitative projections of key variables like greenhouse gas emissions, atmospheric concentrations, energy infrastructure, land usage patterns, and other pertinent factors. IAMs were utilized to analyze and quantify the various trajectories outlined by the SSPs, with select "marker" scenarios incorporated into the ScenarioMIP framework.

The full set of multiple integrated scenarios are denoted as SSPx-y, where x is the specific SSP and y represents the forcing pathway, defined by its long-term global average radiative forcing level.
Figure 2.1 illustrates all the possible ScenarioMIP simulations by a SSP-RCP scenario matrix. Scenarios are arranged into two Tiers: Tier 1, with the SSP-based scenarios as continuations of the RCP2.6, RCP4.5, and RCP8.5 forcing levels, and an additional unmitigated forcing scenario (SSP3-7.0); Tier 2, including additional scenarios of interest (the SSP scenario associated with the RCP6.0, and two mitigation scenarios: SSP4-3.4 and a scenario lower than the RCP 2.6 forcing pathway) as well as additional ensemble members, like the SSP5-3.4-OS (the overshoot pathway), long-term extensions of scenarios (for SSP5-8.5, SSP1-2.6, and the overshoot scenario) and initial condition ensemble members of SSP3-7.0.

Specifically, this study will concentrate on the following scenarios: **SSP5-8.5**, which reaches a RF of 8.5 $\mathrm{W\,m^{-2}}$ by 2100 (very high greenhouse gases (GHG) emissions); **SSP2-4.5**, reaching a radiative forcing of 4.5 $\mathrm{W\,m^{-2}}$ by 2100 (intermediate GHG emissions); and **SSP5-3.4-OS**, representing the overshoot pathway in which a sharp decline in CO_2 concentrations and RF follows the period of steady increase from 1850 until the mid of 21st century. Initially, SSP5-3.4-OS pathway aligns with the high-emission SSP5-8.5 scenario. Then, starting in 2040, it diverges due to intensive mitigation strategies that lead to substantial reductions in CO_2 emissions. These emissions reach zero around 2070, eventually turning net negative, resulting, in a radiative forcing of 3.4 $\mathrm{W\,m^{-2}}$ by 2100.

A more recent study by Meinshausen et al. 2020 [95] presented the extended versions of these scenarios, including data simulations up to 2500, based on simplified assumptions. However, these long-term simulations were not considered in this analysis.

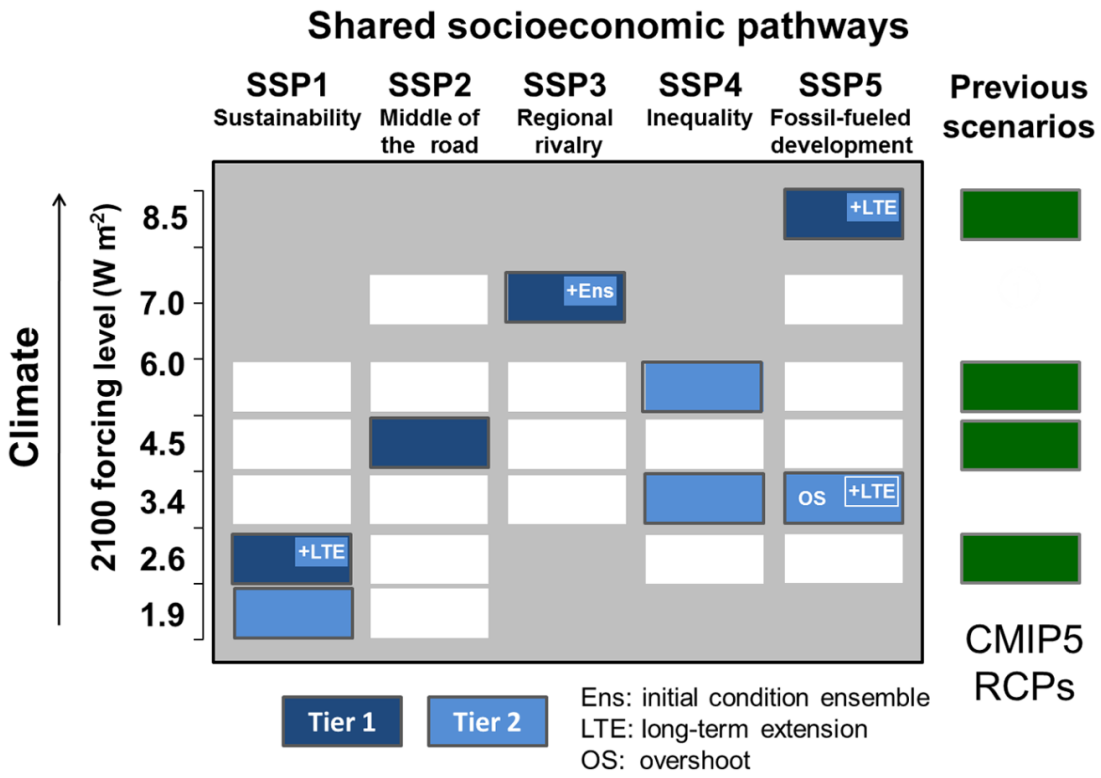

Figure 2.1: **Illustration of the ScenarioMIP simulations by the SSP-RCP scenario matrix provided by O'Neill et al. 2016** [92]. Each cell in the matrix represents a combination of the SSPs and the forcing pathway projected by the IAMs. Dark blue cells denote scenarios in Tier 1, light blue cells scenarios in Tier 2. White cells represent scenarios where climate information will be derived from the SSP scenario indicated in that row. For comparison, CMIP5 Representative Concentration Pathways (RCPs) are also shown in green.

2.2 The IPSL model

Inside the CMIP6 framework, this thesis analyzed in particular the latest version of the climate model of **Institut Pierre-Simon Laplace** (IPSL). IPSL is a university research institute bringing together nine multidisciplinary laboratories, situated primarily at the Pierre and Marie Curie campus of Sorbonne University in Paris (France) and at the campus of the University of Versailles-Saint-Quentin-en-Yvelines in Guyancourt (France).
The IPSL Earth System Model for Phase 6 of CMIP is **IPSL-CM6A-LR** (CM stand for Climate Model and LR Low Resolution). This latest version, presented by Boucher et al. [96] in 2020, marks a notable improvement over its predecessors, IPSL-CM5A-LR and IPSL-CM5A-MR.
Comprised of three components, the IPSL-CM6A-LR integrates the LMDZ atmospheric component (Laboratoire de Météorologie Dynamique Zoom, Version 6A-LR) [97], the ORCHIDEE land surface model (ORganizing Carbon and Hydrology in Dynamic EcosystEms, Version 2.0) for land surface, hydrology, and the land carbon cycle [98], and the NEMO oceanic model (Nucleus for European Models of the Ocean, Version 3.6).

NEMO represents the state-of-the-art in oceanographic research and forecasting. For this latest version of the IPSL model it is used in the configuration eORCA1 (so with a resolution of 1°, with the *e* denoting extended) and comprises three key units: NEMO-OPA for ocean physics, NEMO-LIM3 for sea ice dynamics and thermodynamics, and NEMO-PISCES for ocean biogeochemistry.

This thesis mostly utilises outputs from the biogeochemical component of IPSL-CM6A-LR, given by the coupling of NEMO with **PISCES-v2** (Pelagic Interactions Scheme for Carbon and Ecosystem Studies volume 2). PISCES-v2 was presented by Aumont et al. in 2015 [99] and is a model designed to simulate the carbon cycle, the main nutrient cycles, and the lower trophic levels of marine ecosystems, including phytoplankton, microzooplankton, and mesozooplankton.
It encompasses 24 prognostic variables (tracers), incorporating a description of carbonate chemistry, of two phytoplankton compartments (diatoms and nanophytoplankton) and two zooplankton size classes (microzooplankton and mesozooplankton).[1]

The nutrients simulated are five (nitrate, ammonium, iron, silicate, and phosphate), delivered to the ocean from five sources: atmospheric dust deposition, river inputs, sediment mobilization, sea ice, and hydrothermal vents. The model construction is based on the assumption that nutrient external availability directly limits phytoplankton growth. For all living classes, the model keeps constant the ratios between C, N and P, (P/C, N/C, and N/P) fixing them to the values introduced by Takahashi et al. 1985 [100] (the Redfield ratios C/N/P are set to 122/16/1). This choice is necessary to simplify the representation of complex biological and chemical processes, but it can limit the precision of the model outputs, as observations suggest that in real ocean these ratios actually vary. The internal contents in iron for the two phytoplankton classes and of silicon for diatoms are simulated as a function of the external concentrations in nutrients and of the light level. The ratio between chlorophyll and carbon is simulated with a modified version of the photoadaptation model by Geider et al. (1998) [101].
On the other hand, all the ratios of zooplankton are kept constant.

Here the main characteristics of the two Plankton Functional Types (PFTs) are recalled:

- **Diatoms** are single-celled algae with an external silica skeleton, their vital nutrients include nitrogen, phosphorus, iron, and silicon, and they tend to dominate the phytoplankton community when growth conditions are optimal, such as in high nutrient concentrations.
- **Nanophytoplankton** encompass all non-diatoms, including diazotrophs, calcareous phytoplankton, picophytoplankton, and others. These phytoplankton do not use silicates, relying instead on N, P, and Fe, they are smaller in size and have

[1] This representation includes a limited range of biodiversity and restricts the ability of the model to capture the actual rich diversity within ecosystems. Evaluating the impacts of climate change on a broader range of species would yield more accurate results, as different species may respond and evolve differently under changing environmental conditions.

a smaller half-saturation constants (e.g., for nitrates the minimum half-saturation constant is 0.13 for diatoms versus 0.39 for non-diatoms [99]), so they are favored in regions with reduced nutrient levels.

The most relevant differences between these two groups are that diatoms, differently from nanophytoplankton, need silicates, they require higher amounts of Fe (Sunda and Huntsman, 1995 [102]) and they have higher half-saturation constants because of their larger mean size.

Moreover, in the model there are three non-living compartments: semi labile dissolved organic matter (with timescales of weeks to years), small particles (with a sinking speed of 2 m/d) and big sinking particles (with a sinking speed from 50 to 200 m/d). Constant Redfield ratios are imposed for C/N/P, while for iron and silicon the ratios relative to organic carbon are allowed to vary.

The main variable considered in this thesis is **Net Primary Production** (NPP), defined as the difference between Gross Primary Productivity (GPP), standing for all the carbon that is fixed by the autotrophs organisms by photosynthesis, and respiration (R), since part of the photosynthesised organic matter is utilized for cellular respiration and to upkeep the existing tissues. The relative formula is NPP=GPP−R.
This study did not use observations and only focused on simulations of Earth System Models of the CMIP6 ensemble, due to the difficulties associated to the quantitative measurements of net primary productivity and the lack of adequate datasets of observations to detect climate change impacts, as it will be discussed later on in Chapter 4.2.

In the IPSL model component PISCES, the net formation rate of organic carbon by phytoplankton is represented as the product of phytoplankton biomass (P) and the growth rate (μ): NPP=P $\times \mu$.
The growth rate of a species i, μ^i, is in turn expressed as the product of the maximum growth rate, $\mu^i_{\max}$, the temperature limitation factor, $\mathrm{T}^{\mathrm{P}}_f$, and the nutrient and light limitation factors, $\mathrm{N_{lim}}$ and $\mathrm{L_{lim}}$, respectively. As described in [99] and [103], this relationship can be written as:

$$\mu^i = \mu_{max} \times T^P_f \times N^i_{lim} \times L^i_{lim}. \tag{2.1}$$

Nutrient and light limitation factors are dimensionless values ranging from 0 to 1, where higher values indicate less limitation and therefore higher growth. For instance, the nitrogen growth limitation refers to the ratio of the growth rate of a species in an environment with finite nitrogen availability to its theoretical growth rate in an environment with unlimited nitrogen.
For nutrients, the factor is determined by the minimum value among the nutrients (iron, phosphorous, nitrogen, and silicon), meaning the most limiting nutrient dictates the

overall nutrient limitation:

$$N_{\text{lim}}^{\text{diat}} = \min(N_{\text{Fe}}^{\text{diat}}, N_{\text{PO}_4}^{\text{diat}}, N_{\text{NO}_3+\text{NH}_4}^{\text{diat}}, N_{\text{Si}}^{\text{diat}})$$
$$N_{\text{lim}}^{\text{nano}} = \min(N_{\text{Fe}}^{\text{nano}}, N_{\text{PO}_4}^{\text{nano}}, N_{\text{NO}_3+\text{NH}_4}^{\text{nano}})$$

In particular, nitrogen limitation is associated with the availability of both nitrate and ammonium, specifically:

$$N_{\text{NO}_3+\text{NH}_4}^{\text{i}} = \frac{K_{\text{NH}_4}^i \times \text{NO}_3 + K_{\text{NO}_3}^i \times \text{NH}_4}{K_{\text{NH}_4}^i K_{\text{NO}_3}^i + K_{\text{NH}_4}^i \text{NO}_3 + K_{\text{NO}_3}^i \text{NH}_4}.$$

The temperature limitation in PISCES is, for all nanophytoplankton, diatoms and microzooplankton, an exponential function T_f^{P}:

$$T_f^P = e^{k_{\text{Eppley}} \times T},$$

with k_{Eppley}=0.063913°C^{-1} the temperature dependence factor.

2.3 Sources of uncertainty

Climate change is characterized by high uncertainty which, as highlighted by Hawkins and Sutton 2009 [104], can arise from three distinct sources: internal variability, model uncertainty, and scenario uncertainty. Here there is a brief description:

- **Internal Variability Uncertainty** is associated with the inherent variability of the climate system, the natural fluctuations arising even without radiative forcing. This kind of variability involves small scale processes, weather events or local phenomena, but also larger spatial and temporal scales ones, for instance inter-annual teleconnections like El Niño–Southern Oscillation, the Atlantic Multidecadal Oscillation, or the Pacific Decadal Oscillation, which can affect trends of different variables over the timescale of decades, or even longer-term variability changes in ocean circulation, solar variability, or natural ecosystem dynamics;

- **Model Uncertainty** arises from the limitations and approximations inherent in the models. In response to the same radiative forcing, different models may yield different results due to variations in the simulation of physical and biogeochemical processes. The causes of this uncertainty may lie in the mathematical implementation of the models or in the parameterization used;

- **Scenario Uncertainty** is associated with the unknown future pathways of anthropogenic factors that influence the climate system, such as greenhouse gas emissions, land-use changes, technological developments, and policy decisions, causing uncertainties in future radiative forcing. These uncertainties are represented by the Shared Socioeconomic Pathways in CMIP6.

For the future evolution of the climate system, all of these three uncertainty sources may contribute, potentially interacting in non-trivial ways. Therefore, as highlighted by Lehner et al. 2020 [105] it is fundamental to partition the uncertainty of the projections into the quantitative contributions from each source.

2.4 Variables

In the upcoming dissertation, the data used were mainly processed outputs from the IPSL-CM6A-LR model, which are available for download directly from the CMIP6 database accessible via ESGF (Earth System Grid Federation) [106]. To facilitate comparability across various models, the database underwent homogenization, resulting in regridded files on a 1° resolution grid (360×180 grid).

It is worth noting that multiple simulations were conducted for each model in the ensemble. However, for the purpose of model comparison, only the first member launched after the piControl experiment is considered. In CMIP6, this member is typically labeled as `r1i1p1f1` (sometimes as `r1i1p1f2` or `r1i2p1f1`), where `r1` denotes the realization index, `i1` the initialization index, `p1` the physics index, and `f1` the forcing index.

The main variable taken under investigation will be the vertically integrated net primary productivity (`intpp`, unit of measure $\mathrm{mol\,m^{-2}s^{-1}}$), that represents the rate at which primary producers in an ecosystem create net useful chemical energy.
In this analysis, to evaluate changes in phytoplankton in the ocean, net primary productivity is preferred over biomass, as it is more sensitive to environmental changes and provides a dynamic indicator of the metabolic activity and health of phytoplankton populations over time, directly linking to ecosystem functioning and energy flow within marine ecosystems. While biomass provides information on the static concentrations of a carbon stock, NPP represents an energy/carbon flux that is available to higher trophic levels, so it offers a more comprehensive understanding of the sustainability of marine food webs.

Important variables that can significantly influence the future evolution of net primary productivity are then examined. The primary variable considered is sea surface temperature (`tos`, temperature of the ocean surface), measured in degrees Celsius, indicating the temperature of the upper boundary of the liquid ocean, inclusive of temperatures beneath sea ice and floating ice shelves.
Moreover the study analyses concentrations of dissolved oxygen at a depth of 200 meters (`o2`), measured in units of $\mathrm{mol\,m^{-3}}$, and the ocean mixed layer thickness (measured in meters) defined by sigma T (`mlotst`), where sigma T represents the potential density referenced to the ocean surface. Dissolved nitrate concentration (`no3`, measured in $\mathrm{mol\,m^{-3}}$) will be analysed, both looking at the entire vertical profiles (for selected latitudes), and at specific depths, particularly at the ocean surface and at the depths of 100 and 200 meters. In this thesis, among all nutrients, the focus will be placed especially

on nitrogen, in alignment with most of the literature that gives large attention to this nutrient, as the dominant limiting macronutrient in the global ocean [4], [107].

In the following dissertation, the role of sea level pressure (`psl`) and surface wind stress (`tauu` for the zonal component (unit of measure Pa) and `tauv` for the meridional component (unit of measure Pa)) will be analyzed. In particular, the focus will be on the equatorward surface downward wind stress `tauv`, which serves as a proxy for the upwelling strength to assess the impact of atmospheric circulation variations on primary productivity.
The equatorward surface downward wind stress was chosen over vertical velocity of ocean current because the latter is highly variable, making it challenging to extract clear trends. Moreover, in the following analysis using vertical velocity as a proxy for upwelling would require the identification of the specific depth from which upwelling originates. This is problematic because this depth can vary, both due to short-term internal variability and long-term trends related to climate change. In contrast, equatorward surface downward wind stress provides a more reliable indication of upwelling intensity thanks to its strong relationship with upwelling, due to the physical mechanism of Ekman transport already described in this chapter.

Finally, when investigating the drivers of NPP changes, the mentioned limitation factors are used: T_f^P, N_{lim}, and L_{lim}, respectively for temperature, nutrients, and light limitation (all dimensionless values ranging from 0 to 1). Moreover, to evaluate the different behavior of diatoms and nanophytoplankton, the productions from the two plankton functional types are separated, respectively indicated as `intppdiat` and `intppmisc` (both measured in $\mathrm{mol\,m^{-2}s^{-1}}$). In the end, in the analysis of the overshoot scenario, the Global Mean Air Surface Temperature (GMST) is considered, obtained by averaging globally the near-surface (2m) air temperature `tas` (unit of measure degrees Celsius).

2.5 Analysis methods

In the following study, different types of analyses are conducted. At first, all the CMIP6 members are used, providing SSPs time series and spatial maps, allowing to compare the IPSL model with the other ones. Then, in order to investigate more deeply the mechanisms inducing net primary productivity changes, only IPSL-CM6A-LR is used, and different outputs form that model are studied.

The impact of climate change on many variables is examined by investigating anomalies of future changes, computed as the difference between the projected values of each model and the respective baseline values. Specifically, the historical baseline period is defined by the years 1985–2014, while projections are evaluated for the years 2015–2100 for the SSP5-8.5 and SSP2-4.5 pathways, and for the years 2015–2200 for the SSP5-3.4-OS pathway (where the first years of projection (2015-2039) are, by definition, the same of the SSP5-8.5, and the years 2040-2200 are obtained from the overshoot simulation).

Particular attention is given to **SSPs time series of anomalies** under the different scenarios. In the time series computation, spatial averages are calculated over selected latitudinal and longitudinal extents. In this study, the averages are computed over masked regions, which, in the case of the EBUS, have predefined extents (obtained from the ISIMIP repository). When averaging, a weighted mean is applied, in order to account for the size of each grid cell and ensure that each one contributes proportionally to the average based on its actual area on the Earth's surface.
To present the resulting outputs, smoothing is applied to remove noise due to short-term fluctuations, allowing longer-term trends to be highlighted. A 10-year moving average window is used for this purpose.
Presenting time series, ensemble projections are provided, depicting either the single model trajectories or the ensemble spread, represented by the 25th–75th and by the 10th–90th percentiles.

Moreover, **spatial anomalies** are examined, and time averaging is performed. For historical model outputs the data is averaged over the period 1985–2014, while for projections under SSP5-8.5 over the last 30 years of simulations (2071–2100).
For surface downward and equatorward wind stress, due to missing data for the entire model ensemble, only the IPSL model simulations are used, comparing historical values with the projected SSP5-8.5 anomaly in each region. Instead, for net primary productivity and nitrates at 200m depth, projected anomalies are computed by comparing IPSL-CM6A-LR outputs with the ensemble mean (obtained by averaging simulations from the available CMIP6 models). In the ensemble mean maps, areas where model agreement is high (with more than 80% of models agreeing on the direction of future changes) are stippled to highlight regions of statistical significance.
Additionally, **vertical profiles** of nitrates are provided from the SSP5-8.5 simulations of the IPSL model, obtained by averaging over time and selecting specific latitudes.

Moreover, a deeper focus on the poleward and equatorward portions of the Canary and Benguela EBUS is provided. The two masks are divided at the latitudes of 20°N for the Canary and 24°S for the Benguela, as shown in Figure 2.2.
A **correlation analysis** is then performed on NPP, 200m and surface nitrates in these four subsystems: scatterplots for couples of variables are depicted, computing each time the correlation coefficient `r`[2] and fitting a linear regression line in the cases where p-values are smaller than the 0.05 threshold (to evaluate only the statistically significant correlations).

Furthermore, a **quantitative analysis on the growth rates** is provided by comparing the normal time series of growth rates (obtained using the standard growth rate formula

[2]The correlation coefficient `r` varies between -1 and 1 and measures the strength and direction of the linear relationship between two sets of data. Correlation coefficient equal +1 indicates a perfect positive linear correlation, -1 indicates a perfect negative linear correlation (anticorrelation), 0 indicates no linear correlation.

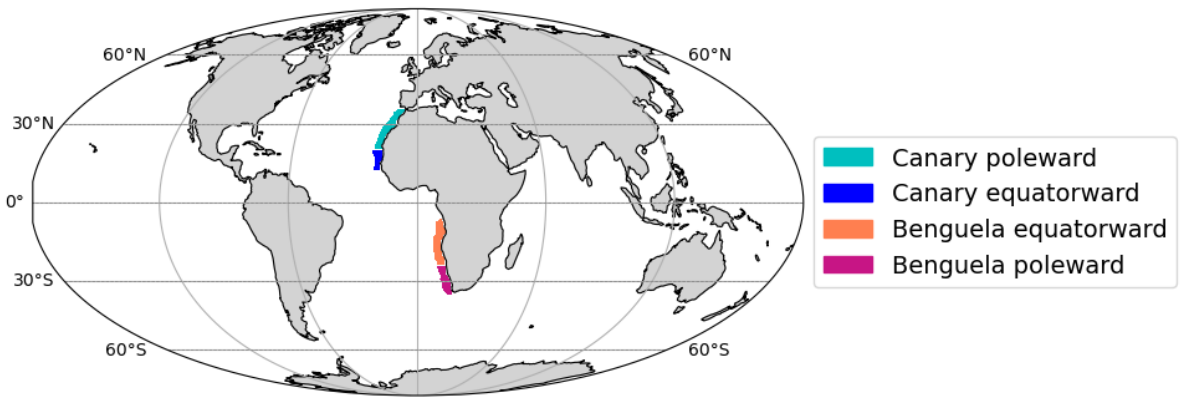

Figure 2.2: **Divided Canary and Benguela EBUS.** Global map depicting the divided masks of the Canary and Benguela EBUS (as defined in the ISIMIP Repository): poleward and equatorward regions were obtained splitting the masks respectively at 20°N and 24°S.

2.1) with three alternative time series. In each one, only one limitation factor is allowed to vary according to its normal SSP5-8.5 projection, while the other two parameters are fixed at their average value over the period 2015-2025. This type of analysis allows to quantify precisely how much the availability of the different factors (temperature, light, and nutrients) limits the growth of phytoplankton.

In the end, in the **overshoot analysis**, instead of presenting conventional time series data, changes in variables are examined in relation to global mean surface temperature. In the investigation of the overshoot scenario, the analysis does not rely on spatial maps, since the use of time-averaged spatial maps could hide important trends and may fail to capture the non-linear responses of certain variables. Instead, analyzing variables in relation to temperature provides a more accurate representation of the Earth system's response to warming, capturing not only the endpoint but also the pathway toward temperature targets.

Chapter 3

Results and discussion

In this chapter the main results of the thesis are presented, with time series and maps of different variables projected changes.
The discussion aims to explain the observed patterns in the EBUS and, using correlative and quantitative analyses, provides an overview of the main factors affecting net primary productivity there, also splitting the Canary and Benguela systems in halves to evaluate separately changes at different latitudes. Finally the analysis of the overshoot scenario SSP5-3.4-OS is provided.

3.1 Global overview

To gain a comprehensive understanding of how climate change may affect the Eastern Boundary Upwelling Systems, the first approach is evaluating the projected changes in key variables on global scale.
Reproducing the results of Bograd et al. 2023 [4], Figure 3.1 presents maps of ensemble mean monthly simulations for Earth System Models of the CMIP6, comparing historical data with the projected changes by the end of the 21st century under the SSP5-8.5 scenario. The latter scenario represents an extreme trajectory and may not eventually be realized, while other less severe pathways are more likely to occur. However, in this analysis, SSP5-8.5 is preferred over the other SSPs because it projects more pronounced changes in the different variables. This larger magnitude of variation provides a clearer view of the potential drivers of shifts in productivity, allowing for a better understanding of the causal mechanisms of climate impacts.

In Figure 3.1, maps 3.1a) and 3.1b) illustrate ensemble mean projected **sea surface temperature**. The historical SST map shows the expected latitudinal temperature gradient, with higher temperatures at lower latitudes, while the projected changes indicate an overall increase in temperature worldwide, particularly in the northern hemisphere, with anomalies exceeding 4°C in some regions.

Net primary productivity is depicted in Figures 3.1c) and 3.1d). The historical map confirms that highest productivity on Earth is found in the Eastern Boundary Upwelling

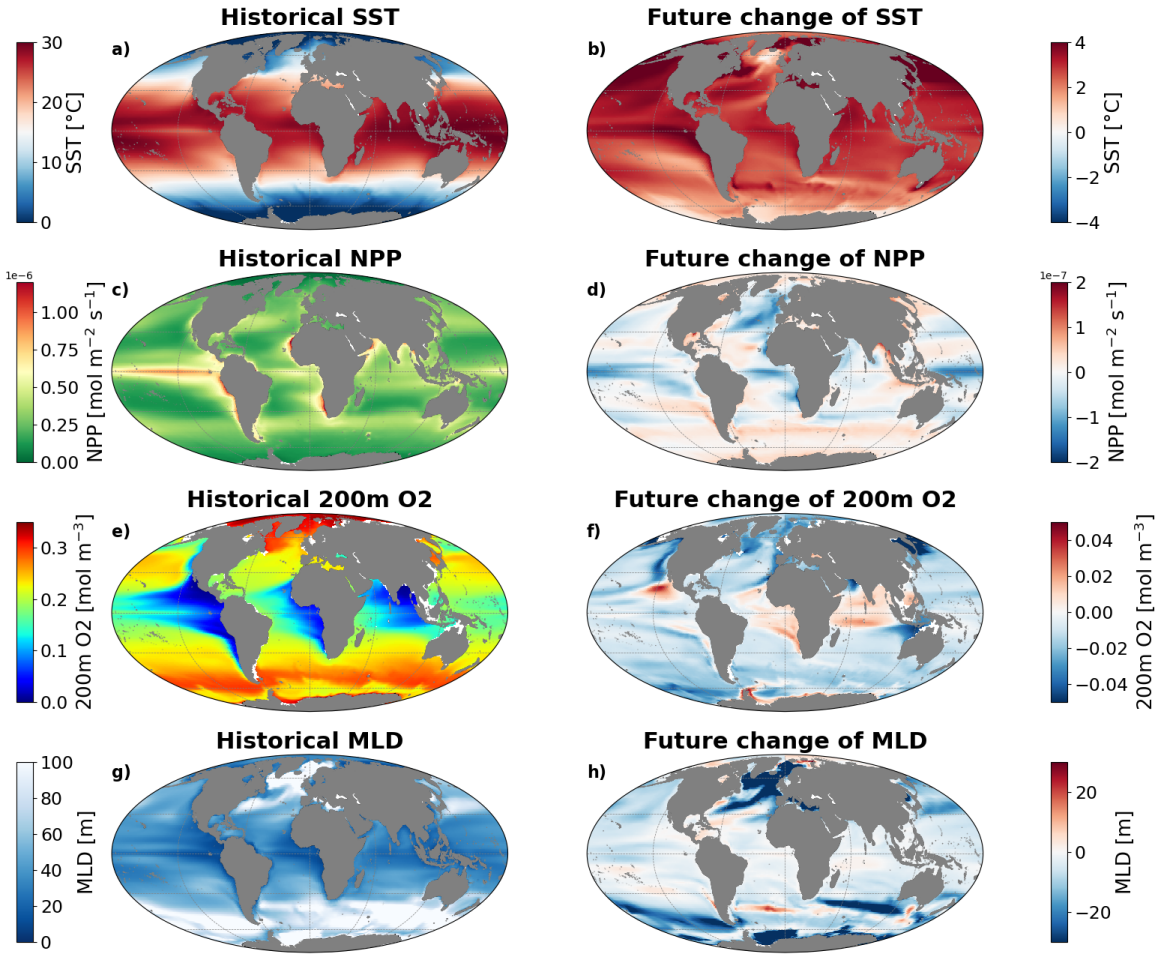

Figure 3.1: **Ensemble mean climate: historical and future changes under SSP5-8.5.** Maps depicting the ensemble mean climate for the historical period from 1985 to 2014 (on the left), and the ensemble mean future changes from 2071 to 2100 relative to 1985–2014 (on the right) for *(a,b)* SST, *(c,d)* net primary productivity, *(e, f)* dissolved oxygen at 200m depth, and *(g,h)* mixed-layer depth.

Systems, especially in the Canary, the Humboldt and the Benguela systems, and high values are also found in the equatorial Pacific Ocean and in the northwestern Arabian Sea. Future projections show large regional variability, with some areas, like the Southern Ocean, experiencing increases in NPP, while others, such as the Northern Atlantic and equatorial Pacific, show decreases.

Describing the global future patterns under the SSP5-8.5, it is relevant to highlight that most models project a primary productivity reduction at a global level, while the IPSL-CM6A-LR simulations show an overall increase. This behavior by the latter version of the IPSL diverges significantly from the majority of the ensemble members and also from its previous version (IPSL-CM5A-LR), that project, by the end of the 21st century, global NPP reduction.

As highlighted by Bopp et al. 2022 in [108], this different response to anthropogenic climate change is mostly related to the parametrisation of N fixation in the PISCES component: in the current model, phosphorus limitation is prevented, resulting in con-

tinued nitrogen fixation, with a key role played by diazotrophy. Carbon uptake and storage, particularly in oligotrophic regions, is significantly affected by diazotrophs, microorganisms able to fix N_2, thus representing in these regions an important source of new nitrogen, leading to increased NPP.
However, the EBUS regions are characterized by large availability of nutrients, and diazotrophy is not thought to be a key feature to investigate when looking at NPP there, because diazotrophy is typically limited to N poor regions in model parametrizations.

Maps 3.1e) and 3.1f) depict dissolved **oxygen** concentrations at 200m depth. In the historical simulations, higher oxygen concentrations are observed at high latitudes and lower concentrations at lower latitudes and along the west coasts of continents. This distribution is influenced by temperature-dependent solubility, with colder waters holding more oxygen, and oceanographic processes, mostly the sinking of oxygen-rich waters in the North Atlantic and Southern Oceans, that further contributes to the higher levels found at higher latitudes. In contrast, tropical and subtropical regions have lower concentrations due to higher biological consumption and respiration by microorganisms. In particular, upwelling regions along the west coasts of continents are characterized, as already discussed, by oxygen-depleted waters in the subsurface, the Oxygen Minimum Zones.
In the projected changes simulation 3.1f), the variations of oxygen concentrations indicate widespread deoxygenation due to anthropogenic climate change, aligning with the findings of Bopp et al. 2002 [109], although the upwelling systems, especially the California, the Canary, and the Benguela experience increases in oxygen levels, particularly in their equatorward portions. The Indian Ocean exhibits positive 200m O_2 anomalies as well.

Finally, **mixed-layer depth** maps are presented in Figures 3.1g) and 3.1h): historical simulations show that mixed layer is deeper at high latitudes (due to stronger winds, colder temperatures and less stratification), while at tropical and subtropical latitudes it is shallower (due to the weaker winds and stronger surface heating, which leads to greater stratification). The map 3.1h) of mixed layer depth anomalies indicate that it is globally getting shallower.
This shoaling is a direct consequence of human-induced global warming: the increasing temperatures during the 21st century heat up surface ocean layers, this warming reduces their density, leading to greater stratification of the water column and diminishing the overall mixing in certain regions.
The consequences of this MLD change on the primary productivity of global oceans vary significantly with the latitude. In polar regions, thanks to the usual large availability of nutrients, the shoaling is projected to lead to the increase of NPP, by mitigating the light scarcity constraint [14]. At lower latitudes, instead, because of the reduced influx of subsurface nutrients into the euphotic zone, it is projected to aggravate nutrient limitation and reduce both net primary production and export production (i.e., sinking particulate flux) [110]. Thus, the shallower source depths and reduced nutrient supply

to the euphotic zone results in a global decrease in primary production [62]. However, as it will be highlighted, in the EBUS increased stratification does not appear to be the first order driver of NPP changes.

Investigating the circulation of the atmosphere, Figure 3.2 presents the historical (1985-2014) global map of the **Surface Wind Stress** Field, overlying the **Sea Level Pressure** field. The data is obtained from the atmospheric set of monthly model simulations of the IPSL-CM6A-LR Earth System Model. Global atmospheric circulation presents trade winds at the equator, blowing from the northeast in the Northern Hemisphere and from the southeast in the Southern Hemisphere. These winds converge in the Intertropical Convergence Zone (ITCZ), region of low pressure. High-pressure systems are found in the subtropical regions, and circulation there is anti-cyclonic (clockwise in the Northern Hemisphere and counterclockwise in the Southern Hemisphere). Mid-latitude regions, instead, are characterised by westerly winds, which are stronger in the Southern Hemisphere, where they blow around the Antarctic continent, due to the smaller coverage of landmasses in this latitude range. In the polar regions low-pressure systems dominate. Focusing on the Eastern Boundary Upwelling Systems, one key feature depicted in the map is the presence of winds flowing towards the equator along the west coasts of the continents.

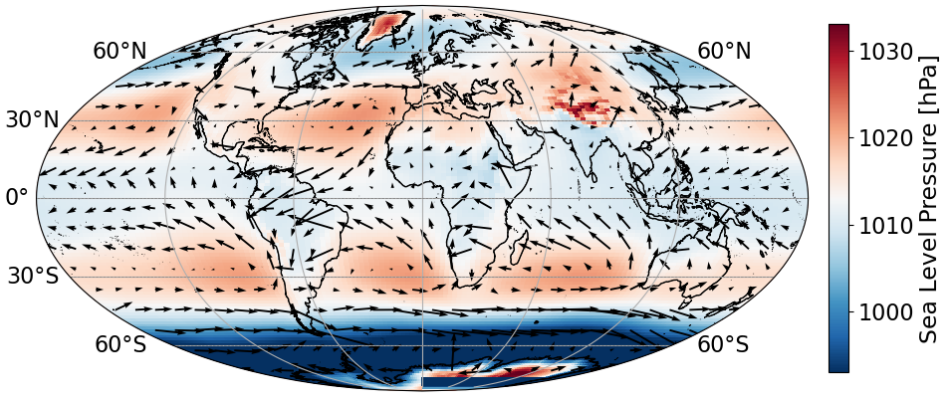

Figure 3.2: **Historical Wind Stress Field for IPSL model.** Maps depicting the IPSL-CM6A-LR model simulations for mean surface wind stress field for the historical period from 1985 to 2014. The wind stress field overlies the corresponding historical sea level pressure field.

In order to investigate more deeply these alongshore winds, Figure 3.3 depicts the global map of surface downward and equatorward wind stress, `tauv`[1]. The historical map (on the left) well shows the presence of alongshore winds, blowing towards the equator along

[1]In the monthly dataset of the IPSL the variable `tauv` was defined positive when directed northward. However, in this study, to highlight better the winds inducing upwelling along the east sides of ocean basins, the data relative to the Southern Hemisphere were changed of sign, so that regions that have positive values (red in figure) are directed equatorward in both Hemispheres, while regions with negative values (blue in figure) are directed poleward.

the west coasts of North and South America, of northern and southern Africa and of Australia. In the SSP5-8.5 anomaly map (on the right), an interesting pattern that can be observed is that in all the four EBUS the meridional winds show a contrasting behavior between the poleward areas, with `tauv` generally strengthening, and the equatorward areas, with `tauv` weakening. This behavior reflects the impact of the projected Hadley cell expansion on the location and intensity of upwelling favorable winds [64], [65]. A deeper analysis around the EBUS will be performed in the next section.

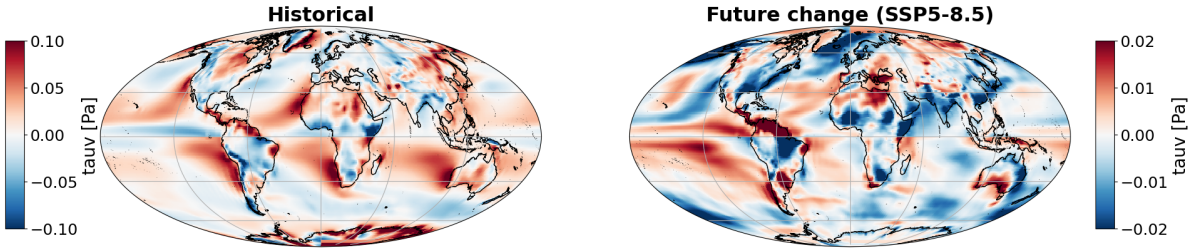

Figure 3.3: **Surface Downward Equatorward Wind Stress: Historical vs. SSP5-8.5 Changes.** Maps depicting the IPSL-CM6A-LR model simulations for mean surface downward and equatorward wind stress for the historical period from 1985 to 2014 (on the left), and the mean future changes from 2071 to 2100 relative to 1985–2014 (on the right).

Finally, Figure 3.4 presents maps of nitrate concentrations, obtained from the oceanic set of yearly simulations, providing insights into the historical and future distributions of nitrates at various ocean depths.
Maps 3.4a) and 3.4b) illustrate **surface NO_3** concentrations: the historical map highlights that the Southern Ocean has the highest nitrate concentrations globally (due to upwelling of deep, nutrient-rich waters), with moderate concentrations also observed in the EBUS and in the poleward portion of the North Pacific, thanks to the sustained upwelling of subsurface waters.
Moving to deeper levels, the concentrations of nitrates increase, particularly in the high-latitude oceans and in upwelling regions. At **200m depth**, Figure 3.4e), the historical distribution of **nitrates** along the west coasts of continents shows an inverse relationship to oxygen levels, which mainly reflects organic carbon remineralization, that consumes oxygen and releases nitrates.
Future changes of NO_3 concentrations appear to have a defined pattern particularly at a depth of 200m, in Figure 3.4f), with the ensemble mean projecting reduced levels in the eastern and equatorial portions of ocean basins (region historically characterized by high concentrations), although strips of increased NO_3 concentrations appear to follow the circulation patterns of the subtropical gyres, increase that may be tied to changes in ocean currents influencing nutrient transport.

This global perspective on historical patterns and projected future changes under the SSP5-8.5 helps to set the Eastern Boundary Upwelling Systems within the framework of global climate change. A purely regional view would only focus on small scale processes,

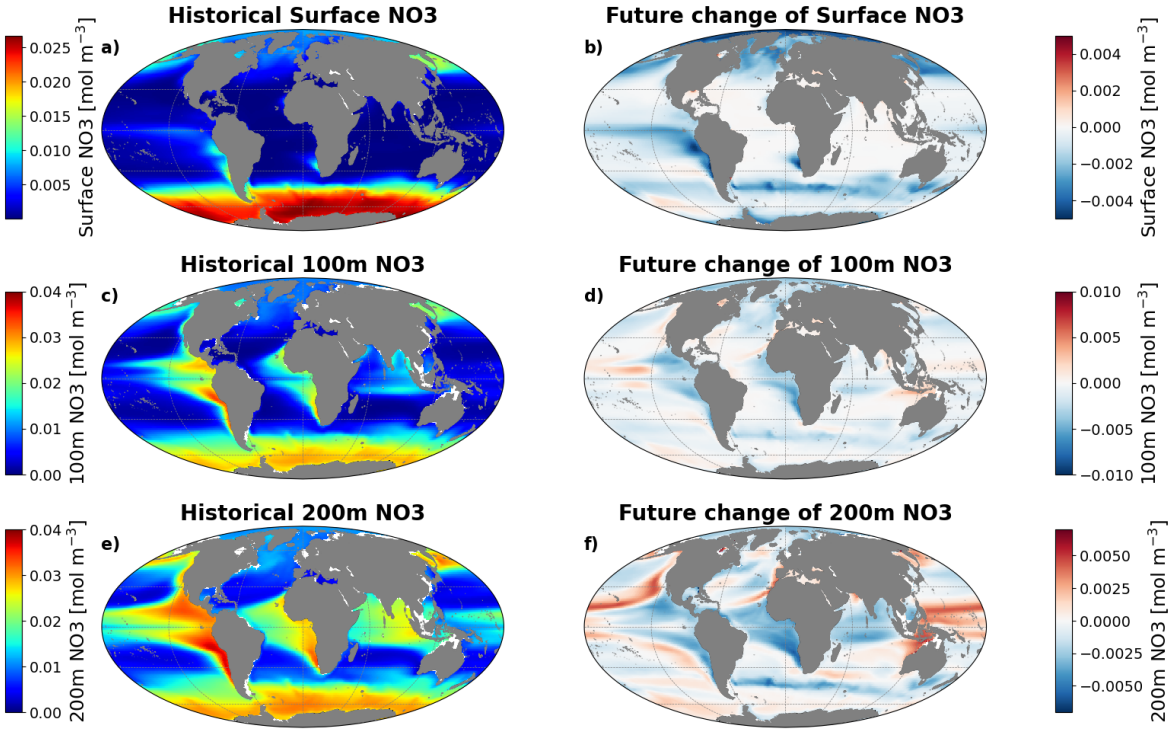

Figure 3.4: **Ensemble mean NO_3: historical and future changes under SSP5-8.5.** Maps depicting the ensemble mean climate for the historical period from 1985 to 2014 (on the left), and the ensemble mean future changes from 2071 to 2100 relative to 1985–2014 (on the right) for *(a,b)* Surface NO_3, *(c,d)* 100m NO_3, *(e, f)* 200m NO_3.

neglecting large scale patterns that play an important role in shaping the biogeochemical and physical processes characterizing these regions.
The maps presented in this section point out the importance of global circulation winds, which drive upwelling in the EBUS, and show the characteristic distribution of different variables on a global scale. Nitrate patterns, in particular, show that their regional concentrations in the EBUS are associated with the oceanic circulation, and nutrients found locally may originate from external sources and then be transported by ocean currents and advection.

3.2 EBUS Net Primary Productivity

Herein, a deeper focus on the Eastern Boundary Upwelling Systems is provided: SSPs time series and anomalies maps are provided, aiming to evaluate future changes of net primary productivity according to the members of the CMIP6 ensemble and to characterize the behavior of the IPSL model with respect to the others.

Figures 3.5 and 3.6 depict model ensemble projections of absolute NPP anomalies under the two scenarios SSP5-8.5 and SSP2-4.5, respectively. These anomalies, as explained in section 2.5, are averaged over the large marine ecosystems associated with each EBUS (although the northern and southern portions of each EBUS often exhibit contrasting

trends, as it will be shown in the following sections).

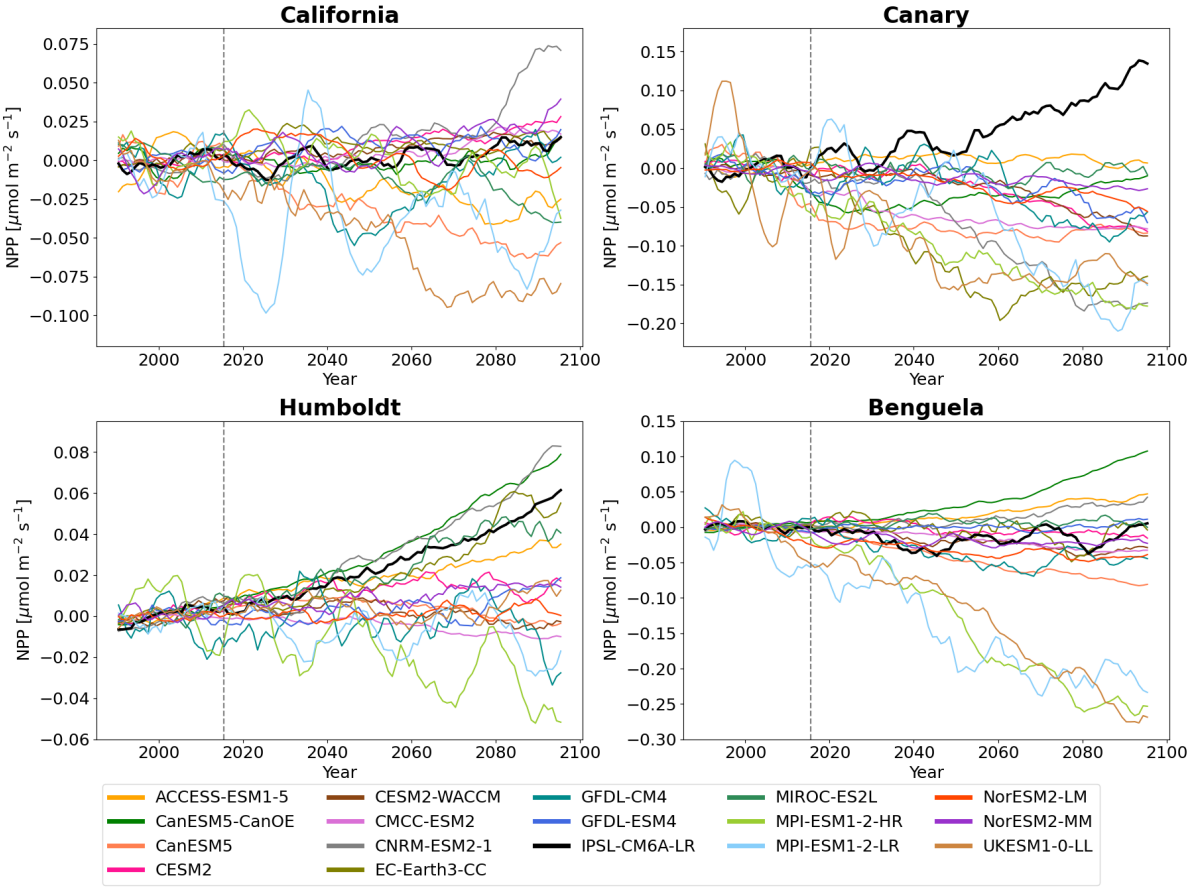

Figure 3.5: **Absolute NPP anomalies: SSP5-8.5 Projections.** Projections of absolute Net Primary Production of different models under SSP5-8.5. IPSL model is the black line. A 10-year smoothing was applied.

At the EBUS scales projections of net primary productivity show **substantial uncertainties**, and significant differences exist between ensemble members: there's wide dispersion and **limited consensus** among them, with little agreement even on the direction of change. Moreover, the level of uncertainty, indicated by the model spread, tends to increase under the higher-emissions scenario (behavior that is observed in general for all variables).
Furthermore, comparing the two scenario projections for each model, it is worth noting that, in the SSP5-8.5 case, the anomalies are much larger, since worse scenarios accentuate the change significantly. For example, the IPSL model in the Canary region projects by 2100 an absolute NPP anomaly of about +0.14 μmol m^{-2} s^{-1} under SSP5-8.5, while for the SSP2-4.5 of +0.07 μmol m^{-2} s^{-1}, so in the highest emission scenario the increase is about the double.

To understand future changes of each region, it is important to evaluate the anomalies with respect to the baseline values of net primary production, since the four regions

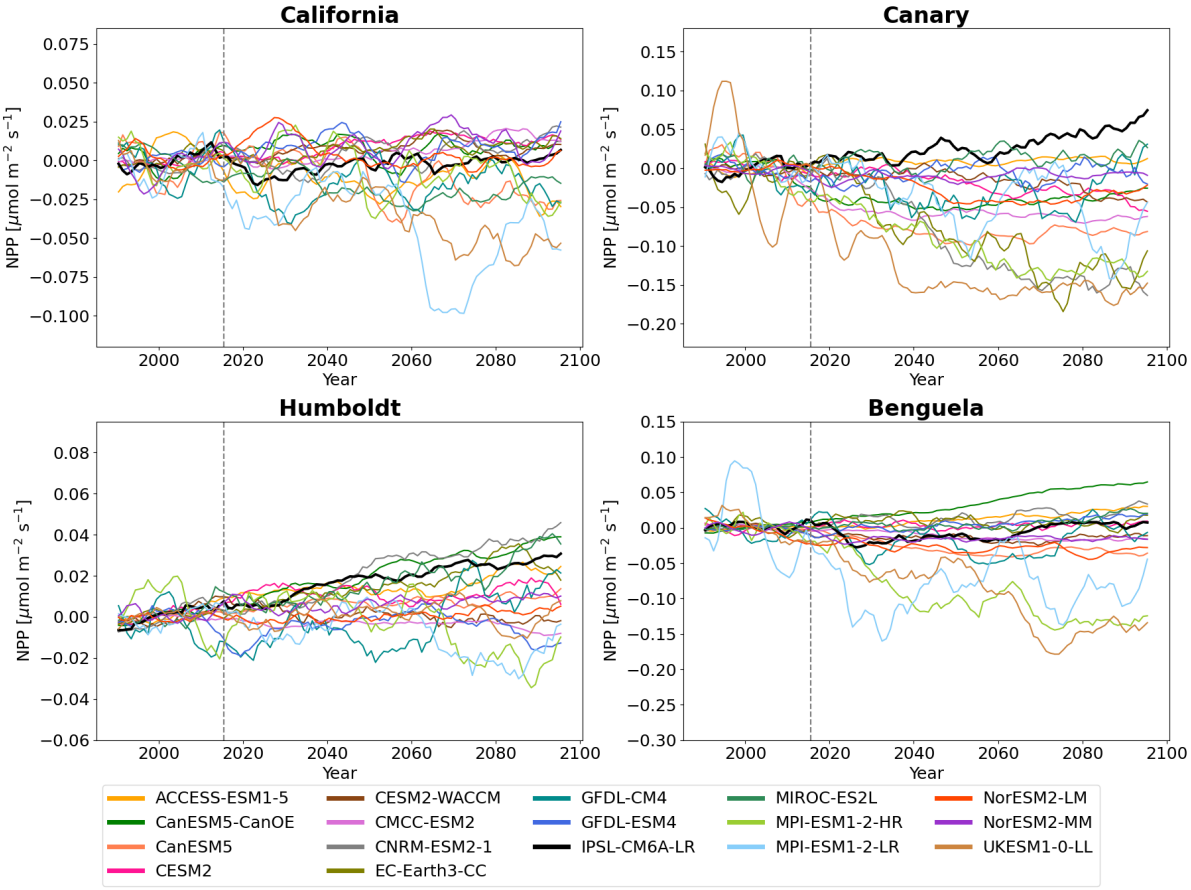

Figure 3.6: **Absolute NPP anomalies: SSP2-4.5 Projections.** Projections of absolute Net Primary Production of different models under SSP2-4.5. IPSL model is the black line. A 10-year smoothing was applied.

show different levels of absolute NPP historically, with the California region being substantially less productive than the other ones (about half of them). For this region, the simulated historical levels of productivity are between 0.1 and 0.5 μmol m^{-2} s^{-1}, while for the other EBUS the simulated historical values are found in a range between 0.2 and 1.1 μmol m^{-2} s^{-1}. By 2100, the projected absolute NPP anomalies for each EBUS vary in different ranges: for the California system from -0.075 to +0.05 μmol m^{-2} s^{-1} under SSP5-8.5, and from -0.05 to +0.025 μmol m^{-2} s^{-1} under the SSP2-4.5; for the Canary system from -0.2 to +0.12 μmol m^{-2} s^{-1} under SSP5-8.5, and from -0.15 to +0.07 μmol m^{-2} s^{-1} under the SSP2-4.5; for the Humboldt from -0.06 to +0.08 μmol m^{-2} s^{-1} under SSP5-8.5, and from -0.03 to +0.04 μmol m^{-2} s^{-1} under the SSP2-4.5; and for the Benguela from -0.25 to +0.12 μmol m^{-2} s^{-1} under SSP5-8.5, and from -0.15 to +0.05 μmol m^{-2} s^{-1} under the SSP2-4.5.

To get a more straightforward comprehension of the strength of these variations, relative changes of net primary productivity are investigated. By normalizing the data against baseline conditions, this approach highlights the magnitude of the projected change compared to historical values.

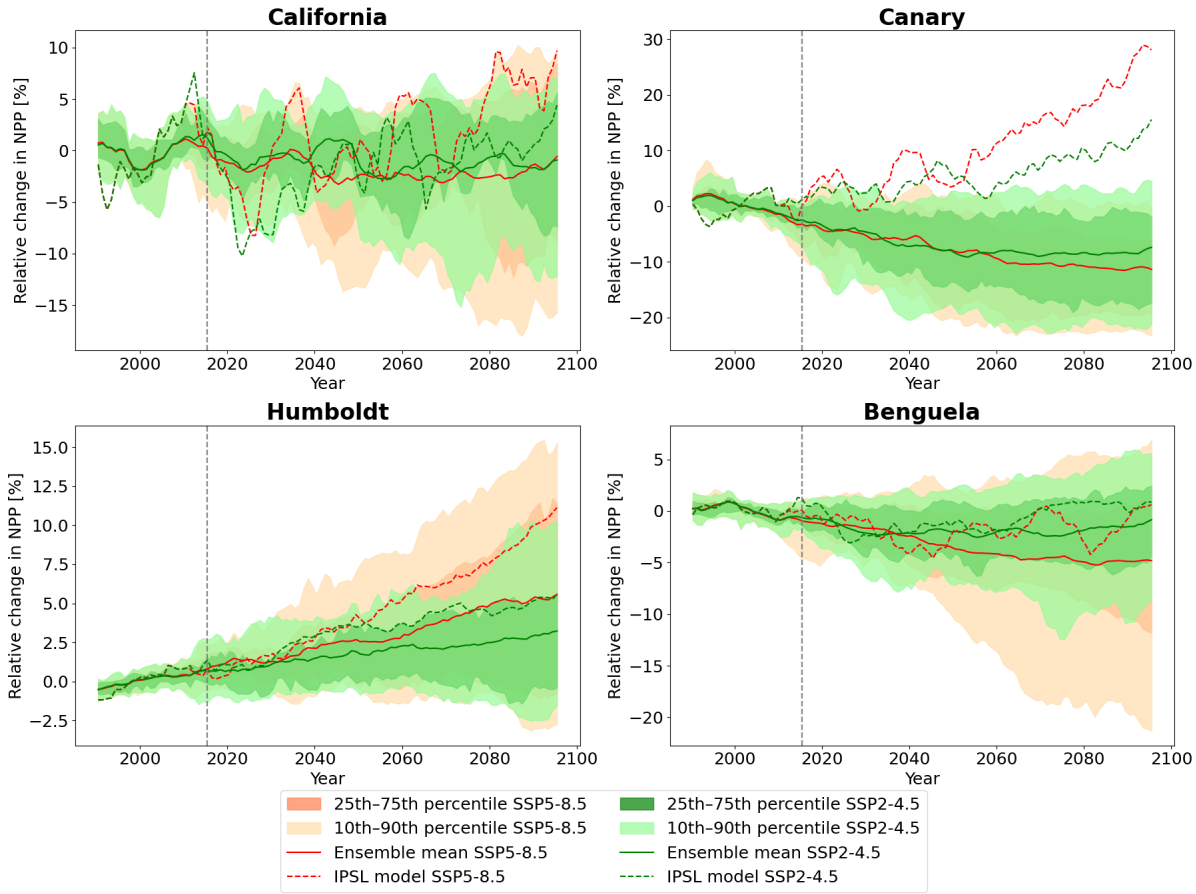

Figure 3.7: **Relative NPP anomalies: SSP5-8.5 vs. SSP2-4.5 Projections.** Projected twenty-first-century relative change in NPP for SSP5-8.5 and SSP2-4.5 of the four EBUS: solid lines are ensemble means, dashed lines are IPSL model; shaded regions indicate 25th–75th (darker shade) and 10th–90th percentile (lighter shade). A 10-year smoothing was applied.

Looking at the projections of anomalies of relative net primary productivity in Figure 3.7, some considerations can be drawn:

- **California EBUS**: Both under the SSP5-8.5 and the SSP2-4.5, large uncertainties exist between models, with little agreement even on the sign of the change of NPP, ranging from more than -15% to +10% under the SSP5-8.5 and from -10% to +7% under the SSP2-4.5. The IPSL models move away from the means of the ensemble in both SSPs, projecting increases in NPP by the end of the century, with a change of around +10% under the SSP5-8.5 and about +5% under the SSP2-4.5.

- **Canary EBUS**: Both under the SSP5-8.5 and the SSP2-4.5, most models agree in projecting a negative change. The 10th–90th percentiles of the ensemble models by 2100 show a range going from -20% to no significant changes. The IPSL model projects instead a positive change in NPP, reaching by 2100 a change of +30% under the SSP5-8.5 and of +15% under the SSP2-4.5.

- **Humboldt EBUS**: Both under the SSP5-8.5 and the SSP2-4.5, most models

agree in projecting a positive change, with ensemble means projecting respectively increases of +5% and +2.5% by the end of the century. The 10th–90th percentiles of the ensemble models by 2100 show a range going from no significant changes to +15%. The IPSL model in both SSP5-8.5 and SSP2-4.5 aligns with the direction of ensemble means trends, projecting a positive change in NPP, with anomalies that by 2100 reach +10% and +5%.

- **Benguela EBUS**: Both under the SSP5-8.5 and the SSP2-4.5, most models agree in projecting a negative change, even if the 10th–90th percentiles of the ensemble models by 2100 show a large range going from almost -20% to +5% under the SSP5-8.5 and from around -10% to +5% under the SSP2-4.5. The IPSL model in both scenarios projects small changes, with a negative NPP change of a few percent under SSP5-8.5 and no significant changes under SSP2-4.5 by the end of the 21st century.

One important observation is that the projected changes are non-monotonic: future trajectories from single models show interannual variability. This behavior arises from the fact that NPP is driven by many factors, which may interact through multiple feedbacks and affect it on varying timescales due to both dynamical and biogeochemical processes. A long-term trend is given by the combination of all the different factors: it may be initially driven mostly by one of them with a short response timescale, and after a while it may change according to another one with a longer time scale, thus causing a variation of the direction of the change. Distinguishing the timings and strength of this influence is a hard problem that should be ideally solved to get a complete and precise overview on the question.

In addition to the analysis of time series, also maps of NPP anomalies are evaluated. Figure 3.8 zooms in on the areas surrounding the Eastern Boundary Upwelling System to provide a more detailed view of the data presented previously in Figure 3.1. NPP anomalies are shown, comparing for each region the ensemble mean (with stippling highlighting areas of strong consensus among models) with the IPSL model data.

Looking at these maps, it can be observed that in the California and Canary regions most models indicate, with good agreement, an overall decrease in NPP, while the IPSL model deviates from this trend. In the first region, IPSL shows a diffused NPP increase, except in the localized region between San Francisco and Los Angeles coasts, where the projected change is strongly negative, while, in the second system, IPSL projects NPP increase in the poleward portion of the EBUS (above 20° of latitude) and decrease in the equatorward portion (below 20° of latitude), pattern partially followed also by the ensemble mean, which shows a stronger decrease in the equatorward portion of the system, however remaining everywhere negative.
In the Humboldt region, model agreement is poor, with a consistent projection of decreased net primary productivity only in its equatorward portion. The IPSL model mirrors the overall direction of changes in this region, albeit exhibiting stronger positive changes.

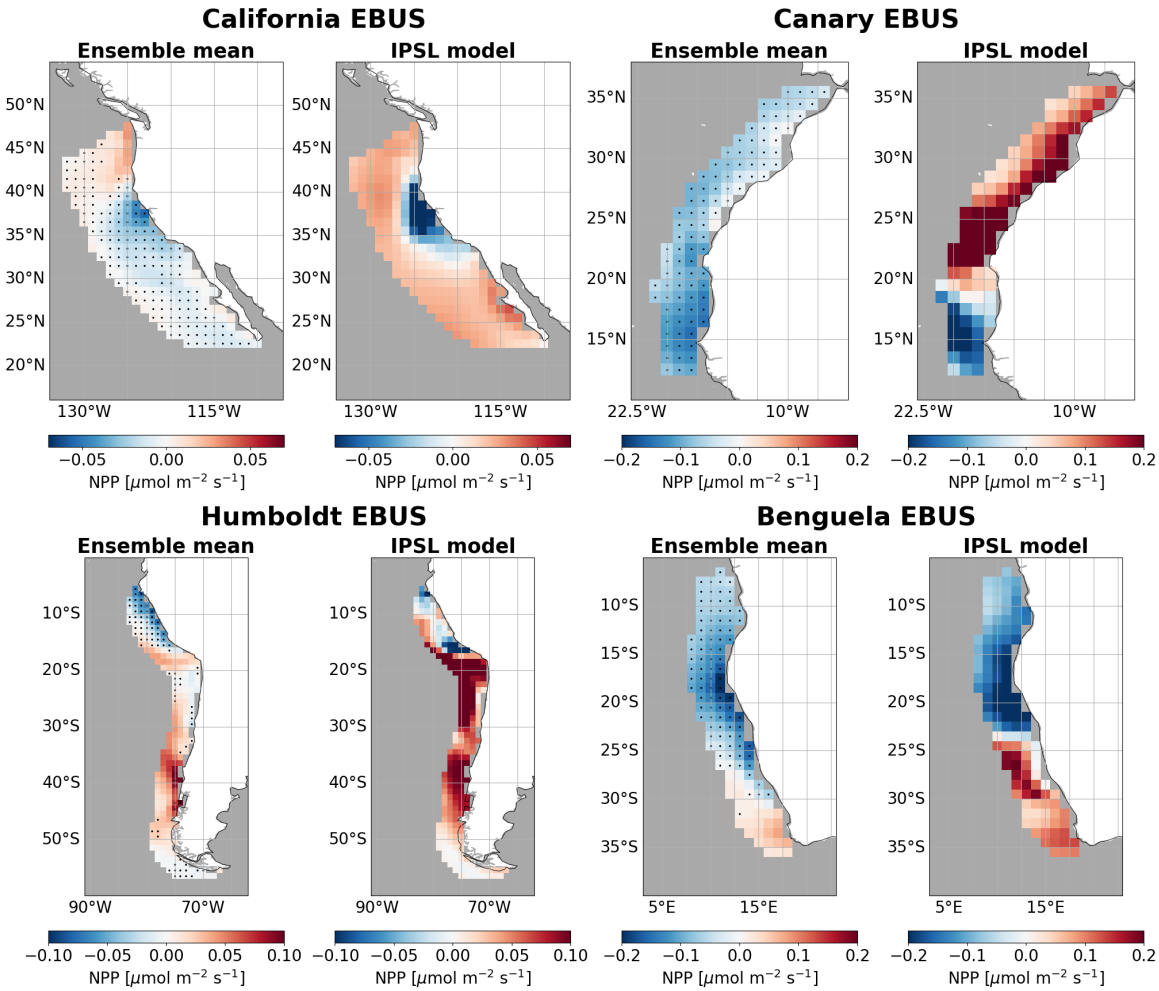

Figure 3.8: **Ensemble mean vs. IPSL NPP: future changes in the EBUS under SSP5-8.5.** Projected net primary productivity (NPP) changes for each Eastern Boundary Upwelling System, comparing the ensemble mean (on the left) and the IPSL (on the right) projected NPP change under the SSP5-8.5 scenario for the period 2071-2100 relative to 1985-2014. Stippling highlights areas where the projected changes are statistically significant across models, with model agreement higher than 80%.

Conversely, model agreement is generally high (except for the poleward area) in the Benguela region. Here, the IPSL model aligns with the ensemble mean, revealing contrasting patterns between the decrease in the equatorward portion and the increase in the poleward one.
In the next section, an analysis on the mechanisms driving these observed projections will be carried on.

3.3 Correlative analysis

Understanding the dynamics of net primary production and projecting its future changes is challenging due to the inherent complexity of marine ecosystems and the difficulties of accurately representing these ecosystems in models. In the EBUS, on one hand, potential contributors to a NPP increase may include stronger upwelling and higher nitrate levels from source waters, reduced light limitation due to stratification, and temperature-driven enhancements in phytoplankton growth rates. Conversely, factors that may lead to a decrease are reduced upwelling and stratification-induced declines in nutrient supply, or temperature-induced increases in zooplankton grazing.

In this section an overview on these potential drivers of net primary productivity changes is provided.
At first, the focus is on the role of nutrients, specifically of nitrates, as the properties of upwelled waters determine nutrient concentrations in the euphotic zone, where phytoplankton live. Therefore, the scenarios of subsurface (200m) NO_3 concentrations are analyzed and compared to the NPP ones, and maps of anomalies depicting ensemble mean and IPSL-CM6A-LR projections are provided, to understand how nitrate availability influences NPP across different models.
Afterwards, a deeper focus only on the IPSL-CM6A-LR is provided to get a specific idea of which are the mechanisms that, according to this model, drive changes in NPP.
Vertical profiles of nitrate concentrations are presented, to assess future changes of the deep ocean nitrate reservoirs. In this context, the mixed layer depth is also considered, to evaluate if stratification changes can alter the availability of nutrients for phytoplankton at shallow levels.

Furthermore, an analysis of the upwelling-favorable winds is provided: using the IPSL model, the hypotheses of past and recent literature are tested, in order to evaluate the impact of atmospheric circulation shifts on upwelling intensity, which is considered as a major factor influencing the availability of nutrients at shallower depths in the EBUS.

Moreover, an additional and more focused investigation is conducted only on the Canary and Benguela regions, dividing them into poleward and equatorward halves[2], as anticipated in section 2.5. The goal of the analysis is to clarify why NPP increases poleward while decreasing equatorward, and to better understand the relationship between nitrate concentrations and primary production, using a linear relationship approach.

[2]The choice of focusing only on the Canary and Benguela system derives from the fact that, with respect to the other two EBUS, the NPP anomalies have well defined patterns of positive anomalies in the poleward portion, and negative in the equatorward one. This may help to understand more easily the causal mechanisms responsible for this dual behavior.

3.3.1 Nitrates

Initially, the focus of the analysis is on NO_3, which is globally the predominant limiting macronutrient. As shown in the global maps of Figure 3.4, the EBUS regions are characterized by the presence of subsurface NO_3 reservoirs. Changes in these deep stocks can affect the availability of nitrates for phytoplankton in shallower well-lit waters, due to the physical process of upwelling, which transports deeper nutrient-rich waters to the surface. Thus, this analysis examines variations in NO_3 concentrations at the depth of 200m and also provides some vertical profiles, to show the extension of the deep water nitrate pools anomalies.

Subsurface nitrates

Nitrate concentrations at 200m depth are analysed under the SSP5-8.5 and SSP2-4.5: similarly to the analysis of Figure 3.7, the projected time series are presented in Figure 3.9.

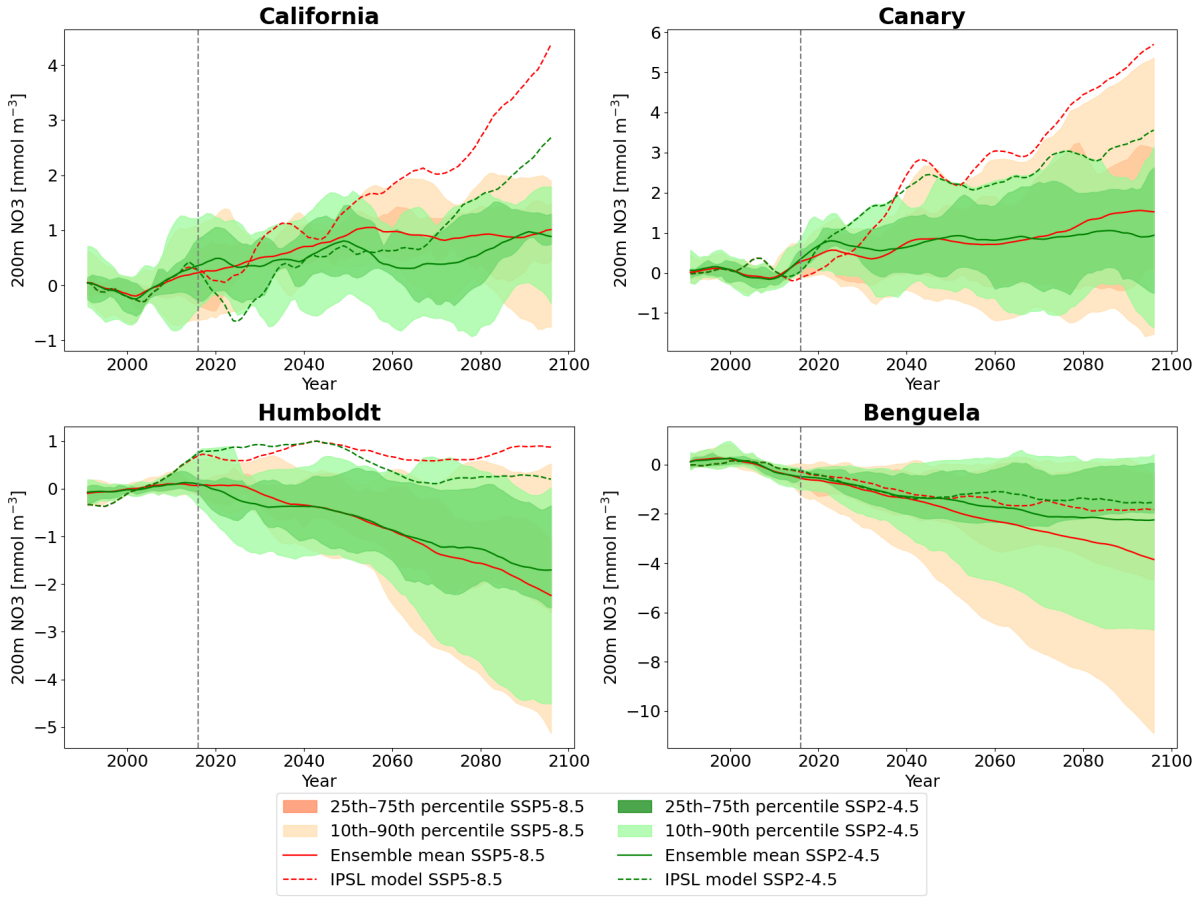

Figure 3.9: **200m NO_3 anomalies: SSP5-8.5 vs. SSP2-4.5 Projections.** Projected twenty-first-century change in 200m NO_3 for SSP5-8.5 and SSP2-4.5 of the four EBUS: solid lines are ensemble means, dashed lines are IPSL model; shaded regions indicate 25th–75th (darker shade) and 10th–90th percentile (lighter shade). A 10-year smoothing was applied.

Looking at each system, it is observed that in the California and Canary region the majority of the models project an overall increase, with ensemble means in both scenarios and in both regions reaching by 2100 similar positive anomalies of about 1 mmol m^{-3}. In these two regions, the IPSL-CM6A-LR projects much stronger increases, which stand out from the majority of the other models: in the California EBUS, anomalies of more than 4 mmol m^{-3} and 2.5 mmol m^{-3} are reached by 2100 under the SSP5-8.5 and SSP2-4.5, respectively, while in the Canary case of about 6 mmol m^{-3} and 3.5 mmol m^{-3}, respectively.
In the Humboldt and the Benguela regions, instead, most models project overall decreases of subsurface nitrates, with ensemble means reaching by 2100 negative anomalies of -2.5 mmol m^{-3} under both scenarios in the Humboldt system, and -4 mmol m^{-3} (under the SSP5-8.5) and -2.2 mmol m^{-3} (under the SSP2-4.5) in the Benguela system. While in the Benguela case the IPSL simulations quite align with the ensemble projections, in the Humboldt EBUS, the IPSL model diverges from most models, projecting under both scenarios slight increases, with anomalies of 0.8 mmol m^{-3} and 0.2 mmol m^{-3} under the SSP5-8.5 and SSP2-4.5, respectively.

Comparing the IPSL trajectories inside the ensemble spreads for 200m NO_3 (Figure 3.9) and NPP (Figure 3.7), it is noticeable that **in the Canary region** there is a similar strong increase in the two variables under the SSP5-8.5. Thus, **the IPSL-projected increase of 200m NO_3** concentrations, which substantially moves away from the majority of the other models, **may be responsible for the same behavior observed for IPSL-projected NPP**. Also in the California and Benguela regions the two variables show quite similar trends, while in the Humboldt EBUS there is not a good correlation between the stable trend of 200m NO_3 and the strongly increasing trajectory of NPP, thus changes in NO_3 concentrations do not appear to be major drivers of NPP variations in this system.

To have an idea on the spatial patterns of the changes, similarly to the analysis made for net primary productivity in Figure 3.7, maps of 200m nitrates anomalies under the SSP5-8.5 are shown in Figure 3.10, comparing for each EBUS the ensemble mean and the IPSL model data.
The IPSL-CM6A-LR model is quite well aligning with other CMIP6 members for some systems, however some differences are present for other ones. In the Canary and Benguela regions, where model agreement is high almost everywhere (except in the poleward Canary area), the simulated patterns are the same, with the IPSL model differentiating from the ensemble only for the intensity of the changes, in particular in the poleward portion of the Canary system, where it projects a very strong NO_3 increase.
However, in the California and Humboldt regions, where the ensemble members show statistically significant changes in subsurface nitrates, the IPSL projections are different. In the first region there are projected decreased levels close to the coast and increased far from it, with the IPSL differentiating from this pattern, with a widespread increase in the whole region. In the second system, a dual pattern on increased concentrations

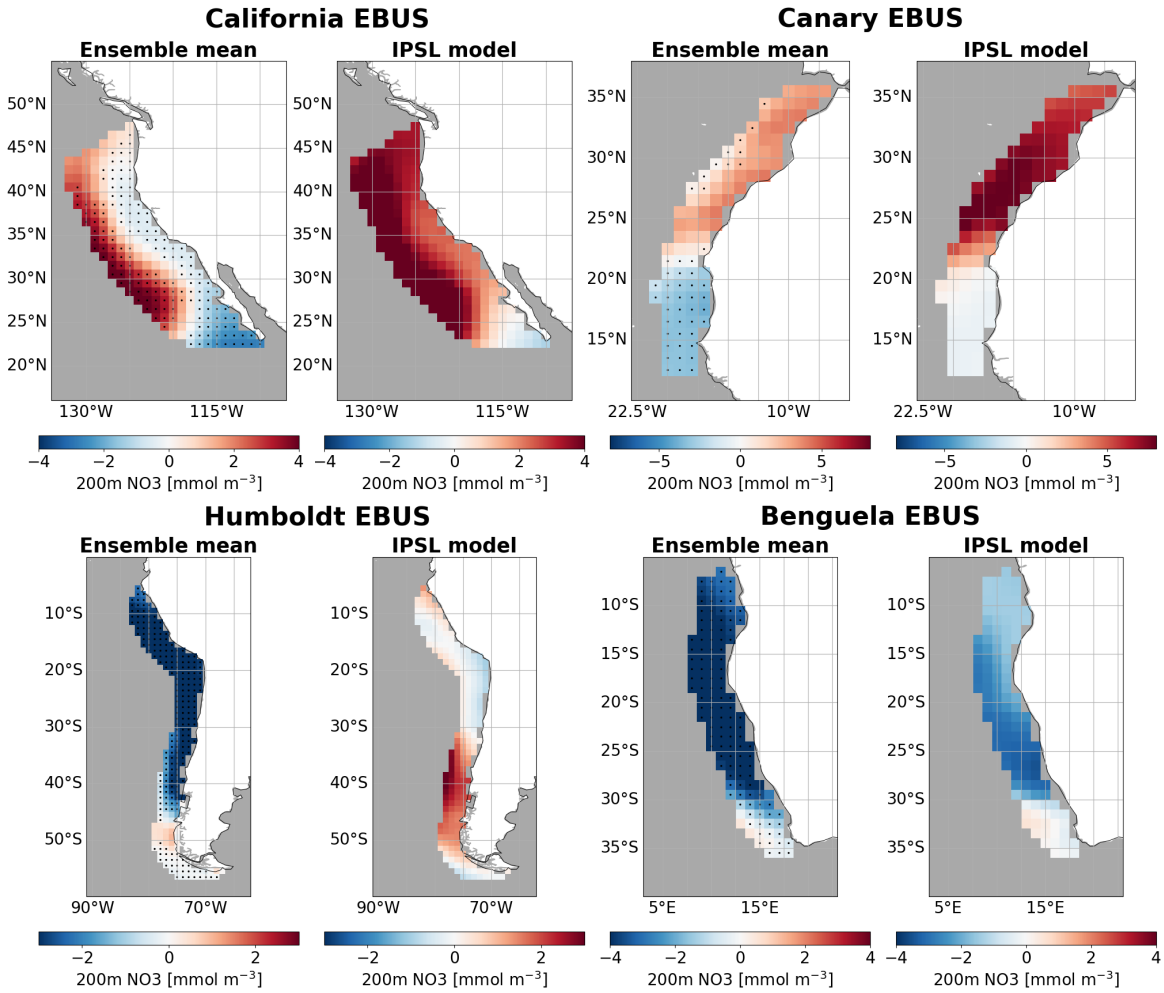

Figure 3.10: **Ensemble mean vs. IPSL 200m NO_3: future changes in the EBUS under SSP5-8.5.**Projected 200m NO_3 changes for each Eastern Boundary Upwelling System, comparing the ensemble mean and the IPSL projected NPP change under the SSP5-8.5 scenario for the period 2071-2100 relative to 1985-2014. Stippling highlights areas where the projected changes are statistically significant across models, with model agreement higher than 80%.

poleward and decreased equatorward is followed both by the ensemble mean and by the IPSL model, but it the first case the decrease is much stronger and reaches lower latitudes.

Comparing the IPSL projections of 200m nitrates of Figure 3.10 with the NPP ones of Figure 3.8, some considerations are provided. For the Benguela and the Humboldt regions, NPP projections are not well mirrored by the subsurface nitrates ones: in the first system the subsurface nitrate concentrations decrease across most of the mask, with almost no change/very slight increase in the poleward edge; in the second system there is a positive anomaly of nitrates in the poleward portion, but it is more limited to the southern portion of the mask with respect to NPP positive anomalies that reach lower latitudes.
Instead, similarities exist between NPP and 200m NO_3 in the Canary and California

EBUS. It is noticeable the great resemblance of the two variables for the Canary EBUS, that shows a precise latitudinal correspondence, with strong increases north of 20°N of latitude. Moreover, in the California region, the pattern of NO_3 increase, stronger in the western edge of the mask, is found also in the observed increase in NPP around the strong decreasing spot. Therefore, it seems that **subsurface NO_3 changes** play an important role in **driving NPP** variability especially **in the California and Canary EBUS**.

Vertical profiles

To get a deeper insight into the mechanisms driving the variability of net primary productivity, form here on out only IPSL-CM6A-LR is used.
To better describe subsurface nutrients and to evaluate the role of vertical mixing occurring in the mixed layer, vertical profiles of nitrate anomalies are presented in Figure 3.11, depicted together with the historical and SSP5-8.5 projected mixed layer depths (MLD) at the selected latitudes across the four upwelling systems.

For each region, two vertical profiles are shown: one representing the equatorward portion and one representing the poleward portion of the upwelling system.
The profiles for the two areas of each upwelling system are defined by specific latitudes[3], while the longitudes are allowed to vary within the predefined masks for each EBUS.
This map reveals some features in the EBUS NO_3 vertical profiles, with subsurface anomalies more commonly positive in the poleward sections while negative or mixed anomalies in the equatorward ones. The strength and distribution of these anomalies vary significantly between regions, with the **Canary poleward region showing the strongest increase in subsurface nitrates**, exhibiting an increase of up to 9 mmol m^{-3} in the subsurface.

Looking more in detail, in the California region both equatorward and poleward portions show increased NO_3 concentration in the subsurface (from the depth of 100-150m), while at shallower levels no significant variations appear.
The Canary upwelling system exhibits different anomalies across latitudes: the equatorward section shows slight negative changes, especially at shallow levels, while the poleward section experiences very strong positive anomalies. In this latter portion, positive anomalies begin to increase at shallower depths near the coast (around 75 meters depth at a longitude of 346°) and progressively deeper levels further offshore (around 150 meters depth at a longitude of 342°).
The Humboldt and the Benguela systems present similar vertical profiles, with the equatorward portions characterized by decreased NO_3 concentrations at shallow levels below

[3]These latitudes were chosen, for each mask, in the equatorward and poleward areas where the direction of change of 200m nitrates is stronger. The fixed latitudes are 27°N (equatorward) and 37°N (poleward) for the California, 17°N (equatorward) and 27°N (poleward) for the Canary, 10°S (equatorward) and 40°S (poleward) for the Humboldt, 15°S (equatorward) and 33°S (poleward) for the Benguela.

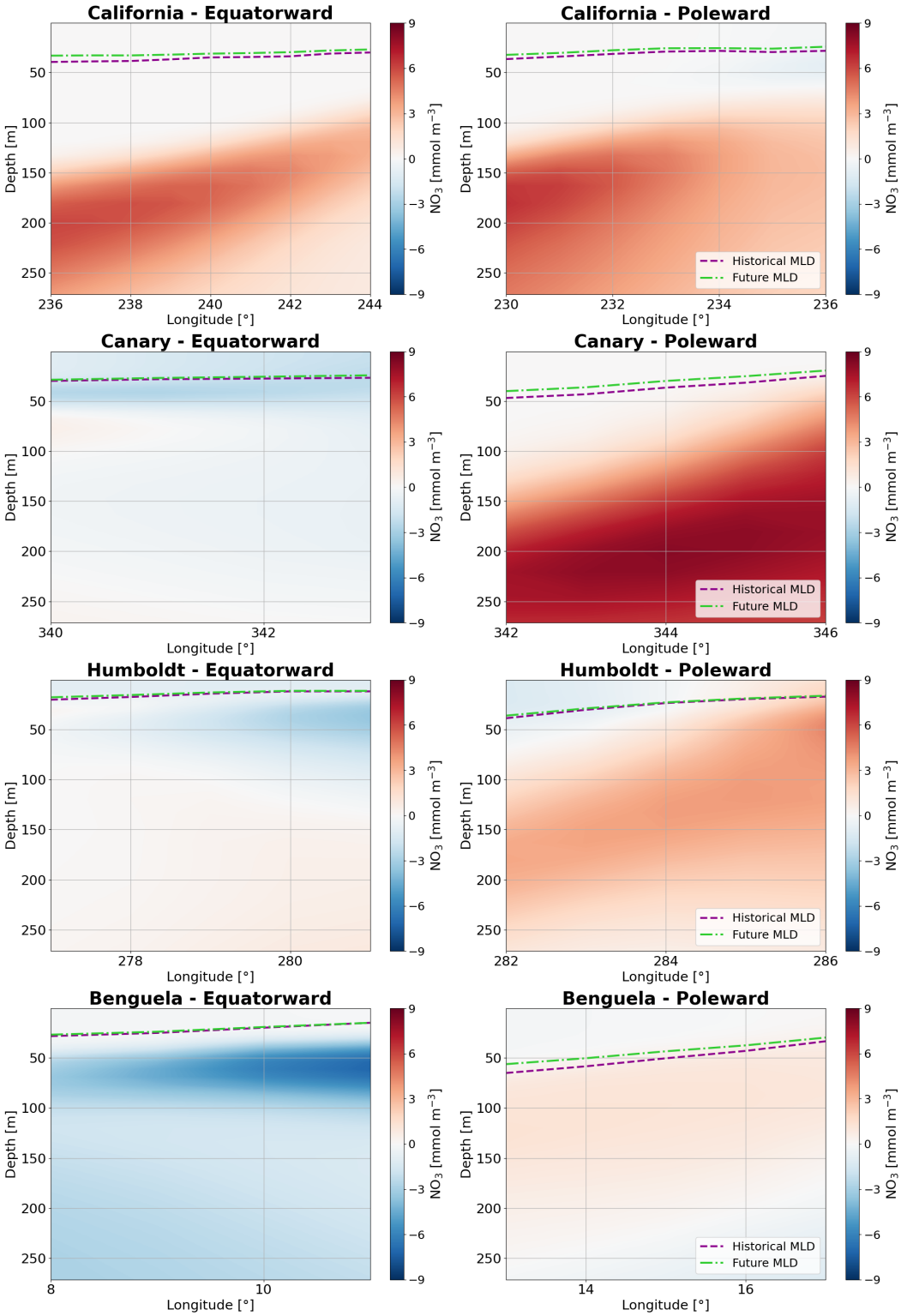

Figure 3.11: **Vertical profiles of nitrate anomalies for IPSL model** in the EBUS regions, poleward and equatorward portions, under SSP5-8.5. Vertical profiles are obtained for varying longitudes and fixed latitudes. Mixed layer depths (MLD) at the selected latitudes are also represented in each map: the historical in purple and the SSP5-8.5 projected in green.

the mixed layer, particularly strong in the Benguela system; while the poleward portions show a prevalent increase in subsurface nitrates, more significant in the Humboldt region.

Moreover, the analysis of the mixed layer depth across all regions reveals that it tends to be deeper in the poleward areas, driven by stronger wind-induced mixing and the influence of major ocean currents. In these portions, the MLD also shows a slanting pattern, becoming deeper moving away from the coast. Moreover, in all regions, the future mixed layer is projected to shoal compared to historical depths due to global warming, which leads to enhanced stratification.
However, in these regions, both historical and projected mixed layers remain well above subsurface nutrient stocks, rarely extending beyond 50 meters in depth (with the exception of the Benguela poleward region). Only in the poleward sections of the Canary, Humboldt, and Benguela systems, near the coasts, the MLD gets closer to the nutrient positive anomalies.
Thus, the **mixing** that occurs **within the mixed layer is not the major responsible for the transport of nutrients** from the deeper reservoirs to shallower levels, role that is rather played by upwelling.

Given the important role of nitrates, understanding the reasons of the observed projected patterns of NO_3 is crucial to get reliable projections of NPP. One feature considered to explain the observed NO_3 patterns was the role of diazotrophy. Indeed, at a global level under the IPSL-CM6A-LR model, nitrogen fixation by diazotrophs was found to be the responsible for the future nitrates increase, which was projected to lead to strong enhancements of global productivity. However, the role of diazotrophs in N fixation is usually significant in oligotrophic regions, far from areas of high nitrate concentrations, where these organisms have better conditions to live[4]. In particular, in the Eastern Boundary Upwelling Systems, they do not appear to represent an important source of new nitrogen. Indeed, the projected levels of nitrogen fixation by diazotrophs in the latest IPSL model were evaluated and low correlations with patterns of projected NPP were found. Thus, diazotrophy is not a primary factor affecting productivity in the four regions of interest.
Rather, the dynamics governing regional patterns of deep nutrient stocks in the ocean are influenced by a variety of physical processes, including horizontal advection or vertical fluxes, as well as biogeochemical processes that may change sources and sinks of nutrients in the ocean (for instance remineralization may be one source).

Beyond understanding the causes of the projected patterns of nutrient reservoirs, it is crucial to assess how these changes will affect the nutrient concentrations in the euphotic layer, where phytoplankton live. Since the key process transporting nutrients to these shallow waters is upwelling, which is controlled by wind patterns, the following analysis focuses on the alongshore winds of these coastal systems.

[4]Even if it was recently discovered a growing variety of microorganisms and thriving diazotrophic communities in unusual habits like coastal waters [111], [112].

3.3.2 Upwelling-favorable winds

As previously introduced, in literature, in the examination of climate change impacts within the Eastern Boundary Upwelling Systems, different hypotheses were made to explain the responses of NPP to different scenarios, and the main driver that has always been identified is the upwelling strength.
The early theory by Bakun 1990 [63] projected that global warming would increase the ocean-land temperature gradient, leading to a strengthening of alongshore winds, intensification of upwelling, and consequently, to an increase in net primary productivity. However, this hypothesis is too simplistic, since it projects homogeneous responses of NPP across the entire systems.
Maps of EBUS net primary productivity of Figure 3.8 demonstrate, instead, that the direction of change is not uniform across the masks, suggesting that climate change impact is likely to be more complex than the simple increase in upwelling, and that it might affect different latitudinal sections of Eastern Boundary Upwelling Systems differently.

Therefore, more recent research (such as Rykaczewski et al. 2015 [34] and Bograd et al. 2023 [4]), were evaluated. These studies identified a different latitudinal response within upwelling regions. They projected a poleward intensification of upwelling, associated with the poleward expansion of the Hadley cell.
The upwelling strength can be crucial in determining the concentrations of nutrients in the well-lit surface layer in the EBUS regions, therefore, in order to test this hypothesis, IPSL-CM6A-LR outputs for meridional winds were analysed.
Figure 3.12 compares surface downward and equatorward wind stress (`tauv`, unit of measure Pa) for historical simulations (1985-2014) and the projected changes under the SSP5-8.5 scenario (2071-2100 with respect to the baseline), simulations derived from the IPSL-CM6A-LR. In all the four EBUS, historical maps show that atmospheric circulation along the west coasts of continents is predominantly characterized by equatorward winds, with the exception of the poleward portion of the Humboldt system, due to the more complex dynamics associated with the very low latitudes.
From maps of projected changes, instead, significant variations in high-pressure systems are evident. In the Canary, Humboldt and Benguela regions, a meridional gradient of wind changes is projected, with a decrease in the equatorward portion and an increase in the poleward portion (although in the Humboldt system there is again a different behavior in the latest high-latitude portion, more associated with other processes and linked to the vicinity of the Southern Ocean).
In the California EBUS, the majority of the region shows a projected decrease in the equatorward wind stress. However, similar to the other systems, the poleward edge of this EBUS exhibits increased alongshore wind stress, positive anomaly that is found just after the final portion of the mask's defined limits obtained from the ISIMIP repository. Moreover, in the California region, a notable strong negative wind anomaly appears near the coast around the 35° latitude.

The observed dual behavior of winds of Figure 3.12 **confirms Rykaczewski's hypoth-**

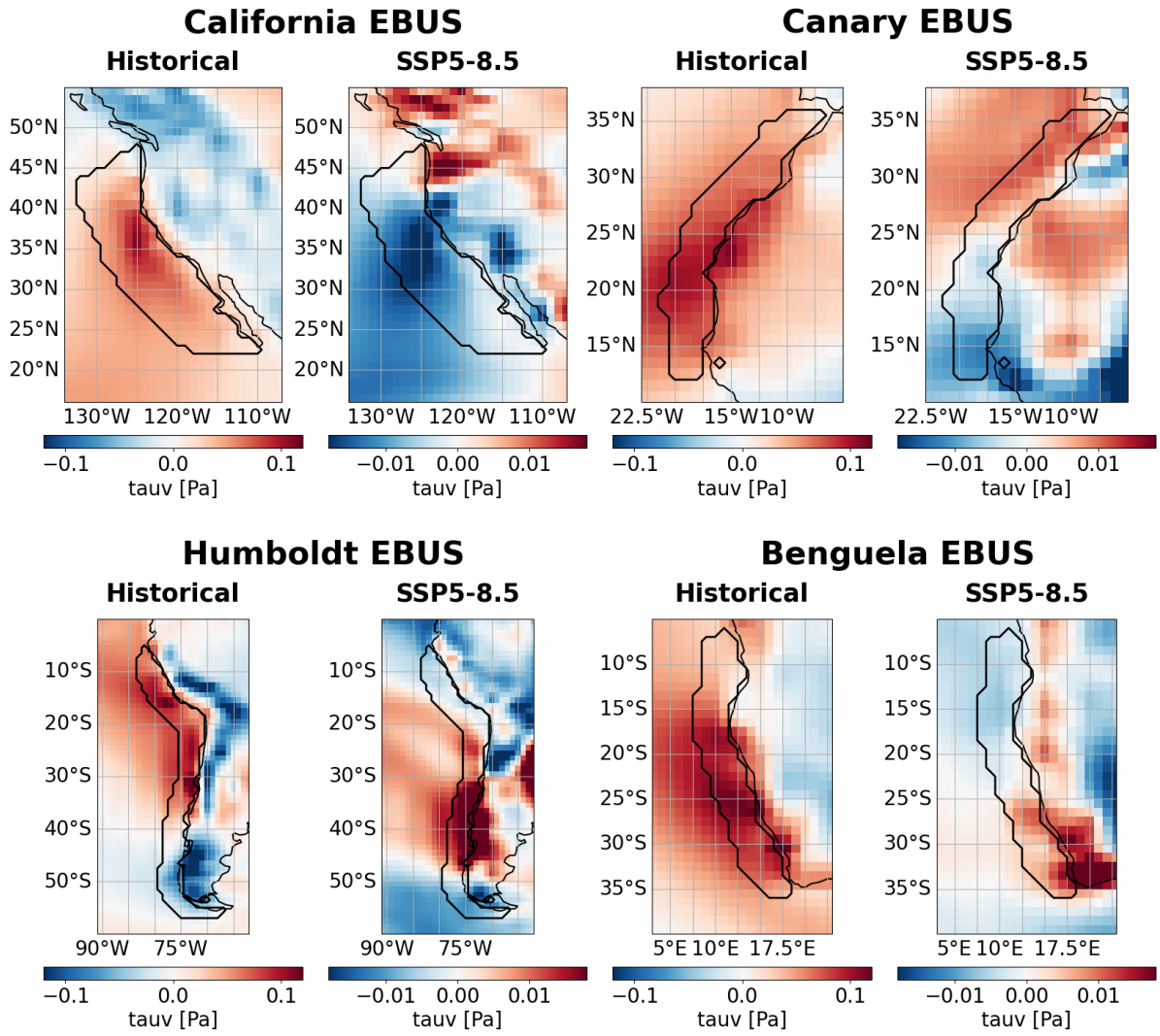

Figure 3.12: **Surface Downward Equatorward Wind Stress: Historical vs. SSP5-8.5 Changes.** Surface Downward Equatorward Wind Stress for each Eastern Boundary Upwelling System, comparing the historical (1985-2014) and projected change under the SSP5-8.5 scenario for the period 2071-2100 (relative to 1985-2014). Positive wind stress is toward the equator.

esis [34], with increased land-sea temperature gradients due to global warming leading to **enhanced upwelling-favorable winds poleward and weaker winds equatorward** across all four EBUS regions.

When comparing the IPSL-projected changes in net primary productivity shown in Figure 3.8 with the upwelling-favorable winds in Figure 3.12, insights into the mechanisms driving NPP changes emerge. In the Canary, Humboldt, and Benguela regions, there is a consistent latitudinal correspondence between the two variables. In the Humboldt and Benguela region the correspondence is quite precise, with regions of increased (decreased) net primary productivity almost coinciding with the increased (decreased) equatorward winds; in the Canary region the dual pattern is followed, even though the NPP increase

extends in the poleward portion up to the latitude of 20°N, while the wind stress positive anomaly only reaches the 25°N latitude.
Instead, in the California region, the projected reduction in upwelling strength explains the significant negative NPP anomaly hotspot, with both variables showing strong negative anomalies in the same location. However, the increased NPP observed elsewhere in the California system is not explained by the projected upwelling changes.

From this analysis, it is evident that upwelling strength is a major factor impacting NPP, thanks to the enhanced supply of nutrients at shallower levels provided by the increased upwelling. Particularly **in the Humboldt, Benguela, and in a localized area of the California EBUS, upwelling strength is the major driver of NPP** changes.

However, the upwelling strength does not explain the NPP patterns everywhere. Past and present research of anthropogenic changes in EBUS only emphasize the role of upwelling, often neglecting to consider other potential factors, mainly the changes in subsurface nutrients concentrations, whose variations may alter significantly the concentrations found in the euphotic layer.
Looking at the California case, for instance, it is observed that, despite the projected decrease in upwelling across the entire mask, NPP is expected to decrease only in the localized spot of very strong upwelling reduction, while, all around that spot, it is projected to intensify. This is because the increase in subsurface nutrient levels is so intense that, despite the reduced volume of water being upwelled, enough nitrates reach the surface and significantly boost NPP.

The analysis so far indicates that no single factor can fully explain future NPP projections, and both subsurface nitrate concentrations and upwelling strength may contribute to the changes. A quantitative assessment of how much each factor influences NPP would be enlightening. In particular, the understanding of the interconnected changes in nitrate levels and upwelling dynamics, such as the depth from which waters are drawn and brought to the surface would offer a clearer picture of the mechanisms driving changes in marine primary production.

3.3.3 Community composition changes

To get deeper into the understanding on the causal mechanisms driving NPP in the euphotic zone, a deeper analysis using IPSL-CM6A-LR outputs was carried on. The relation between NPP, surface and subsurface nutrients was investigated, and the approach used involved linear regression.

As previously illustrated in the NPP map of Figure 3.8, under the SSP5-8.5 scenario, the IPSL-CM6A-LR projections for the four EBUS show internal contrasting trends in NPP, with a dichotomy between the poleward and equatorward parts, particularly pronounced in the Canary and Benguela regions, while California and Humboldt exhibit less orderly patterns. Hence, the two Atlantic regions are split in halves at the latitudes where the

NPP anomalies change sign in each EBUS, as shown in Figure 2.2 of section 2.5.

The linear dependencies of NPP, surface NO_3, and 200m NO_3 in the equatorward and poleward halves of the Canary and Benguela regions are analysed. More precisely, Figure 3.13 presents scatterplots of historical and projected anomalies from the IPSL model, with the linear regression line that is derived for each couple of variables having a statistically significant relation (p-value smaller than 0.05).
The first column represents, for each of the four subsystems, the linear relation between surface nitrates and net primary productivity, the second one between 200m nitrates and net primary productivity, the last one between 200m and surface nitrates.

In the majority of the plots the correlation coefficient `r` is very high. In particular, in the Canary poleward and in the Benguela equatorward portions, `r` values are everywhere higher than 0.8; also in the Canary equatorward area, even if `r` values are lower, the correlations are positive. This aligns with the physical descriptions discussed earlier: phytoplankton can only thrive in the sunlit surface waters if sufficient nutrients are available. Therefore, it is reasonable that high NPP values correspond with elevated nitrate concentrations at both the surface and 200m, as these depths represent the range of nutrient levels accessible to phytoplankton.
Also, in these three areas, subsurface and surface nitrates appear to be coupled, which is expected given the upwelling in these regions, that brings deep waters to the surface. However, interestingly, the Benguela poleward region presents high correlation values only between subsurface and surface nitrates (`r`=0.77), while NPP is negatively correlated with 200m NO_3 (`r`$=-0.52$) and there is no statistically significant correlation with 200m NO_3 (p-value>0.05).

This decoupling of NO_3 and NPP in the Benguela poleward region suggests that variations in nitrate levels are not a straightforward driver of productivity in this area.
A deeper study is conducted by distinguishing between diatoms and nanophytoplankton, as they may be affected by diverse factors due to their size, morphology, and biogeochemical characteristics.
The same analysis of Figure 3.13 is repeated for diatoms and nanophytoplankton separately across the halves of the Canary and Benguela regions.
The results highlights that the net primary productivity of the two plankton functional types behave differently in the poleward portion of the Benguela. A substantial different pattern characterises the two classes: NPP shows positive correlation values with both 200m and surface nutrients for diatoms, while for nanophytoplankton there is no significant correlation (p-value>0.05).
To understand this discrepancy, Figure 3.14 shows the time series of SSP5-8.5 projected total NPP and NPP from nanophytoplankton and diatoms, using the IPSL model in the equatorward and poleward halves of the Canary and Benguela regions. It can be observed that in the two equatorward portions and in the Canary poleward region, total NPP and productions from the two PFTs behave in the same way in each region (in the

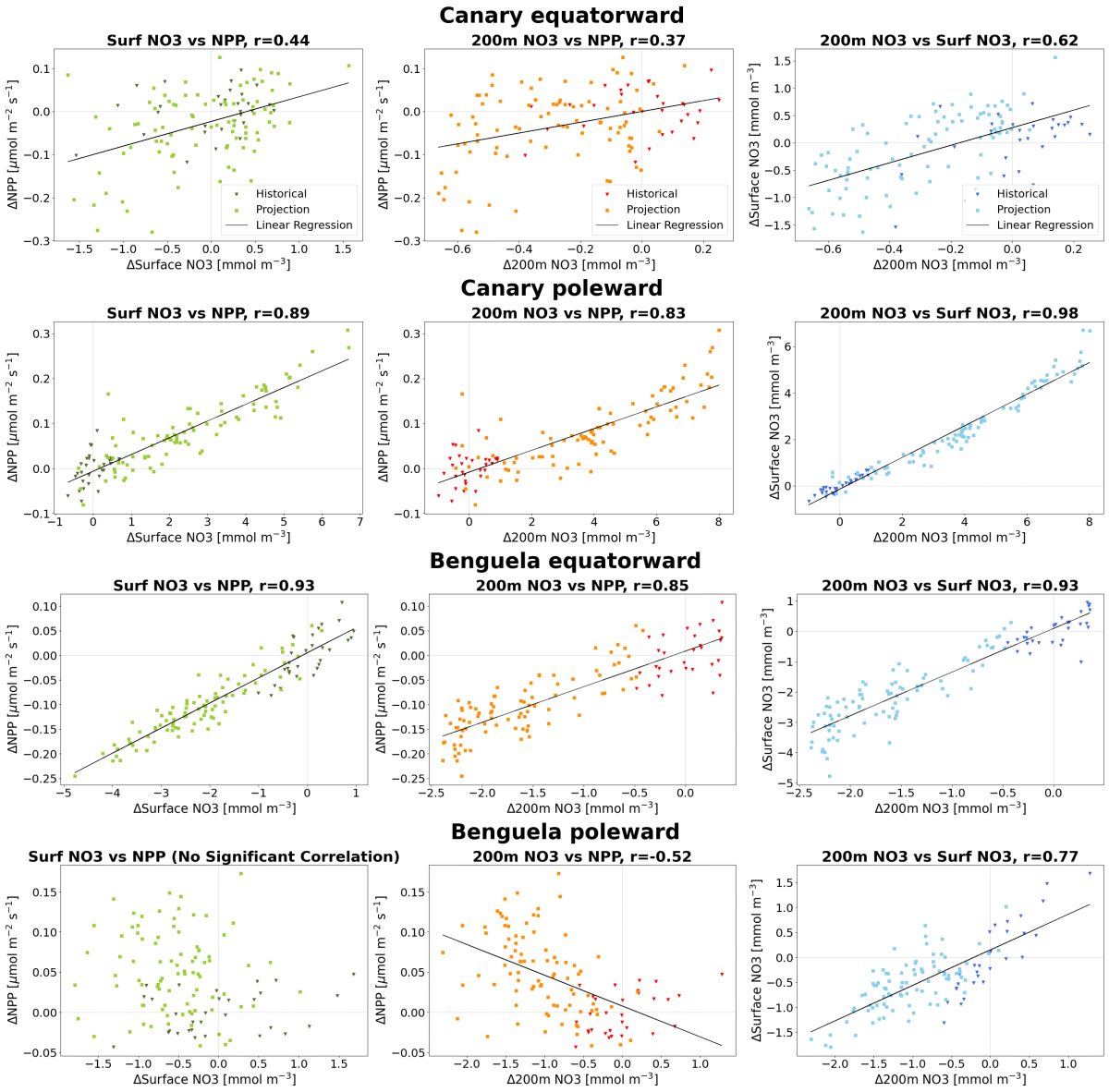

Figure 3.13: **NPP, surface NO_3 and 200m NO_3 linear relations.** Scatterplots of anomalies of surface NO_3 vs. NPP in the first column (dark green triangles are historical data, light green squares are projected data); 200m NO_3 vs. NPP in the second column (red triangles are historical data, orange squares are projected data); 200m NO_3 vs. surface NO_3 in the third column (blue triangles are historical data, light blue squares are projected data). Each row corresponds to a portion of a system, from the top: Canary equatorward, Canary poleward, Benguela equatorward, and Benguela poleward. In each plot, the black line represents the regression line. All correlation values are statistically significant (p-value<0.05), except for the surface NO_3 vs. NPP relationship. Data from the IPSL-CM6A-LR model output.

equatorward cases they all decrease, while in the Canary poleward they all increase). In contrast, in the poleward portion of the Benguela there is an opposing trend between nanophytoplankton NPP, projected to increase from 0.8 to 1 μmol m^{-2} s^{-1}, and diatoms, projected to decrease from 0.16 to 0.08 μmol m^{-2} s^{-1}.

Figure 3.14 also shows the fraction of net primary productivity given by the two plankton functional types, and it is observed that nanophytoplankton are the dominant type across all regions. In the equatorward portion of the Canary system, nanophytoplankton NPP is about five times larger around 2020 and grows to seven times larger by 2100, while in the poleward Canary region, the ratio between nanophytoplankton and diatoms net primary productions decreases slightly, from about 3.5 in 2020 to 2.5 by 2100. The Benguela system shows a more pronounced imbalance: in the equatorward region, nanophytoplankton are seven times larger around 2020, increasing to 12 times by 2100, while in the poleward Benguela region, the ratio of nanophytoplankton over diatoms NPP goes from 5 to 13 times larger, which is a significant change in the relative concentrations of the two PFTs. Thus, the increasing trend in total net primary production in the Benguela poleward region is primarily driven by the rising NPP of nanophytoplankton, and it is not affected by the decreasing diatoms tendency.

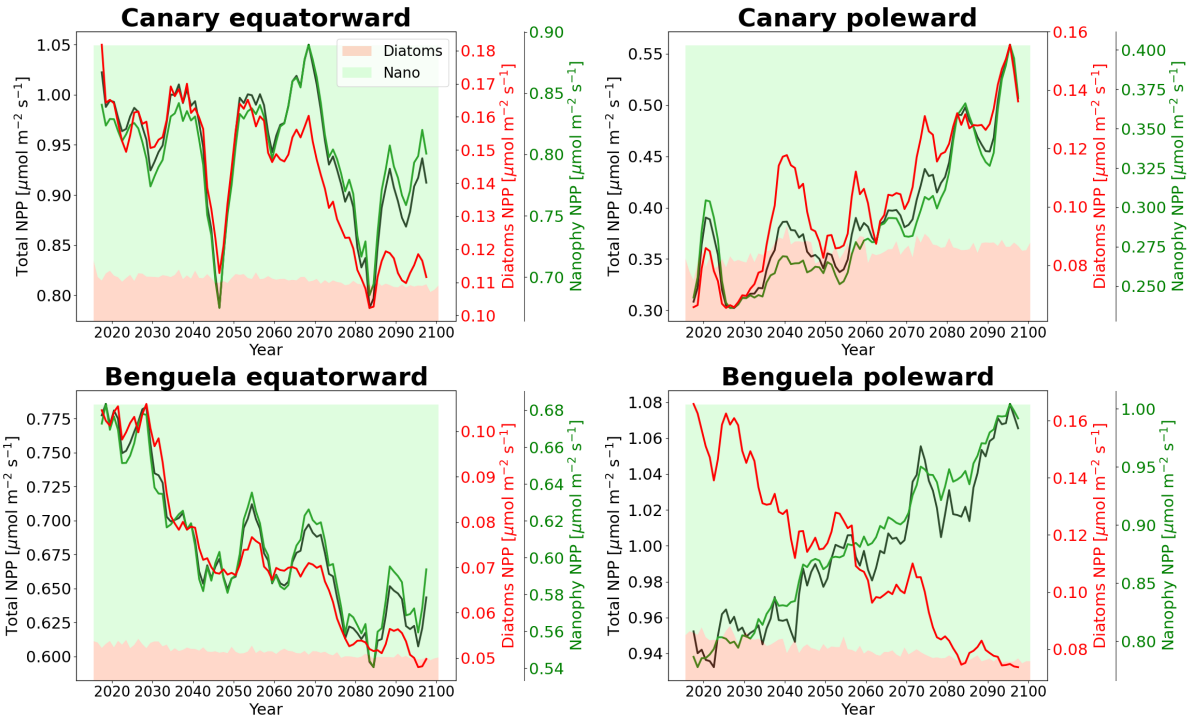

Figure 3.14: **Nanophytoplankton, diatoms and total net primary productivity for IPSL model (SSP5-8.5).** Time series of SSP5-8.5 IPSL-projected absolute values of total NPP (black), NPP by diatoms (red), and NPP by nanophytoplankton (green) in the equatorward and poleward halves of the Canary and Benguela regions. A 5-years smoothing was applied. In the background, the fractions of NPP by diatoms (light red) and by nanophytoplankton (light green).

There may be several reasons for this shift in the community structure. Different studies, such as Bopp et al. 2005 [113] or Marinov et al. 2010 [114], have highlighted how nutrient-depleted conditions in the surface ocean may favor small phytoplankton at the expense of diatoms. The latter tend to dominate the phytoplankton community when

growth conditions are optimal, while, where nutrients are depleted, smaller phytoplankton, with lower half-saturation coefficients, are favored.
In the poleward Benguela region, however, despite the projected decrease in NO_3 levels (both at the surface and in deeper waters), the nitrogen limitation factor[5] is projected to increase (less limitation), so nitrogen does not appear to be the cause of this trend.

This suggests that other factors could be more significant in driving community changes. The main investigation made in this study was on the role of silicates, whose lacking availability affects diatoms, the only phytoplankton functional type that requires this nutrient, and so may be badly affected by its scarcity.
However, analyzing the projected anomalies of silicates in these regions, no large explanations are found. In the poleward Benguela system, positive anomalies of silicates are projected, while a decrease would be expected if they were responsible for the projected diatoms reduction. Thus, it loos like silicates are not the responsible for the observed decrease in diatoms.

To conclude, the trends in net primary productivity and the nutrient dynamics in the Benguela poleward region require deeper investigation, due to the complex interplay between nutrient availability, phytoplankton community composition, and their respective nutrient utilization efficiencies. In the next section, another approach will shed more light on this question.

3.4 Growth rates decomposition

In this section, a quantitative approach is used to evaluate the different factors influencing NPP.
As already introduced, an expression for net primary productivity is: $NPP = P \times \mu$, where P is the phytoplankton biomass and μ is the growth rate. Therefore, NPP changes can be associated with variations in biomass P (which may be due to changes in the zooplankton grazing pressure) or with changes in the growth rates of phytoplankton.
Dealing with this last aspect, it is provided an evaluation of the relative importance of different factors on the growth rate variability.

A quantitative analysis of the limitation factors is made. Taking into account limitation of temperature, light and nitrogen (described in Section 2.4), time series of growth rates are examined. As explained in Section 2.5, the standard time series of growth rates are compared against three alternative time series that, in each case, have only one limiting factor allowed to vary according to its SSP5-8.5 projection, while the other two factors are held constant.
Figure 3.15 presents the resulting projections for diatom growth rates in the four systems, as modeled by the IPSL model under the SSP5-8.5 scenario.

[5]The nitrogen limitation factor does not only depend on nitrate (NO_3) but also on ammonium (NH_4).

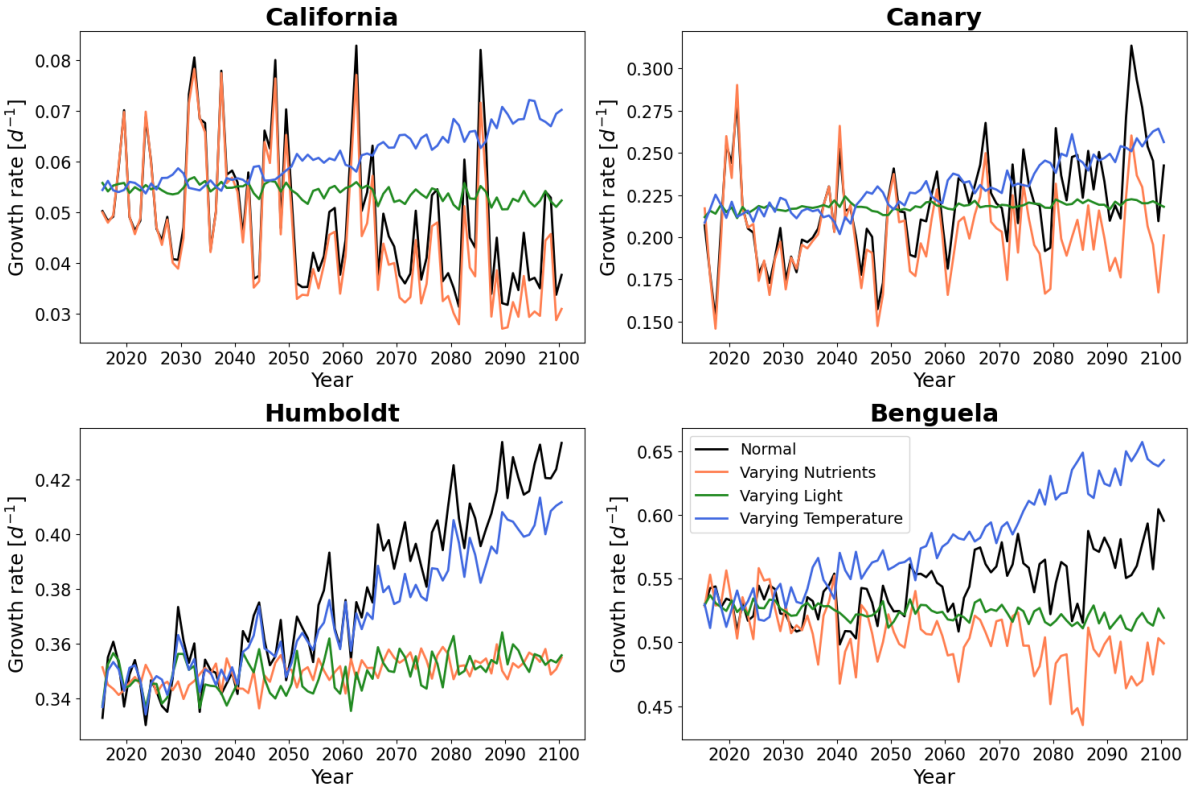

Figure 3.15: **Decomposition of diatom growth rate changes under SSP5-8.5 for IPSL model.** Time series of projected growth rates of diatoms under the SSP5-8.5 for the IPSL model in the four EBUS. Black lines are normal growth rates; orange, green, and blue lines are growth rates obtained allowing to vary respectively only nutrients, light, and temperature (according to their normal SSP5-8.5 projection), while keeping the other two factors fixed at their average value over the period 2015-2025.

The first consideration is that nutrient limitation has the greatest impact on growth rates across all four regions: the reduction of the growth rate is the strongest when there is only nutrient limitation, rather than when there is only light or temperature limitation. Moreover, in the California and Canary regions, nutrients can be identified as the primary drivers of changes in growth rates, as it is deduced from the significant resemblance between the normal and nutrient-varying growth rate time series, although the actual growth rates are higher due to the positive impact of temperature (which increases the rate almost linearly in response to global warming).
In contrast, **in the Benguela and Humboldt systems temperature is a central driver of NPP variability**, since temperature limitation shapes the final growth rate projections. In the Benguela region, temperature strongly determines the increasing trend in the growth rate, although interannual variability is mostly explained by the nitrogen factor. In the Humboldt system, temperature has an even stronger influence, determining the intense increasing trend and also affecting interannual variability.
The effect of increasing temperatures, in these systems, is of speeding up the metabolic processes, leading to a more efficient nutrient uptake. This allows for faster growth rates, even when nutrient availability is low.

It is noted that, among the four EBUS, the Benguela and Humboldt regions exhibit the highest growth rates, followed by the Canary region, and, lastly, the California region. The latter experiences significant nutrient limitation, resulting in much lower growth rates, approximately one order of magnitude smaller compared to the other regions. This limitation is responsible for the reduced productivity observed in this region. Specifically, the upwelling hotspot of the California region has an average historical NPP of $0.5\times10^{-6}\,\mathrm{mol\,m^{-2}s^{-1}}$, whereas the other regions have an average historical NPP about twice that amount. This result aligns with a previous study by Lachkar et al. 2011 [115], which compared the California and Canary current systems and highlighted that nutrient use efficiency may depend on topography and the degree of eddy activity, suggesting that the broader continental shelves and lower mesoscale activity in the Canary region contribute to longer residence times for upwelled waters, thus leading to a greater buildup of biomass.

Coming back to all the four EBUS, the analysis just presented for diatoms was conducted also for nanophytoplankton, which yielded similar results. However, the growth rates for these last ones were generally higher across all regions, a difference that is attributed to their greater capacity to adapt to unfavorable conditions.

Harking back to the analysis of Section 3.3.3, one interesting result, obtained using this growth rate decomposition, regards the poleward Benguela portion. In that region, where NPP was highlighted to be negatively correlated to 200m nitrates and not correlated to surface nitrates, the same approach was used. The decomposition of diatom and nanophytoplankton growth rate changes highlighted that, in that area, the most limiting factor is temperature: while in both portions of the Canary and in the equatorward Benguela, nitrates are the major limitation factor, given the good similarity between the normal and nutrient-varying growth rate time series, in the poleward Benguela the dominant influencing factor is temperature. This strong limiting role played by temperature, rather than by nutrients, may explain the unexpected linear relations between NPP and NO_3 concentrations at the two depths observed in Figure 3.13. However, a more complete understanding of this peculiar behavior and of the projected community shift should also investigate the changes in the recycling of nutrients in the euphotic zone and the variations of the zooplankton grazing pressure.

3.5 Overshoot scenario

Focusing on the scenarios SSP5-8.5 and SSP2-4.5, in the previous sections it was proved how hard it is to project the evolution of primary productivity, given the wide range of projected trajectories of ESMs of the ensemble. The issue becomes particularly relevant, and more complicated, when investigating reversibility of the changes.
To evaluate the response to mitigation strategies, it was employed the overshoot scenario

SSP5-3.4-OS, component of the ScenarioMIP introduced in section 2.1.

The ensemble available for the overshoot scenario comprises 8 members, a smaller set with respect to the previous one, which included 17 models for SSP5-8.5 and SSP2-4.5. This is a significant drawback because a smaller ensemble size increases the risk of model uncertainty, that is typically mitigated with a larger number of members.

Dealing with this new overshoot pathway, the first variable examined is the Global Mean Surface Temperature (GMST), since the knowledge of its evolution can provide direct and clear information on the severity of the climate crisis.
Similar to the projections of the previous sections, but now looking at a global level, Figure 3.16 illustrates the ensemble anomalies of GMST, comparing the SSP5-8.5 and the SSP5-3.4-OS.

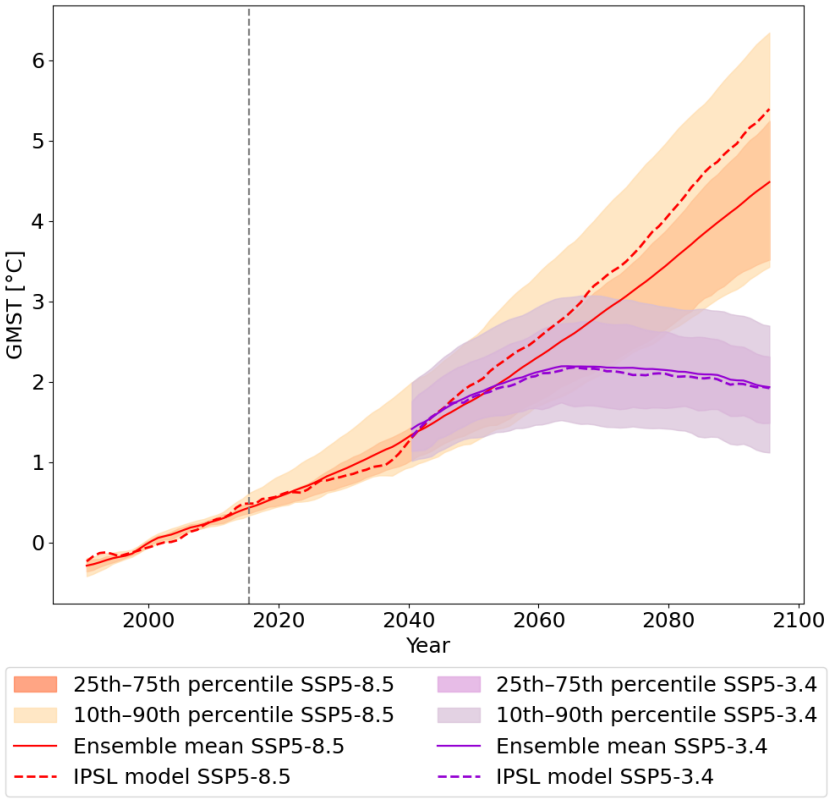

Figure 3.16: **Global Mean Surface Temperature anomalies: SSP5-8.5 vs. SSP5-3.4-OS Projections.** Projected twenty-first-century change in Global Mean Air Surface Temperature for SSP5-8.5 and SSP5-3.4-OS: solid lines are ensemble means, dashed lines are IPSL model; shaded regions indicate 25th–75th (darker shade) and 10th–90th percentile (lighter shade). A 10-year smoothing was applied.

Model agreement across both scenarios is strong, with ensemble spreads showing a range of around 1°C between the 25th and 75th percentiles, and of 2°C between the 10th and 90th percentiles, with the IPSL simulations aligning with the ensemble means.
Under the SSP5-8.5 scenario, all members project strong warming, with the ensemble

mean temperature reaching an anomaly of about 5°C by 2100. In contrast, under the SSP5-3.4-OS pathway, despite the emission reductions from 2040, the atmosphere keeps warming for about 25 more years. The ensemble mean exceeds the 2°C threshold around 2060, peaks around 2065, and only then it starts to slowly decrease, eventually falling back below the 2°C anomaly by 2090.
It should be noted that, due to the different sizes of the ensembles for the SSP5-8.5 and the SSP5-3.4-OS, the ensemble means of the two scenarios do not exactly coincide in the year 2040, even though the overshoot scenario directly branches off from SSP5-8.5 at that time.

After establishing the projected evolution of global mean surface temperature, a useful next step is to assess how other variables behave in response to specific levels of warming. Therefore, in this section, variables changes are presented in relation to GMST, rather than as time series.
Given the findings of the previous sections, which highlighted the peculiar behavior of NPP anomalies in the different portions of the Canary and Benguela regions, the overshoot projections of NPP, SST, and 200m NO_3 are presented for both the equatorward and poleward areas of these two systems. Due to limited availability of long time series data from other models, this analysis was conducted using only the IPSL simulations.
Moreover, a similar analysis was performed for the entire four EBUS regions, however those projections did not yield valuable insights into the understanding of the processes driving marine productivity changes. Rather, the focus on these specific areas helps to understand better the mechanisms influencing NPP variability.

Figure 3.17 presents the projected relative change in net primary productivity for the two scenarios, plotted against the GMST anomaly. The SSP5-8.5 scenario extends until 2100, while the SSP5-3.4-OS pathway continues up to 2200, providing a longer view on future evolution under non-monotonic forcing. In the SSP5-8.5 scenario, the findings of the previous section are confirmed: NPP decreases in the equatorward areas and increases in the poleward areas as GMST (that is linearly related with time) increases.
Instead, under SSP5-3.4-OS, a characteristic behavior emerges for the poleward and equatorward portions of these systems. In the poleward areas, both the Canary and the Benguela systems show reversibility in NPP changes. After the GMST exceeds the 2°C threshold (around 2060), NPP anomalies continue to rise for about 5 more years, peaking near 2065 at +20% in the Canary poleward and +6% in the Benguela poleward regions. After this, NPP reverses direction, gradually decreasing toward past levels. By 2200, with a GMST anomaly of around 1°C, NPP anomalies are approximately +10% in the Canary poleward and +2% in the Benguela poleward areas, values that were characterizing the system around the year 2040, when the overshoot scenario branched off the SSP5-8.5.
In contrast, the equatorward portions of the two systems show a different response, with strong intensification of NPP with respect to baseline values. In both cases, in the overshoot scenario, NPP shows a decreasing tendency (similar to the one of the SSP5-8.5)

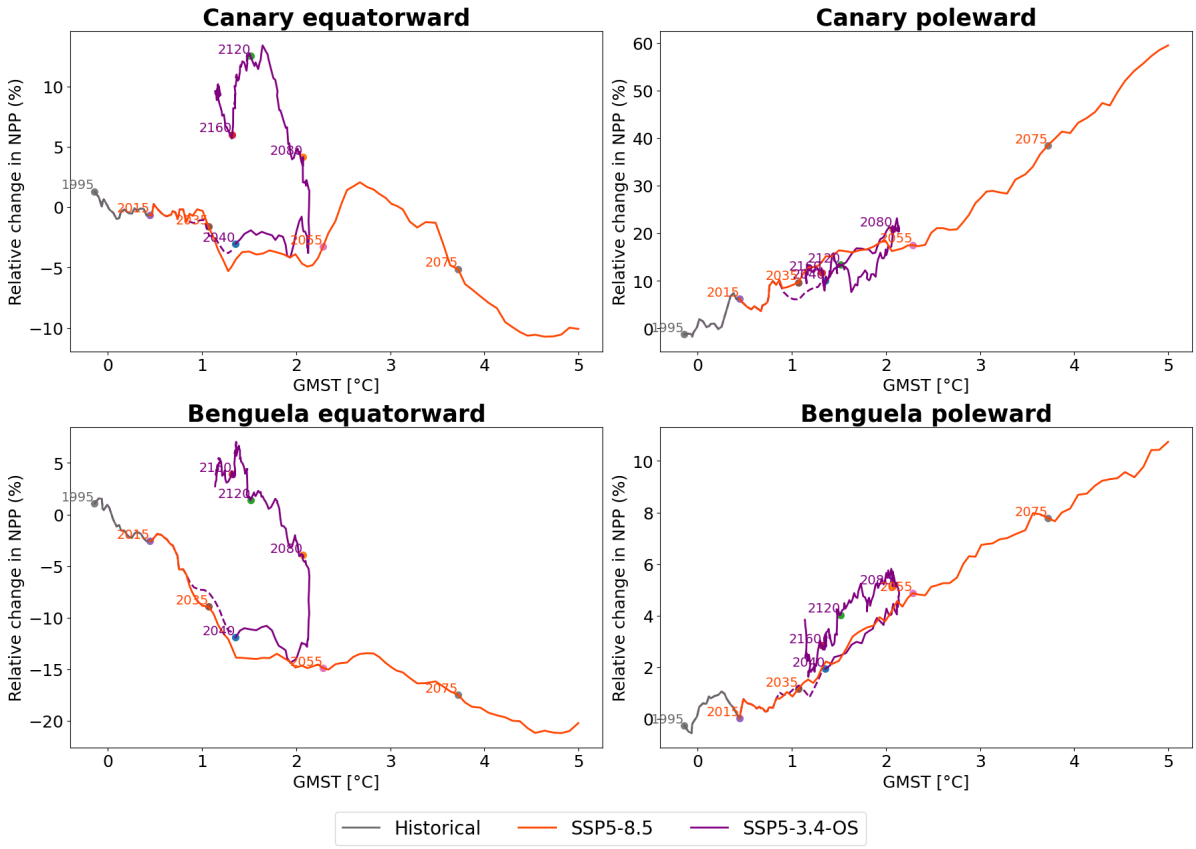

Figure 3.17: **Relative NPP change against GMST: SSP5-8.5 vs. SSP5-3.4-OS Projections.** IPSL projections of relative NPP changes for the equatorward and poleward halves of the Canary and Benguela regions are shown. The changes, relative to the baseline period 1985-2014, are plotted against GMST. Data for the SSP5-8.5 scenario (orange) are up to 2100, with the years indicated every 20 years, while data for the SSP5-3.4-OS scenario (purple) are up to 2200, with the years indicated every 40 years. A 10-year smoothing was applied.

until the GMST anomaly reaches 2°C. Then, around 2065, in the equatorward regions the trend changes. In the Canary case, NPP rises sharply, reaching a +10% anomaly by 2100 (with a GMST anomaly of about 1.5°C), followed by a slight decline over the next century. Similarly, the Benguela equatorward region experiences a strong rebound in NPP, that, increasing, returns to historical values by 2200 (with a GMST anomaly of around 1°C).
In both cases, the increase in relative NPP is more than 10% in only a hundred years, a very steep tendency, especially in the case of the Canary region.

These results can be compared with the already cited study by Heinze et al. 2023 [90], where NPP in the Arctic Ocean was studied under a mitigation scenario and was found to go back to past values, reversing the direction of change around 2065. In that study, the considered region of investigation was different, but the lag of the response of NPP in the overshoot scenario was the same. Thus, it can be confirmed that the lag of response of net primary production is of about 25 years after aggressive mitigation efforts are carried on.

Moreover, trying to understand the reasons of the different directions of anomalies observed in the two portions of the EBUS after the overshoot, the same analysis is performed on the drivers of NPP variability.

The first variable analyzed is sea surface temperature. Figure 3.18 presents the same type of plots as in Figure 3.17, but for SST. Under the SSP5-8.5 scenario, SST shows a consistent increase in all regions for increasing GMST and time. By the end of the 21st century, the Canary region experiences a SST anomaly of more than 3°C and of 2.5°C, respectively in its equatorward and poleward portions, while for the Benguela EBUS of about 4°C and almost 3°C, respectively in the equatorward and poleward portions. Instead, in the case of the SSP5-3.4-OS, in all the considered regions, SST shows re-

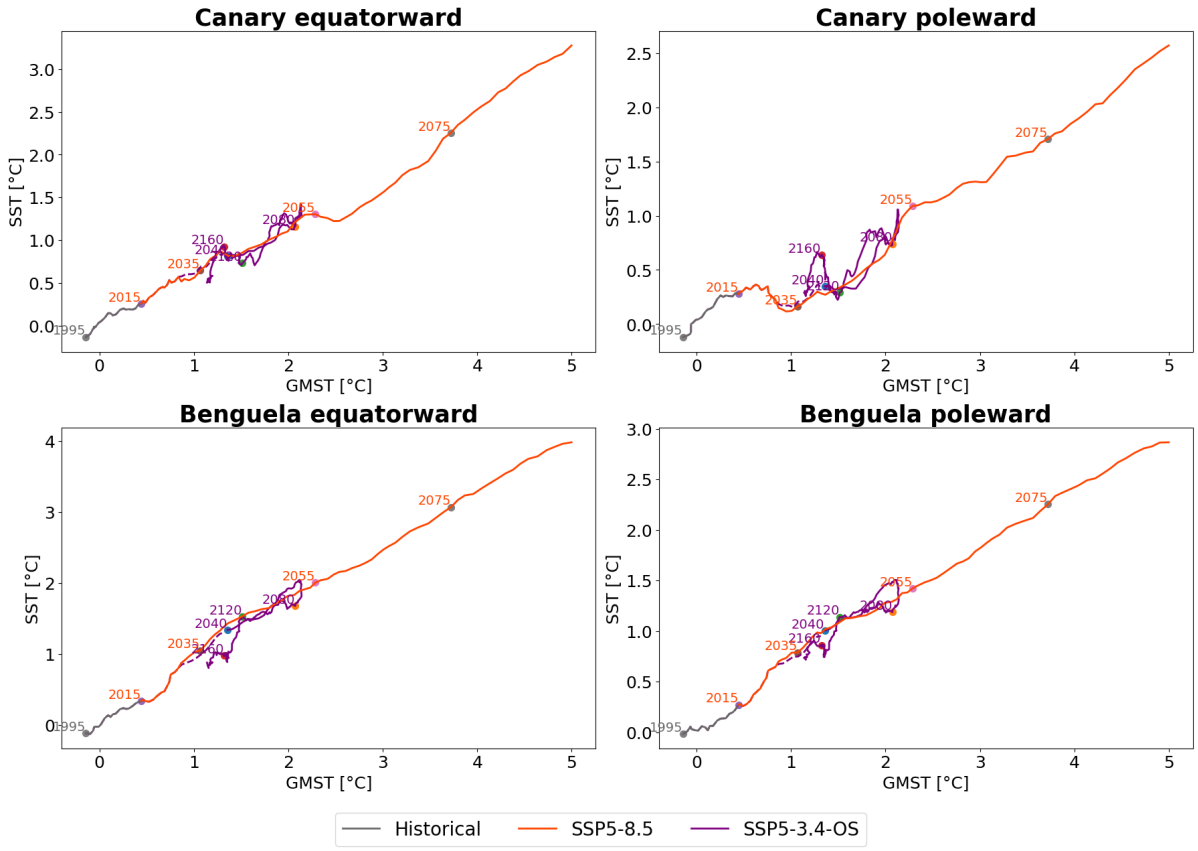

Figure 3.18: **SST change against GMST: SSP5-8.5 vs. SSP5-3.4-OS Projections.** IPSL projections of SST changes for the equatorward and poleward halves of the Canary and Benguela regions are shown. The changes, relative to the baseline period 1985-2014, are plotted against GMST. Data for the SSP5-8.5 scenario (orange) are up to 2100, with the years indicated every 20 years, while data for the SSP5-3.4-OS scenario (purple) are up to 2200, with the years indicated every 40 years. A 10-year smoothing was applied.

versibility: it keeps rising as GMST increases and until the latter reaches an anomaly of about 2.1°C (around 2070). After this point, as GMST begins to decrease, and SST follows suit, tracing backwards its previous pathway.

Hence, SST shows everywhere good reversibility: temperature of ocean surface tends to go back to past values under the overshoot scenario, with a lag of around 30 years after the onset of intense mitigation strategies in 2040.
This indicates that SST is not directly responsible for the behavior observed in the projected NPP, so other factors are probably driving the observed changes in NPP.

A similar analysis was performed also for the equatorward surface wind stress, but the resulting plots were quite noisy. No evidence of reversibility was observed in the changes of this variable in the considered regions, and the trajectories were difficult to interpret, offering little insight into the behavior of NPP across the different portions of the EBUS. Trying to understand this complexity, it was considered the study by Kim et al. 2023 [116], which explores the reversibility of the poleward Hadley cell expansion. The study suggests that under a carbon dioxide removal scenario, the Hadley cell does not return to its present-day state. Instead, it shows an asymmetric behavior between the two Hemispheres: in the Southern one, the HC edge shows a slower recovery and remains poleward of its current position, instead in the Northern Hemisphere, the HC edge recovers faster and shifts equatorward of its current position. This asymmetric behavior makes it complicated to interpret the impact of wind stress on NPP trends.

Rather, the investigation of subsurface nitrate levels provides interesting and straightforward results. Figure 3.19 illustrates the 200m NO_3 concentrations, investigated in the same way as the previous NPP analysis of Figure 3.17.
Under the SSP5-8.5 scenario, with increasing GMST over time, the Canary region exhibits a strong increase in subsurface NO_3 concentrations poleward (anomaly of +7 mmol m^{-3} by 2100), while a slight decrease is observed equatorward (about -0.25 mmol m^{-3} by the end of the 21st century); instead, in both the poleward and equatorward portions of the Benguela EBUS, subsurface nitrates are projected to decrease (respectively reaching by 2100 anomalies of -2 mmol m^{-3} and -1.5 mmol m^{-3}). These results well align with the findings of the previous sections on projected subsurface nitrates.
Dealing with the SSP5-3.4-OS, instead, the interesting result is that the plots show very similar patterns to the ones of relative NPP in Figure 3.17. In the poleward regions of both the Canary and Benguela systems, subsurface nitrate concentrations show reversibility: they initially follow the respective trends of SSP5-8.5 until the GMST anomaly of 2.1°C (around 2070), then concentrations reverse and retrace backwards the previous trajectory.
Instead, in the equatorward portions, the nitrate concentrations follow the SSP5-8.5 decreasing trend until the 2.1°C GMST anomaly, and afterwards they increase. In the equatorward Canary region, concentrations reach anomalies of approximately 1.5 mmol m^{-3} by the year 2180, while in the Benguela portion, nitrate levels rebound to historical values and slightly surpass them, with anomalies approaching 1 mmol m^{-3} by 2180.

Thus, NPP and NO_3 responses are characterized by a similar lag of 25-30 years after the emission reduction strategies actuation. The trajectories of both variables show large

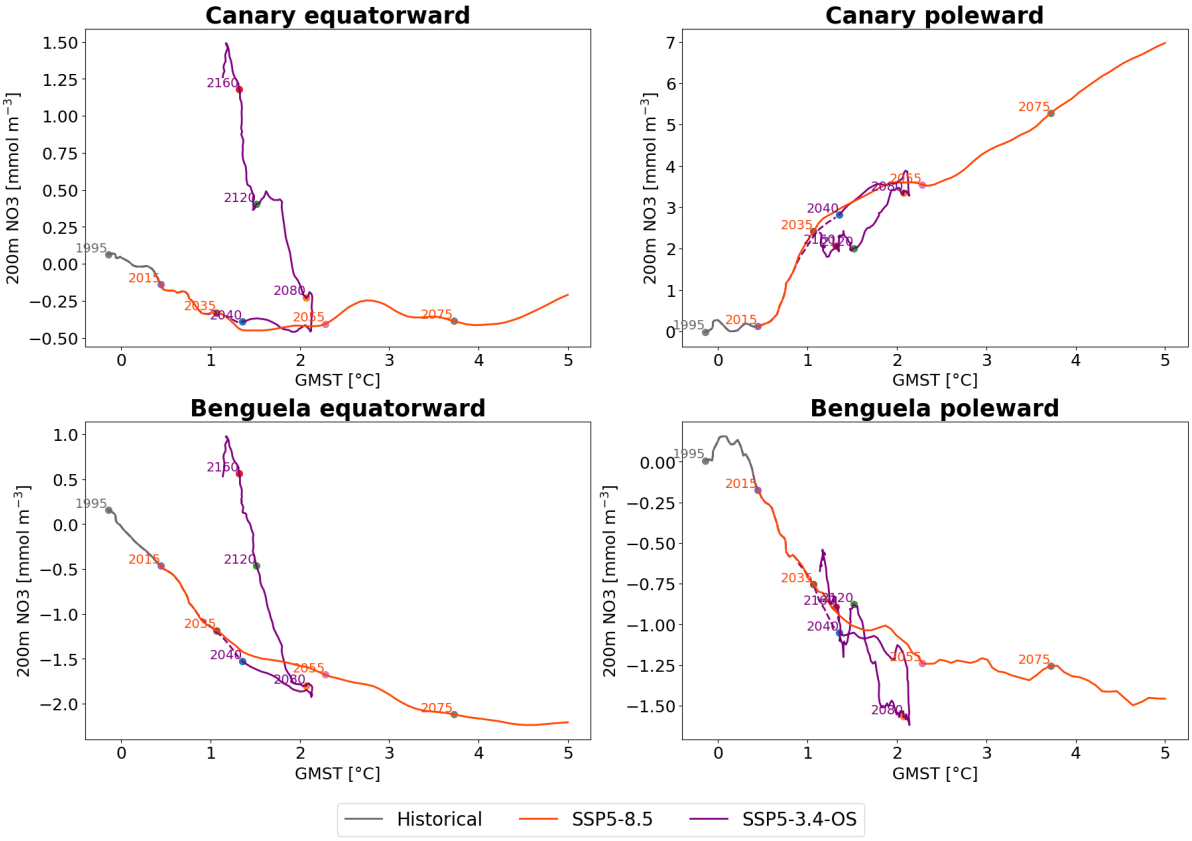

Figure 3.19: **200m NO_3 change against GMST: SSP5-8.5 vs. SSP5-3.4-OS Projections.** IPSL projections of 200m NO_3 changes for the equatorward and poleward halves of the Canary and Benguela regions are shown. The changes, relative to the baseline period 1985-2014, are plotted against GMST. Data for the SSP5-8.5 scenario (orange) are up to 2100, with the years indicated every 20 years, while data for the SSP5-3.4-OS scenario (purple) are up to 2200, with the years indicated every 40 years. A 10-year smoothing was applied.

differences between poleward and equatorward regions. **In the poleward areas, NPP and 200m NO_3 exhibit strong reversibility**, almost tracing backwards their previous trajectories. In contrast, **the equatorward regions show significant increases in both variables**: in the Benguela system, net primary productivity and nitrate levels rebound back to historical values, while in the Canary system, they increase substantially above the historical values.

These projections shed light on the causal mechanisms driving NPP in these ecosystems: subsurface nitrates play a central role in shaping surface phytoplankton dynamics, given the similarities of the plots in Figures 3.17 and 3.19, which suggest that increased concentrations in subsurface waters can significantly enhance marine production.
Since the upwelling-favorable wind stress projections under the overshoot scenario did not explain the projected changes of relative NPP, it can be concluded that under this SSP5-3.4-OS, the major driver of primary productivity variability is the change in the subsurface nitrate concentrations.

These results were compared to the study by John et al. 2015 [91], that, using a ramp-up and ramp-down scenario, found a similar pattern of increased NPP levels above contemporary means after the implementation of mitigation strategies.
That study attributed this unexpected increase in NPP to a deeper mixing in the ocean: during the ramp-down phase the surface temperatures cool more rapidly, while the deeper ocean continues to warm due to its thermal inertia. The resulting increased temperature gradient leads to enhanced mixing in a deeper mixed layer, process that brings more nitrates from deeper waters to the surface, inducing higher productivity.
In particular, the study highlighted that the subtropics have the largest relative primary productivity amplifications under climate mitigation due to this kind of process.

This amplification in the subtropics could explain the strong increase in NPP observed only in the equatorward portions of EBUS and not in the poleward ones. However, this remains a hypothesis, and several factors need consideration. In the EBUS regions, major driver of surface nutrient levels is upwelling, rather than the vertical mixing caused by temperature gradients between surface and deeper waters. Moreover, as past literature suggests, upwelling in EBUS may counteract the warming effect by bringing cold, deep water to the surface. This could slow the subsurface warming in response to climate change, reducing the temperature gradient and thereby limiting vertical mixing.

A precise quantification of the impact of these processes in the overshoot scenario remains an open challenge, and potentially interesting findings may yield from analysing changes in upwelling strength, vertical temperature gradients, and mixed layer depth.
Future and more detailed studies on this topic should focus on these dynamical processes, on subsurface ocean currents and on biogeochemical processes that may alter nitrate concentrations of deep reservoirs. In this way a more quantitative overview on future changes in nutrients concentrations, found to be major drivers of NPP under the overshoot scenario, would be obtained.

Chapter 4

Future work and open questions

As highlighted in the development of the thesis, diagnosing changes in net primary productivity in upwelling systems is a challenging issue. The complexity arises from the multitude of interacting factors, both dynamical and biogeochemical, which include feedbacks operating on different time and spatial scales.
This chapter illustrates the main limitations of the study, highlighting the difficulties encountered during the analysis and suggesting possible solutions to adopt for future investigations.

4.1 Biogeochemical aspects

To get reliable projections of future climate variables, enhancing the biorealism of Earth System Models is crucial. Accurate models must effectively simulate biological processes (like photosynthesis, respiration, and nutrient uptake), biogeochemical cycles, and the dynamics, interactions, and biodiversity of organisms, in order to get a comprehensive view of the ecosystem.
One shortcoming of this study is the disproportionate importance given to nitrogen among all nutrients. This analysis only evaluated the limiting role of nitrogen on phytoplankton productivity, since it is globally the dominant limiting macronutrient, however other nutrients might also be important drivers of NPP evolution in the EBUS regions. For instance, as explained previously, silicates are essential for the life of diatoms, so variations in their concentrations could impact their populations. In addition, other nutrients like phosphorus, iron, or ammonium should be investigated to get a complete overview. Future studies should adopt a more comprehensive approach, evaluating also co-limitations of nutrients [117] and making full budgets of them, for example analyzing fluxes using a box model, similarly to what has been done for oxygen by Bopp et al. 2002 [109].

Another weakness of this study is that it did not analyse the role of zooplankton. As highlighted in studies such as Le Quéré et al. 2016 [118], zooplankton are essential in their relationship with phytoplankton, because they regulate the marine carbon cycle, influencing export production below the surface mixed layer and the remineralization

and recycling of organic matter in the upper ocean. Therefore, considering the grazing pressure on different phytoplankton species by zooplankton is important, as well as analysing the resulting food-web dynamics.
In particular, past studies suggest that the global response of phytoplankton productivity decrease may amplify throughout the trophic food web [119], with more dramatic responses at higher trophic levels [120].
Therefore, due to the role of phytoplankton as base of the oceanic food chain, future studies should focus on the implications of thier changes on higher trophic levels. Assessing quantitatively the impact in the EBUS regions and evaluating the possibility of trophic cascades is essential, because of the important environmental, but also social and economic, service supported by the regions.
To do this, a useful approach would be the coupling with a high trophic level model like APECOSM (see Duponet al. 2022 [121]), in order to represent marine animals in Earth System Models and get a better understanding about the potential for climate change effects to intensify as they move up the marine food web.

4.2 Observations

This study only analyzed output data from model simulations of Earth System Models, neglecting observations. However, comparing these ones with historical simulations may be valuable for assessing the accuracy of models, identifying gaps in the understanding of the mechanisms driving net primary productivity, and potentially improving model algorithms and the represented processes.
The issue is that, when it comes to phytoplankton, observations generally provide reliable information only on biomass, which is measured from space by analyzing chlorophyll concentrations looking at ocean color. Observing net primary production, instead, is more complex, and there are significant uncertainties related to its observations predating satellite remote sensing.
Quantitatively measuring NPP involves using algorithms that combine satellite measurements of chlorophyll (from sensors like the Moderate Resolution Imaging Spectroradiometer, MODIS, and the Sea-viewing Wide Field-of-view Sensor, SeaWiFS) with incident light data and descriptions of phytoplankton physiology. Different algorithms have been developed for this purpose. For instance, Kwiatkowski et al. 2017 [122] compared four different algorithms over the SeaWiFS satellite record: the Vertically Generalised Production Model (VGPM), the Carbon-based Production Model (CbPM), the Marra model, and the Carr model. However, these algorithms often produce contrasting results, and there is still no consensus on the best way to estimate NPP, with no agreement on global trends over the past century.
Additionally, evaluating the impact of climate change on NPP from observations is challenging because the time series of data often show discontinuities and are too short (satellite observations have only been available since 1997) to differentiate between anthropogenic impacts and natural variability.

Furthermore, comparing model outputs with observations has inherent limitations, since models that perform well today may not be suitable in the future due to possible changes in processes and emergence of newly important drivers of NPP. These factors might not be well-parameterized in present models, and since they are not currently the primary drivers of NPP changes, their influence may not yet be evident. As these new factors become more significant, the accuracy and reliability of existing models may decline.

4.3 Spatial resolution

In the process of understanding the drivers of NPP changes, one challenge was that the main model used, IPSL-CM6A-LR, is coarse, with a resolution of 1° (NEMO-PISCES in the ORCA1 configuration). This low-resolution global model was chosen over a high-resolution regional one because the processes influencing NPP do not occur only at a local level, but also at a larger scale. For instance, it was described how global atmospheric circulation changes associated with the expansion of the Hadley cell can influence upwelling strength. Additionally, subsurface dynamics, such as currents and circulation processes, may affect nutrient concentrations in the subsurface stock.

However, while a global model is necessary to account for these large-scale processes, smaller-scale phenomena like mesoscale eddies, coastal undercurrents, tides or sediments processes may not be resolved with a 1° resolution. Ideally, global high-resolution models would be used, but this is currently too expensive computationally, given the long time series and large number of models required for this study. Moreover, less models in the ensemble are available at a high resolution. Future analyses may attempt to couple the low-resolution model with a higher-resolution one, possibly using NEMO-PISCES at a resolution of 0.25°, or by integrating a regional high-resolution model such as CROCO [123], which is designed for regional configurations and fine scales analysis.

4.4 Projection uncertainty

As introduced in 2.3, when analyzing outputs of scenario simulations from Earth System Models, different sources can contribute to increase the uncertainty of the projection. In this study, the **scenario uncertainty** was addressed by exploring different trajectories of plausible futures based on human activities and policy decisions, focusing on the scenarios SSP5-8.5, SSP2-4.5, and SSP5-3.4-OS.

Internal variability was found to be the dominant source of uncertainty in most coastal large marine ecosystems over the next few decades [124], therefore, when looking at the Eastern Boundary Upwelling Systems, it becomes crucial to quantitatively assess its impact. One approach to distinguish internal variability from the human-induced is using large ensembles, that can better capture the range of possible outcomes due to inherent randomness within the climate system [125].
However, in this thesis, the data used were the outputs of single simulations for each

model: as explained in section 2.4, even if multiple simulations were available, for each model of the ensemble, only the first member was considered (usually `r1i1p1f1`). In this way it was not considered the potential impact of initial conditions in the evolution of the different variables, which may be strongly determining. Using a large ensemble approach and considering all the available simulations from the Earth System Models may help to capture the range of possible outcomes due to the inherent randomness within the climate system.

To address **model uncertainty**, a common approach is to use multi-model ensembles. In this study, the CMIP6 one was adopted, and the attention was put on the IPSL-CM6A-LR member. Comparing the behavior of the latter with the other models helps to identify the causes of its different projections and to evaluate its sensitivity to processes that may occur at different spatial and time scales, which may be parametrized differently. For instance, as previously explained, the diverse parametrisation of nitrogen fixation in the IPSL-CM6A-LR model has a huge impact on projections of NPP globally, leading to projected increasing trends that significantly differ from most of the other ensemble members. An effective method to assess this type of uncertainty, as demonstrated in [108], is to compare two versions of the same model to understand the effects of recent modifications in the model.
In future research, it would be ideal to apply this approach to Eastern Boundary Upwelling Systems with the global models IPSL-CM5A-LR and IPSL-CM6A-LR. The comparison would help quantify the contribution of nitrogen fixation by diazotrophy originating from the oligotrophic waters of central ocean gyres, since the investigation conducted by now only evaluated local fixation, neglecting potential sources from outside of the EBUS.

4.5 Natural variability

As introduced in section 1.3.1, variability of marine ecosystems is driven by the combination of natural and anthropogenic forcings. Through interannual or decadal modes, it can superimpose and alter the impacts of anthropogenic changes.
Unfortunately, it is hard to differentiate between variability associated to natural low-frequency modes such as the already mentioned El Niño-Southern Oscillation (ENSO), Pacific Decadal Oscillation (PDO), North Pacific Gyre Oscillation (NPGO), North Atlantic Oscillation (NAO), Atlantic Multidecadal Oscillation (AMO), and human-induced changes, due to the possible superimposition of effects and alterations that climate change may have on natural variability.

One possible approach would be running simulations over longer periods (of centuries or more) to establish a more solid baseline against which changes due to anthropogenic influences can be detected. However, this distinction requires long-term observations that are not available, moreover the data from the fishery sector are mostly limited to

commercial species and often overlook some aspects of variability in the trophic chain. In future, it will be auspicious to be able to recognize the specific impact of anthropogenic climate change on the regions of interest.

Chapter 5

Conclusions

This thesis analysed the potential evolution of marine primary productivity in the Eastern Boundary Upwelling Systems under climate change. These regions were shown to play a disproportionately significant role in global ocean productivity, providing crucial ecosystem services to human society. However, the present comprehension of future net primary productivity evolution is still partial and a quantitative evaluation of its drivers is still missing. This study used simulations of different scenarios (SSP5-8.5, SSP2-4.5, and SSP5-3.4-OS) from many Earth Systems Models of the CMIP6 ensemble, with a focus on IPSL-CM6A-LR, the latest model by the IPSL institute.

Considerable uncertainties were found to characterize net primary productivity projections, with the ensemble members showing limited consensus and barely agreeing on the sign of the changes. The IPSL model generally aligns, in the various systems, to the ensemble means, while in the Canary region, it stands out from the majority of the models projecting significant NPP increases particularly under the SSP5-8.5.

To explain the projected patterns of net primary productivity, IPSL-CM6A-LR was mostly used, providing a comprehensive analysis of the different potential drivers. While previous studies mainly focused on upwelling variations driven by wind changes, this research examined also the critical roles of subsurface nutrients and temperature. For each specific Eastern Boundary Upwelling System, the response to climate change was found to be influenced by a combination of factors, with their overall variations shaping the future trajectory of NPP in each system.

By analyzing the growth rates under the SSP5-8.5, and decomposing it to quantify the influence of each limiting factor, it was highlighted that temperature is a major driver in the Humboldt EBUS, with a significant role played in the Benguela system as well. In such regions, warmer waters can influence the growth rates by accelerating the metabolic processes, making more efficient the nutrient uptake; this can act to offset the nutrient limitation, allowing organisms to make a more efficient use of the available resources. The Benguela system was found to be influenced also by nutrient limitation, which is the dominant limitation factor in the California and Canary EBUS.

Focusing on the mechanisms driving changes in nutrient availability, this study considered the influence of upwelling-favorable winds and of subsurface nutrient concentrations. In the case of winds, the analysis of alongshore equatorward wind stress led to the rejection of Bakun's (1990) theory, which proposed that the global warming-induced intensification of alongshore winds would enhance net primary production. This theory is insufficient to explain the projected latitude-dependent behavior of NPP changes. Instead, this thesis confirmed Rykaczewski's and Bograd's hypotheses of poleward intensification of coastal upwelling-favorable winds associated to the poleward migration of the major atmospheric high-pressure cells due to global warming. Using a comparative analysis, this wind pattern was found to significantly shape NPP across all four Eastern Boundary Upwelling Systems, particularly the Humboldt and Benguela regions. In the Canary and California region, in addition to wind effects, subsurface nitrate levels also played a crucial role.

A correlative analysis highlighted almost everywhere positive correlations between NPP and both surface and 200m nitrate concentrations, therefore corroborating the hypothesis of the large influence played by nutrients in sustaining productivity. However, in the poleward portion of the Benguela EBUS, an unexpected lack of correlation was found between anomalies of surface nitrate concentrations and NPP, and a negative correlation between anomalies of subsurface nitrate concentrations and NPP. The reasons for this behavior were explored evaluating the community composition, projected to shift toward a dominance of nanophytoplankton at the expense of diatoms, and the temperature limitation, which emerged as a key factor limiting productivity there. Other potential explanations, including limitations of silicate availability and increased zooplankton grazing pressure, were also proposed, but the question remains open.

Moreover, the analysis of net primary productivity projections under the SSP5-3.4-OS scenario highlighted the central role of nitrates in shaping surface phytoplankton dynamics. Posing the problem of reversibility and revealing a similar lag of NPP and subsurface nitrates in the response to mitigation strategies (25-30 years), the overshoot-projections revealed a precise resemblance of the two variables in the equatorward and poleward portions of the Canary and Benguela EBUS. Particularly, the poleward areas show good reversibility toward past values, while the equatorward areas are characterized by steep increases, in the Canary case to values much higher than the historical ones. To explain these patterns, some hypotheses were presented, but the precise cause is still to be understood.

Overall, this study tried to find out the drivers of net primary productivity in the different Eastern Boundary Upwelling Systems: a gap in the current understanding of the mechanisms driving net primary productivity changes in the coastal upwelling regions was identified, with dynamical and biogeochemical processes yet to be fully explored.
Future analyses on this question will take into account even more mechanisms, which

may operate at many scales, so the integration of low-resolution global models with high-resolution local ones will be necessary. Moreover, it will be necessary to quantify the impact of each driver, distinguishing between anthropogenic effects and natural variability, and to determine the role of zooplankton grazing pressure and the implications for higher trophic levels. Considering the environmental, social, and economic value of the Eastern Boundary Upwelling Systems, this deeper understanding will be crucial for adapting to and mitigating the urgent climate challenges.

Bibliography

[1] Samar Khatiwala, Toste Tanhua, S Mikaloff Fletcher, Markus Gerber, Scott C Doney, Heather D Graven, Nicolas Gruber, GA McKinley, Akihiko Murata, AF Ríos, et al. "Global ocean storage of anthropogenic carbon". In: *Biogeosciences* 10.4 (2013), pp. 2169–2191.

[2] Jorge L Sarmiento. *Ocean biogeochemical dynamics*. Princeton university press, 2006.

[3] Lester Kwiatkowski, Olivier Torres, Laurent Bopp, Olivier Aumont, Matthew Chamberlain, James R Christian, John P Dunne, Marion Gehlen, Tatiana Ilyina, Jasmin G John, et al. "Twenty-first century ocean warming, acidification, deoxygenation, and upper-ocean nutrient and primary production decline from CMIP6 model projections". In: *Biogeosciences* 17.13 (2020), pp. 3439–3470.

[4] Steven J Bograd, Michael G Jacox, Elliott L Hazen, Elisa Lovecchio, Ivonne Montes, Mercedes Pozo Buil, Lynne J Shannon, William J Sydeman, and Ryan R Rykaczewski. "Climate change impacts on eastern boundary upwelling systems". In: *Annual Review of Marine Science* 15.1 (2023), pp. 303–328.

[5] Marina Lévy, Damien Couespel, Clément Haëck, Madhavan Girijakumari Keerthi, Inès Mangolte, and Channing J Prend. "The impact of fine-scale currents on biogeochemical cycles in a changing ocean". In: *Annual Review of Marine Science* 16.1 (2024), pp. 191–215.

[6] NASA Earth Observatory. *Importance of phytoplankton*. https://earthobservatory.nasa.gov/features/Phytoplankton/page2.php. Accessed: [Your access date].

[7] Nathalie Simon, Anne-Lise Cras, Elodie Foulon, and Rodolphe Lemée. "Diversity and evolution of marine phytoplankton". In: *Comptes rendus biologies* 332.2-3 (2009), pp. 159–170.

[8] C. L. de La Rocha and U. Passow. "The biological pump". In: *Treatise on geochemistry*. Vol. 6. 2006, pp. 83–111.

[9] Morten H Iversen. "Carbon export in the ocean: a biologist's perspective". In: *Annual Review of Marine Science* 15.1 (2023), pp. 357–381.

[10] Michael R Stukel, John P Irving, Thomas B Kelly, Mark D Ohman, Christian K Fender, and Natalia Yingling. "Carbon sequestration by multiple biological pump pathways in a coastal upwelling biome". In: *Nature Communications* 14.1 (2023), p. 2024.

[11] Nicole Dubilier, Claudia Bergin, and Christian Lott. "Symbiotic diversity in marine animals: the art of harnessing chemosynthesis". In: *Nature Reviews Microbiology* 6.10 (2008), pp. 725–740.

[12] Kristen R Hunter-Cevera, Michael G Neubert, Robert J Olson, Andrew R Solow, Alexi Shalapyonok, and Heidi M Sosik. "Physiological and ecological drivers of early spring blooms of a coastal phytoplankter". In: *Science* 354.6310 (2016), pp. 326–329.

[13] Jan Taucher and Andreas Oschlies. "Can we predict the direction of marine primary production change under global warming?" In: *Geophysical Research Letters* 38.2 (2011).

[14] Scott C Doney. "Plankton in a warmer world". In: *Nature* 444.7120 (2006), pp. 695–696.

[15] Elliot Sherman, J Keith Moore, Francois Primeau, and David Tanouye. "Temperature influence on phytoplankton community growth rates". In: *Global Biogeochemical Cycles* 30.4 (2016), pp. 550–559.

[16] James H Brown, James F Gillooly, Andrew P Allen, Van M Savage, and Geoffrey B West. "Toward a metabolic theory of ecology". In: *Ecology* 85.7 (2004), pp. 1771–1789.

[17] Marco Steinacher, Fortunat Joos, TL Frölicher, L Bopp, P Cadule, Valentina Cocco, SC Doney, M Gehlen, Keith Lindsay, JK Moore, et al. "Projected 21st century decrease in marine productivity: a multi-model analysis". In: *Biogeosciences* 7.3 (2010), pp. 979–1005.

[18] Michael J Behrenfeld, Robert T O'Malley, David A Siegel, Charles R McClain, Jorge L Sarmiento, Gene C Feldman, Allen J Milligan, Paul G Falkowski, Ricardo M Letelier, and Emmanuel S Boss. "Climate-driven trends in contemporary ocean productivity". In: *Nature* 444.7120 (2006), pp. 752–755.

[19] Brenda Côté and Trevor Platt. "Day-to-day variations in the spring-summer photosynthetic parameters of coastal marine phytoplankton". In: *Limnology and Oceanography* 28.2 (1983), pp. 320–344.

[20] C Garcia-Soto, I De Madariaga, F Villate, and E Orive. "Day-to-day variability in the plankton community of a coastal shallow embayment in response to changes in river runoff and water turbulence". In: *Estuarine, Coastal and shelf science* 31.3 (1990), pp. 217–229.

[21] Michael J Behrenfeld, James T Randerson, Charles R McClain, Gene C Feldman, Sietse O Los, Compton J Tucker, Paul G Falkowski, Christopher B Field, Robert Frouin, Wayne E Esaias, et al. "Biospheric primary production during an ENSO transition". In: *Science* 291.5513 (2001), pp. 2594–2597.

[22] Harald U Sverdrup. "On conditions for the vernal blooming of phytoplankton". In: *J. Cons. Int. Explor. Mer* 18.3 (1953), pp. 287–295.

[23] Michele D DuRand, Robert J Olson, and Sallie W Chisholm. "Phytoplankton population dynamics at the Bermuda Atlantic Time-series station in the Sargasso Sea". In: *Deep Sea Research Part II: Topical Studies in Oceanography* 48.8-9 (2001), pp. 1983–2003.

[24] Vamara Koné, Olivier Aumont, Marina Lévy, and Laure Resplandy. "Physical and biogeochemical controls of the phytoplankton seasonal cycle in the Indian Ocean: A modeling study". In: *Indian Ocean biogeochemical processes and ecological variability* 185 (2009), p. 350.

[25] ISIMIP. *ISIMIP Output Data Repository*. URL: https://www.isimip.org/outputdata/isimip-repository/.

[26] D. L. Mackas, P. T. Strub, A. Thomas, and V. Montecino. "Eastern ocean boundaries pan-regional overview". In: *The Sea* 14 (2006), pp. 21–59.

[27] Priscilla Le Mezo, Stelly Lefort, Roland Seferian, Olivier Aumont, Olivier Maury, Raghu Murtugudde, and Laurent Bopp. "Natural variability of marine ecosystems inferred from a coupled climate to ecosystem simulation". In: *Journal of Marine Systems* 153 (2016), pp. 55–66.

[28] Roland Séférian, Aurélien Ribes, and Laurent Bopp. "Detecting the anthropogenic influences on recent changes in ocean carbon uptake". In: *Geophysical Research Letters* 41.16 (2014), pp. 5968–5977.

[29] Michael G Jacox, Steven J Bograd, Elliott L Hazen, and Jerome Fiechter. "Sensitivity of the California Current nutrient supply to wind, heat, and remote ocean forcing". In: *Geophysical Research Letters* 42.14 (2015), pp. 5950–5957.

[30] Fanny Chenillat, Pascal Rivière, Xavier Capet, Emanuele Di Lorenzo, and Bruno Blanke. "North Pacific Gyre Oscillation modulates seasonal timing and ecosystem functioning in the California Current upwelling system". In: *Geophysical Research Letters* 39.1 (2012).

[31] Thomas E Cropper, Edward Hanna, and Grant R Bigg. "Spatial and temporal seasonal trends in coastal upwelling off Northwest Africa, 1981–2012". In: *Deep Sea Research Part I: Oceanographic Research Papers* 86 (2014), pp. 94–111.

[32] Patrick Marchesiello and P Estrade. "Upwelling limitation by onshore geostrophic flow". In: (2010).

[33] Luis Bravo, Marcel Ramos, Orlando Astudillo, Boris Dewitte, and Katerina Goubanova. "Seasonal variability of the Ekman transport and pumping in the upwelling system off central-northern Chile (30° S) based on a high-resolution atmospheric regional model (WRF)". In: *Ocean Science* 12.5 (2016), pp. 1049–1065.

[34] Ryan R Rykaczewski, John P Dunne, William J Sydeman, Marisol García-Reyes, Bryan A Black, and Steven J Bograd. "Poleward displacement of coastal upwelling-favorable winds in the ocean's eastern boundary currents through the 21st century". In: *Geophysical Research Letters* 42.15 (2015), pp. 6424–6431.

[35] Marisol García-Reyes, William J Sydeman, David S Schoeman, Ryan R Rykaczewski, Bryan A Black, Albertus J Smit, and Steven J Bograd. "Under pressure: Climate change, upwelling, and eastern boundary upwelling ecosystems". In: *Frontiers in Marine Science* 2 (2015), p. 109.

[36] Lynne D Talley. *Descriptive physical oceanography: an introduction*. Academic press, 2011.

[37] Denise Breitburg, Lisa A Levin, Andreas Oschlies, Marilaure Grégoire, Francisco P Chavez, Daniel J Conley, Véronique Garçon, Denis Gilbert, Dimitri Gutiérrez, Kirsten Isensee, et al. "Declining oxygen in the global ocean and coastal waters". In: *Science* 359.6371 (2018), eaam7240.

[38] RCJ Dugdale. "Nutrient limitation in the sea: Dynamics, identification, and significance 1". In: *Limnology and Oceanography* 12.4 (1967), pp. 685–695.

[39] RC Dugdale and JJ Goering. "Uptake of new and regenerated forms of nitrogen in primary productivity 1". In: *Limnology and oceanography* 12.2 (1967), pp. 196–206.

[40] Monique Messié, Jesus Ledesma, Dorota D Kolber, Reiko P Michisaki, David G Foley, and Francisco P Chavez. "Potential new production estimates in four eastern boundary upwelling ecosystems". In: *Progress in Oceanography* 83.1-4 (2009), pp. 151–158.

[41] Zhiyan Chen, Tianyi Nie, Xin Zhao, Jiwei Li, Bin Yang, Dongyang Cui, and Xinxin Li. "Organic carbon remineralization rate in global marine sediments: A review". In: *Regional Studies in Marine Science* 49 (2022), p. 102112.

[42] Boris Dewitte, J Vazquez-Cuervo, Katerina Goubanova, Serena Illig, Ken Takahashi, Gildas Cambon, Sara Purca, D Correa, Dimitri Gutiérrez, Abdel Sifeddine, et al. "Change in El Niño flavours over 1958–2008: Implications for the long-term trend of the upwelling off Peru". In: *Deep Sea Research Part II: Topical Studies in Oceanography* 77 (2012), pp. 143–156.

[43] Daniel Pauly and Villy Christensen. "Primary production required to sustain global fisheries". In: *Nature* 374.6519 (1995), pp. 255–257.

[44] Ove Hoegh-Guldberg, Rongshuo Cai, Elvira S Poloczanska, Peter G Brewer, Svein Sundby, Karim Hilmi, Victoria J Fabry, Sukgeun Jung, William Skirving, Dáithí A Stone, et al. "The ocean". In: (2014).

[45] Sea Around Us. *Sea Around Us*. https://www.seaaroundus.org/.

[46] Rui Seabra, Rubén Varela, António M Santos, Moncho Gómez-Gesteira, Claudia Meneghesso, David S Wethey, and Fernando P Lima. "Reduced nearshore warming associated with eastern boundary upwelling systems". In: *Frontiers in Marine Science* 6 (2019), p. 104.

[47] Rubén Varela, Fernando P Lima, Rui Seabra, Claudia Meneghesso, and Moncho Gómez-Gesteira. "Coastal warming and wind-driven upwelling: A global analysis". In: *Science of the Total Environment* 639 (2018), pp. 1501–1511.

[48] Weiwei Fu, James T Randerson, and J Keith Moore. "Climate change impacts on net primary production (NPP) and export production (EP) regulated by increasing stratification and phytoplankton community structure in the CMIP5 models". In: *Biogeosciences* 13.18 (2016), pp. 5151–5170.

[49] Andreas Oschlies, Peter Brandt, Lothar Stramma, and Sunke Schmidtko. "Drivers and mechanisms of ocean deoxygenation". In: *Nature Geoscience* 11.7 (2018), pp. 467–473.

[50] National Oceanic and Atmospheric Administration (NOAA). *Ocean acidification*. https://www.noaa.gov/education/resource-collections/ocean-coasts/ocean-acidification. Accessed: [Your access date].

[51] Laurent Bopp, Laure Resplandy, James C Orr, Scott C Doney, John P Dunne, M Gehlen, P Halloran, Christoph Heinze, Tatiana Ilyina, Roland Seferian, et al. "Multiple stressors of ocean ecosystems in the 21st century: projections with CMIP5 models". In: *Biogeosciences* 10.10 (2013), pp. 6225–6245.

[52] Scott C Doney, Victoria J Fabry, Richard A Feely, and Joan A Kleypas. "Ocean acidification: the other CO2 problem". In: *Annual review of marine science* 1.1 (2009), pp. 169–192.

[53] Long Cao, Han Zhang, Meidi Zheng, and Shuangjing Wang. "Response of ocean acidification to a gradual increase and decrease of atmospheric CO2". In: *Environmental Research Letters* 9.2 (2014), p. 024012.

[54] James C Orr, Victoria J Fabry, Olivier Aumont, Laurent Bopp, Scott C Doney, Richard A Feely, Anand Gnanadesikan, Nicolas Gruber, Akio Ishida, Fortunat Joos, et al. "Anthropogenic ocean acidification over the twenty-first century and its impact on calcifying organisms". In: *Nature* 437.7059 (2005), pp. 681–686.

[55] Ana C Franco, Nicolas Gruber, Thomas L Frölicher, and L Kropuenske Artman. "Contrasting impact of future CO2 emission scenarios on the extent of CaCO3 mineral undersaturation in the Humboldt Current System". In: *Journal of Geophysical Research: Oceans* 123.3 (2018), pp. 2018–2036.

[56] Claudine Hauri, Nicolas Gruber, Meike Vogt, Scott C Doney, Richard A Feely, Zouhair Lachkar, A Leinweber, Andrew MP McDonnell, M Munnich, and G-K Plattner. "Spatiotemporal variability and long-term trends of ocean acidification in the California Current System". In: *Biogeosciences* 10.1 (2013), pp. 193–216.

[57] Zouhair Lachkar. "Effects of upwelling increase on ocean acidification in the California and Canary Current systems". In: *Geophysical Research Letters* 41.1 (2014), pp. 90–95.

[58] Malin L Pinsky, Gabriel Reygondeau, Richard Caddell, Juliano Palacios-Abrantes, Jessica Spijkers, and William WL Cheung. "Preparing ocean governance for species on the move". In: *Science* 360.6394 (2018), pp. 1189–1191.

[59] Caren Barceló, Lorenzo Ciannelli, and Richard D Brodeur. "Pelagic marine refugia and climatically sensitive areas in an eastern boundary current upwelling system". In: *Global change biology* 24.2 (2018), pp. 668–680.

[60] Morten Frederiksen, Martin Edwards, Anthony J Richardson, Nicholas C Halliday, and Sarah Wanless. "From plankton to top predators: bottom-up control of a marine food web across four trophic levels". In: *Journal of Animal Ecology* 75.6 (2006), pp. 1259–1268.

[61] Dean Roemmich and John McGowan. "Climatic warming and the decline of zooplankton in the California Current". In: *Science* 267.5202 (1995), pp. 1324–1326.

[62] MG Jacox and CA Edwards. "Effects of stratification and shelf slope on nutrient supply in coastal upwelling regions". In: *Journal of Geophysical Research: Oceans* 116.C3 (2011).

[63] Andrew Bakun. "Global climate change and intensification of coastal ocean upwelling". In: *Science* 247.4939 (1990), pp. 198–201.

[64] Jian Lu, Gabriel A Vecchi, and Thomas Reichler. "Expansion of the Hadley cell under global warming". In: *Geophysical Research Letters* 34.6 (2007).

[65] Kevin M Grise and Sean M Davis. "Hadley cell expansion in CMIP6 models". In: *Atmospheric Chemistry and Physics* 20.9 (2020), pp. 5249–5268.

[66] Ryan R Rykaczewski and John P Dunne. "Enhanced nutrient supply to the California Current Ecosystem with global warming and increased stratification in an earth system model". In: *Geophysical Research Letters* 37.21 (2010).

[67] United Nations Framework Convention on Climate Change (UNFCCC). "Paris Agreement". In: *Report of the Conference of the Parties to the United Nations Framework Convention on Climate Change (21st session, 2015: Paris)*. Retrieved December 2017, HeinOnline, Getzville, NY, USA. 2015.

[68] Tabbi Wilberforce, AG Olabi, Enas Taha Sayed, Khaled Elsaid, and Mohammad Ali Abdelkareem. "Progress in carbon capture technologies". In: *Science of The Total Environment* 761 (2021), p. 143203.

[69] Klaus S Lackner, Sarah Brennan, Jürg M Matter, A-H Alissa Park, Allen Wright, and Bob Van Der Zwaan. "The urgency of the development of CO2 capture from ambient air". In: *Proceedings of the National Academy of Sciences* 109.33 (2012), pp. 13156–13162.

[70] Megan Mills-Novoa and Diana M Liverman. "Nationally determined contributions: material climate commitments and discursive positioning in the NDCs". In: *Wiley Interdisciplinary Reviews: Climate Change* 10.5 (2019), e589.

[71] Peiran R Liu and Adrian E Raftery. "Country-based rate of emissions reductions should increase by 80% beyond nationally determined contributions to meet the 2 C target". In: *Communications earth & environment* 2.1 (2021), p. 29.

[72] Carl-Friedrich Schleussner, Joeri Rogelj, Michiel Schaeffer, Tabea Lissner, Rachel Licker, Erich M Fischer, Reto Knutti, Anders Levermann, Katja Frieler, and William Hare. "Science and policy characteristics of the Paris Agreement temperature goal". In: *Nature Climate Change* 6.9 (2016), pp. 827–835.

[73] United Nations. *Climate action. For a livable climate: Net-zero commitments must be backed by credible action.* https://www.un.org/en/climatechange/net-zero-coalition.

[74] Niklas Höhne, Michel den Elzen, Joeri Rogelj, Bert Metz, Taryn Fransen, Takeshi Kuramochi, Anne Olhoff, Joseph Alcamo, Harald Winkler, Sha Fu, et al. "Emissions: world has four times the work or one-third of the time". In: *Nature* 579.7797 (2020), pp. 25–28.

[75] Irina Melnikova, Olivier Boucher, Patricia Cadule, Philippe Ciais, Thomas Gasser, Yann Quilcaille, Hideo Shiogama, Kaoru Tachiiri, Tokuta Yokohata, and Katsumasa Tanaka. "Carbon cycle response to temperature overshoot beyond 2 C: An analysis of CMIP6 models". In: *Earth's Future* 9.5 (2021), e2020EF001967.

[76] Joeri Rogelj, Drew Shindell, Kejun Jiang, Solomone Fifita, Piers Forster, Veronika Ginzburg, Collins Handa, Haroon Kheshgi, Shigeki Kobayashi, Elmar Kriegler, et al. "Mitigation pathways compatible with 1.5 C in the context of sustainable development". In: *Global warming of 1.5 C*. Intergovernmental Panel on Climate Change, 2018, pp. 93–174.

[77] Toshihiko Masui, Kenichi Matsumoto, Yasuaki Hijioka, Tsuguki Kinoshita, Toru Nozawa, Sawako Ishiwatari, Etsushi Kato, Priyadarshi R Shukla, Yoshiki Yamagata, and Mikiko Kainuma. "An emission pathway for stabilization at 6 Wm- 2 radiative forcing". In: *Climatic change* 109 (2011), pp. 59–76.

[78] Keywan Riahi, Shilpa Rao, Volker Krey, Cheolhung Cho, Vadim Chirkov, Guenther Fischer, Georg Kindermann, Nebojsa Nakicenovic, and Peter Rafaj. "RCP 8.5—A scenario of comparatively high greenhouse gas emissions". In: *Climatic change* 109 (2011), pp. 33–57.

[79] Detlef P Van Vuuren, Michel GJ Den Elzen, Paul L Lucas, Bas Eickhout, Bart J Strengers, Bas Van Ruijven, Steven Wonink, and Roy Van Houdt. "Stabilizing greenhouse gas concentrations at low levels: an assessment of reduction strategies and costs". In: *Climatic change* 81 (2007), pp. 119–159.

[80] Detlef P Van Vuuren, Jae Edmonds, Mikiko Kainuma, Keywan Riahi, Allison Thomson, Kathy Hibbard, George C Hurtt, Tom Kram, Volker Krey, Jean-Francois Lamarque, et al. "The representative concentration pathways: an overview". In: *Climatic change* 109 (2011), pp. 5–31.

[81] Malte Meinshausen, Nicolai Meinshausen, William Hare, Sarah CB Raper, Katja Frieler, Reto Knutti, David J Frame, and Myles R Allen. "Greenhouse-gas emission targets for limiting global warming to 2 C". In: *Nature* 458.7242 (2009), pp. 1158–1162.

[82] Joeri Rogelj, William Hare, Jason Lowe, Detlef P Van Vuuren, Keywan Riahi, Ben Matthews, Tatsuya Hanaoka, Kejun Jiang, and Malte Meinshausen. "Emission pathways consistent with a 2 C global temperature limit". In: *Nature Climate Change* 1.8 (2011), pp. 413–418.

[83] Nathan P Gillett, Vivek K Arora, Kirsten Zickfeld, Shawn J Marshall, and William J Merryfield. "Ongoing climate change following a complete cessation of carbon dioxide emissions". In: *Nature Geoscience* 4.2 (2011), pp. 83–87.

[84] Gaurav Ganti, Thomas Gasser, Mai Bui, Oliver Geden, William F Lamb, Jan C Minx, Carl-Friedrich Schleussner, and Matthew J Gidden. "Evaluating the near- and long-term role of carbon dioxide removal in meeting global climate objectives". In: *Communications Earth & Environment* 5.1 (2024), p. 377.

[85] O Boucher, PR Halloran, EJ Burke, M Doutriaux-Boucher, CD Jones, J Lowe, MA Ringer, E Robertson, and P Wu. "Reversibility in an Earth System model in response to CO2 concentration changes". In: *Environmental Research Letters* 7.2 (2012), p. 024013.

[86] J.B.R. Matthews, V. Möller, R. van Diemen, J.S. Fuglestvedt, V. Masson-Delmotte, C. Méndez, S. Semenov, and A. Reisinger. "Annex VII: Glossary". In: *Climate Change 2021: The Physical Science Basis. Contribution of Working Group I to the Sixth Assessment Report of the Intergovernmental Panel on Climate Change*. Ed. by V. Masson-Delmotte, P. Zhai, A. Pirani, S.L. Connors, C. Péan, S. Berger, N. Caud, Y. Chen, L. Goldfarb, M.I. Gomis, M. Huang, K. Leitzell, E. Lonnoy, J.B.R. Matthews, T.K. Maycock, T. Waterfield, O. Yelekçi, R. Yu, and B. Zhou. Cambridge University Press, 2021, pp. 2215–2256. URL: https://www.ipcc.ch/report/ar6/wg1/downloads/report/IPCC_AR6_WGI_AnnexVII.pdf.

[87] Chris D Jones, Thomas L Frölicher, Charles Koven, Andrew H MacDougall, H Damon Matthews, Kirsten Zickfeld, Joeri Rogelj, Katarzyna B Tokarska, Nathan P Gillett, Tatiana Ilyina, et al. "The Zero Emissions Commitment Model Intercomparison Project (ZECMIP) contribution to C4MIP: quantifying committed climate changes following zero carbon emissions". In: *Geoscientific Model Development* 12.10 (2019), pp. 4375–4385.

[88] Bill Hare and Malte Meinshausen. "How much warming are we committed to and how much can be avoided?" In: *Climatic change* 75.1 (2006), pp. 111–149.

[89] Timothy M Lenton, Johan Rockström, Owen Gaffney, Stefan Rahmstorf, Katherine Richardson, Will Steffen, and Hans Joachim Schellnhuber. "Climate tipping points—too risky to bet against". In: *Nature* 575.7784 (2019), pp. 592–595.

[90] Christoph Heinze, Thorsten Blenckner, Peter Brown, Friederike Fröb, Anne Morée, Adrian L New, Cara Nissen, Stefanie Rynders, Isabel Seguro, Yevgeny Aksenov, et al. "Reviews and syntheses: Abrupt ocean biogeochemical change under human-made climatic forcing–warming, acidification, and deoxygenation". In: *Biogeosciences Discussions* 2023 (2023), pp. 1–131.

[91] Jasmin G John, Charles A Stock, and John P Dunne. "A more productive, but different, ocean after mitigation". In: *Geophysical Research Letters* 42.22 (2015), pp. 9836–9845.

[92] Brian C O'Neill, Claudia Tebaldi, Detlef P Van Vuuren, Veronika Eyring, Pierre Friedlingstein, George Hurtt, Reto Knutti, Elmar Kriegler, Jean-Francois Lamarque, Jason Lowe, et al. "The scenario model intercomparison project (ScenarioMIP) for CMIP6". In: *Geoscientific Model Development* 9.9 (2016), pp. 3461–3482.

[93] Malte Meinshausen, Steven J Smith, Katherine Calvin, John S Daniel, Mikiko LT Kainuma, Jean-Francois Lamarque, Kazuhiko Matsumoto, Stephen A Montzka, Sarah CB Raper, Keywan Riahi, et al. "The RCP greenhouse gas concentrations and their extensions from 1765 to 2300". In: *Climatic change* 109 (2011), pp. 213–241.

[94] Keywan Riahi, Detlef P Van Vuuren, Elmar Kriegler, Jae Edmonds, Brian C O'neill, Shinichiro Fujimori, Nico Bauer, Katherine Calvin, Rob Dellink, Oliver Fricko, et al. "The Shared Socioeconomic Pathways and their energy, land use, and greenhouse gas emissions implications: An overview". In: *Global environmental change* 42 (2017), pp. 153–168.

[95] Malte Meinshausen, Zebedee RJ Nicholls, Jared Lewis, Matthew J Gidden, Elisabeth Vogel, Mandy Freund, Urs Beyerle, Claudia Gessner, Alexander Nauels, Nico Bauer, et al. "The shared socio-economic pathway (SSP) greenhouse gas concentrations and their extensions to 2500". In: *Geoscientific Model Development* 13.8 (2020), pp. 3571–3605.

[96] Olivier Boucher, Jérôme Servonnat, Anna Lea Albright, Olivier Aumont, Yves Balkanski, Vladislav Bastrikov, Slimane Bekki, Rémy Bonnet, Sandrine Bony, Laurent Bopp, et al. "Presentation and evaluation of the IPSL-CM6A-LR climate model". In: *Journal of Advances in Modeling Earth Systems* 12.7 (2020), e2019MS002010.

[97] Frédéric Hourdin, Catherine Rio, Jean-Yves Grandpeix, Jean-Baptiste Madeleine, Frédérique Cheruy, Nicolas Rochetin, Arnaud Jam, Ionela Musat, Abderrahmane Idelkadi, Laurent Fairhead, et al. "LMDZ6A: The atmospheric component of the IPSL climate model with improved and better tuned physics". In: *Journal of Advances in Modeling Earth Systems* 12.7 (2020), e2019MS001892.

[98] Gerhard Krinner, Nicolas Viovy, Nathalie de Noblet-Ducoudré, Jérôme Ogée, Jan Polcher, Pierre Friedlingstein, Philippe Ciais, Stephen Sitch, and I Colin Prentice. "A dynamic global vegetation model for studies of the coupled atmosphere-biosphere system". In: *Global Biogeochemical Cycles* 19.1 (2005).

[99] Olivier Aumont, Christian Éthé, Alessandro Tagliabue, Laurent Bopp, and Marion Gehlen. "PISCES-v2: an ocean biogeochemical model for carbon and ecosystem studies". In: *Geoscientific Model Development Discussions* 8.2 (2015), pp. 1375–1509.

[100] Taro Takahashi, Wallace S Broecker, and Sara Langer. "Redfield ratio based on chemical data from isopycnal surfaces". In: *Journal of Geophysical Research: Oceans* 90.C4 (1985), pp. 6907–6924.

[101] Richard J Geider, Hugh L MacIntyre, and Todd M Kana. "A dynamic regulatory model of phytoplanktonic acclimation to light, nutrients, and temperature". In: *Limnology and oceanography* 43.4 (1998), pp. 679–694.

[102] William G Sunda and Susan A Huntsman. "Iron uptake and growth limitation in oceanic and coastal phytoplankton". In: *Marine chemistry* 50.1-4 (1995), pp. 189–206.

[103] Charlotte Laufkötter, Meike Vogt, Nicolas Gruber, Maki Aita-Noguchi, Olivier Aumont, Laurent Bopp, Erik Buitenhuis, Scott C Doney, J Dunne, Taketo Hashioka, et al. "Drivers and uncertainties of future global marine primary production in marine ecosystem models". In: *Biogeosciences* 12.23 (2015), pp. 6955–6984.

[104] Ed Hawkins and Rowan Sutton. "The potential to narrow uncertainty in regional climate predictions". In: *Bulletin of the American Meteorological Society* 90.8 (2009), pp. 1095–1108.

[105] Flavio Lehner, Clara Deser, Nicola Maher, Jochem Marotzke, Erich M Fischer, Lukas Brunner, Reto Knutti, and Ed Hawkins. "Partitioning climate projection uncertainty with multiple large ensembles and CMIP5/6". In: *Earth System Dynamics* 11.2 (2020), pp. 491–508.

[106] Earth System Grid Federation. *Earth System Grid Federation (ESGF)*. URL: https://esgf-node.ipsl.upmc.fr/projects/cmip6-ipsl/.

[107] Monique Messié and Francisco P Chavez. "Seasonal regulation of primary production in eastern boundary upwelling systems". In: *Progress in Oceanography* 134 (2015), pp. 1–18.

[108] Laurent Bopp, Olivier Aumont, Lester Kwiatkowski, Corentin Clerc, Léonard Dupont, Christian Ethé, Roland Séférian, and Alessandro Tagliabue. "Diazotrophy as a key driver of the response of marine net primary productivity to climate change". In: *Biogeosciences Discussions* 2021 (2021), pp. 1–31.

[109] Laurent Bopp, Corinne Le Quéré, Martin Heimann, Andrew C Manning, and Patrick Monfray. "Climate-induced oceanic oxygen fluxes: Implications for the contemporary carbon budget". In: *Global Biogeochemical Cycles* 16.2 (2002), pp. 6–1.

[110] Laurent Bopp, Patrick Monfray, Olivier Aumont, Jean-Louis Dufresne, Hervé Le Treut, Gurvan Madec, Laurent Terray, and James C Orr. "Potential impact of climate change on marine export production". In: *Global Biogeochemical Cycles* 15.1 (2001), pp. 81–99.

[111] Mary R Gradoville, Deniz Bombar, Byron C Crump, Ricardo M Letelier, Jonathan P Zehr, and Angelicque E White. "Diversity and activity of nitrogen-fixing communities across ocean basins". In: *Limnology and Oceanography* 62.5 (2017), pp. 1895–1909.

[112] Weiyi Tang, Seaver Wang, Debany Fonseca-Batista, Frank Dehairs, Scott Gifford, Aridane G Gonzalez, Morgane Gallinari, Hélène Planquette, Géraldine Sarthou, and Nicolas Cassar. "Revisiting the distribution of oceanic N2 fixation and estimating diazotrophic contribution to marine production". In: *Nature communications* 10.1 (2019), p. 831.

[113] Laurent Bopp, Olivier Aumont, Patricia Cadule, Séverine Alvain, and Marion Gehlen. "Response of diatoms distribution to global warming and potential implications: A global model study". In: *Geophysical Research Letters* 32.19 (2005).

[114] Irina Marinov, SC Doney, and ID Lima. "Response of ocean phytoplankton community structure to climate change over the 21st century: partitioning the effects of nutrients, temperature and light". In: *Biogeosciences* 7.12 (2010), pp. 3941–3959.

[115] Zouhair Lachkar and Nicolas Gruber. "What controls biological production in coastal upwelling systems? Insights from a comparative modeling study". In: *Biogeosciences* 8.10 (2011), pp. 2961–2976.

[116] Seo-Yeon Kim, Yeong-Ju Choi, Seok-Woo Son, Kevin M Grise, Paul W Staten, Soon-Il An, Sang-Wook Yeh, Jong-Seong Kug, Seung-Ki Min, and Jongsoo Shin. "Hemispherically asymmetric Hadley cell response to CO2 removal". In: *Science advances* 9.30 (2023), eadg1801.

[117] Thomas J Browning and C Mark Moore. "Global analysis of ocean phytoplankton nutrient limitation reveals high prevalence of co-limitation". In: *Nature Communications* 14.1 (2023), p. 5014.

[118] Corinne Le Quéré, Erik T Buitenhuis, Róisín Moriarty, Séverine Alvain, Olivier Aumont, Laurent Bopp, Sophie Chollet, Clare Enright, Daniel J Franklin, Richard J Geider, et al. "Role of zooplankton dynamics for Southern Ocean phytoplankton biomass and global biogeochemical cycles". In: *Biogeosciences* 13.14 (2016), pp. 4111–4133.

[119] Lester Kwiatkowski, Olivier Aumont, and Laurent Bopp. "Consistent trophic amplification of marine biomass declines under climate change". In: *Global change biology* 25.1 (2019), pp. 218–229.

[120] Heike K Lotze, Derek P Tittensor, Andrea Bryndum-Buchholz, Tyler D Eddy, William WL Cheung, Eric D Galbraith, Manuel Barange, Nicolas Barrier, Daniele Bianchi, Julia L Blanchard, et al. "Global ensemble projections reveal trophic amplification of ocean biomass declines with climate change". In: *Proceedings of the National Academy of Sciences* 116.26 (2019), pp. 12907–12912.

[121] Léonard Dupont, Priscilla Le Mézo, Olivier Aumont, Laurent Bopp, Corentin Clerc, Christian Ethé, and Olivier Maury. "High trophic level feedbacks on global ocean carbon uptake and marine ecosystem dynamics under climate change". In: *Global Change Biology* 29.6 (2023), pp. 1545–1556.

[122] Lester Kwiatkowski, Laurent Bopp, Olivier Aumont, Philippe Ciais, Peter M Cox, Charlotte Laufkötter, Yue Li, and Roland Séférian. "Emergent constraints on projections of declining primary production in the tropical oceans". In: *Nature Climate Change* 7.5 (2017), pp. 355–358.

[123] S. Jullien, M. Caillaud, R. Benshila, L. Bordois, G. Cambon, F. Dufois, F. Dumas, J. Gula, M. Le Corre, S. Le Gentil, F. Lemarié, P. Marchesiello, G. Morvan, and S. Theetten. *Technical and numerical doc, Release 1.2.* https://data-croco.ifremer.fr/DOC/model-v1.2.pdf. 2019.

[124] Thomas L Frölicher, Keith B Rodgers, Charles A Stock, and William WL Cheung. "Sources of uncertainties in 21st century projections of potential ocean ecosystem stressors". In: *Global Biogeochemical Cycles* 30.8 (2016), pp. 1224–1243.

[125] Clara Deser, Flavio Lehner, Keith B Rodgers, Toby Ault, Thomas L Delworth, Pedro N DiNezio, Arlene Fiore, Claude Frankignoul, John C Fyfe, Daniel E Horton, et al. "Insights from Earth system model initial-condition large ensembles and future prospects". In: *Nature Climate Change* 10.4 (2020), pp. 277–286.